

EXCITATION AND DAMPING
OF
SOLAR P-MODES

Thesis by
Pawan Kumar

In Partial Fulfillment of the Requirements
for the Degree of
Doctor of Philosophy

California Institute of Technology
Pasadena, California

1988

(Submitted 21 August, 1987)

ACKNOWLEDGEMENTS

My thesis advisor Professor Peter Goldreich introduced me to solar oscillations, suggested the excitation problem and provided constant guidance and encouragement. He spared time from his busy schedule for countless number of discussions with me. I can not express enough gratitude to him.

It was always a delight to talk to Professor Ken Libbrecht. He provided many observational results which were essential to some of the work done here. It was a great pleasure to collaborate with Professor Joel Franklin on the energy statistics of stochastically driven oscillators. I am grateful to Professor Harold Zirin and Wal Sargent for providing financial support for the summer of 1982 and 1983 respectively.

My special thanks is due to Jim Kaufman for reading the early drafts of two papers and also providing helpful comments on my talks. I am indebted to Charles Lawrence for helping me with numerous \TeX questions. I am thankful to many of my colleagues particularly Jim McCarthy, Dave Hough, Alain Porter, Alex Filipenko, Fernando Selman, Steven Myers, Dean Chou, Kwok-Wai Cheung and Haimin Wang for numerous discussions and also helping to make my stay at Caltech so pleasant.

During the course of my stay at Caltech I took many courses. I particularly enjoyed and benefited from the courses offered by Richard Feynman, Jerry Sussman, Kip Thorne, John Preskill and Gerald Whitham. Peter Goldreich's seminar course on the early universe was very exciting. It started out as a one term course but due to the active participation of Peter Goldreich, Craig Hogan, David Tytler and Jeremy Goodman it continued for almost two years! It is a great pleasure to thank them all.

Kathleen Campbell of Planetary Science was always very helpful with paper works or travel arrangements. I am particularly grateful to her for helping me to make photocopies of my thesis on a Friday afternoon, when every thing was going wrong, so that I could submit the thesis in time. I am thankful to Donna Lathrop for typing the first chapter of my thesis. Nora Knicker, of solar astronomy, impressed me with her efficiency and pleasantness. Helen Knudsen, of the Astronomy library, saved me trouble countless number of times in finding a reference or providing a

literature search. I am grateful to Liselotte Hauck, an exceptionally warm and hard working person of Palomar office, for her concern that I don't stay up too late at night working.

ABSTRACT

I have carried out detailed analysis of the interaction of acoustic radiation with homogeneous turbulence in order to understand the excitation of solar p-modes by turbulent convection. The most significant outcome of this investigation is the finding that, for certain types of forced turbulences, the absorption of acoustic waves is no greater than a free turbulence, whereas the emission is always enhanced by a factor M^{-2} , where M is the Mach number of the turbulence. Turbulent convection in the sun is an example of this kind of turbulence. This leads to the conclusion that energies in solar p-modes, due to their interaction with the convection, should be approximately equal to the thermal energy in a resonant eddy. This is found to be in good agreement with the observations. The ideas developed in the above work have been applied to explain the recently observed absorption of acoustic waves by sunspots as well. Work has also been carried out to determine the probability distribution function for the time averaged energy of stochastically excited modes. We hope to learn about the nature of the excitation and damping processes for the solar modes by comparing this theoretically determined distribution with the observations.

In an effort towards resolving the overstability question of solar p-modes, I have investigated the effectiveness of 3-mode couplings, the most plausible process for limiting the amplitudes of overstable modes. The 3-mode coupling mechanism is also a good candidate for exciting fundamental modes which are found to be linearly stable, but are observed to have energies comparable to p-modes of similar frequencies. The issue of mode stability remains inconclusive due to the unknown energies of modes with period ~ 3.5 minutes. However, we find the fundamental modes to be damped as a result of mode couplings and hence they require excitation by a mechanism other than the overstability.

TABLE OF CONTENTS

Acknowledgements	ii
Abstract	iv
Chapter 1. Introduction to solar oscillations	1
Chapter 2. The interaction of acoustic radiation with turbulence	30
Chapter 3. Absorption of acoustic waves by sunspots	88
Chapter 4. Distribution functions for the time averaged energies of stochastically excited solar p-modes	95
Chapter 5. 3-mode coupling of solar p-modes	121

CHAPTER 1

Introduction to solar oscillations

1. Preliminaries

Solar oscillations with periods near five minutes were discovered by Leighton, Noyes and Simon (1961) and Evans and Michard (1962). About ten years later, Ulrich (1970) and, Leibacher and Stein (1971) described them as standing acoustic waves trapped between two reflecting surfaces in the sun, the upper surface lying just below the photosphere. About five years later, Deubner (1975) observationally determined the power in these oscillations as a function of frequency and horizontal wavenumber and found that the power lies along ridges in the resultant $k - \omega$ diagram. This finding established the global nature of these oscillations. The ridges found by Deubner corresponded well to those predicted by Ulrich (1970) and Ando and Osaki (1975).

There are three restoring forces which act on a displaced fluid element in the sun: thermal pressure, buoyancy and magnetic tension. When one of these restoring forces is dominant, the corresponding oscillation is called an acoustic, gravity and magnetic wave, respectively. If the gravity, or g-modes, are excited in the sun, they would be trapped below ~ 0.7 solar radius, and thus provide information predominantly about the solar interior. At present, the observational evidence for g-modes in the sun (Severny *et al.* 1976, Brooks *et al.* 1976, Delache and Scherrer 1983, Scherrer 1984, Kuhn *et al.* 1986), is disputable. Therefore, I shall concentrate on the well established pressure or p-modes which are simply sound waves trapped in the sun. There are several excellent reviews of this subject (Stein and Leibacher 1974, Goldreich and Keeley 1977c, Christensen-Dalsgaard 1984, Deubner and Gough 1984, Christensen-Dalsgaard *et al.* 1985, Brown *et al.* 1986), which should be consulted for a complete survey of the subject. My goal here is to give a quick overview of the main observational and theoretical results. Needless to say, my selection of papers is far from complete and reflects my own interests and prejudices.

The p-modes are classified by the number of nodes, n , in the radial displacement component of the eigenfunction, the spherical harmonic degree ℓ , and the azimuthal

eigenvalue, m . For $\ell = 0$, the periods of the p-modes range from 0 to 60 minutes. However, the observed p-modes have periods between 4 and 10 minutes; this is called the 5-minute band because the observed power peaks at about five minutes. The degree, ℓ , for the modes in this band ranges from 0 to about 2000. For fixed frequency, the number of radial nodes depends on ℓ . For $\ell = 0$, the modes in the 5-minute band have $10 \leq n \leq 30$, for $\ell = 900$, $1 \leq n \leq 4$. As usual, m takes values from $-\ell$ to ℓ . Thus, there are about ten million modes in the five minute band.

I mentioned before that the p-modes are stationary sound waves. There are two reasons for the reflection of sound waves in the interior of the sun. Firstly, the sound speed increases with increasing depth in the sun so a downward, nonradial, ray is deflected away from the radial direction, and is eventually refracted upward (mirages occur for the same reason). Secondly, even for a homogeneous sphere, a ray starting out at a distance r from the center and directed at an angle θ from the inward radial direction does not come closer than $r \sin \theta$ to the center. More precisely, for an inhomogeneous sphere like the sun, given a mode of degree ℓ there are ℓ nodes along the longitude, (considering $m=0$, without loss of generality) independent of the radial distance from the center, so the horizontal component of wave number $k_h^2 = \ell(\ell + 1)/r^2$. Since $k^2 = k_h^2 + k_r^2$, $k_r = \sqrt{\omega^2/c^2 - \ell(\ell + 1)/r^2}$. For fixed ω and ℓ , there would be a critical r , R_c , at which $k_r = 0$. For $r < R_c$, $k_r^2 < 0$ so the wave cannot propagate inside the radius R_c . The reflection of the wave at the outer boundary below the solar photosphere is due to a sharp increase in both the Brunt-Väisälä and acoustic cut off frequencies which attain a value of 5 mHz. For a p -wave to propagate, its frequency must be greater than the local acoustic cut off frequency and the Brunt-Väisälä frequency, or more physically, its wavelength should be smaller than the density scale height. So an acoustic wave with frequency less than 5 mHz will be trapped inside the sun.

The distance of the inner reflection point (R_{in}) from the center of the sun depends on both the frequency and ℓ , $R_{in} = c\sqrt{\ell(\ell + 1)}/\omega$. The higher the frequency

and the lower the ℓ , the deeper the mode can probe inside the sun. For example, with $\ell = 2$ and $\nu = 1.7$ mHz (10 minute), $R_{in} = 0.15 R_{\odot}$. For $\ell = 2$ and $\nu = 3.4$ mHz, $R_{in} \simeq 0$. For a five minute period, the $\ell = 100$ mode has $R_{in} = 0.85 R_{\odot}$ and the $\ell = 1000$ has $R_{in} = 0.99 R_{\odot}$. By contrast, the outer boundary remains nearly fixed for different ω and ℓ . The eigenfrequencies give information about some weighted average of the sound speed in the cavity in which the mode is trapped. As the depth of the cavity is a function of ω and ℓ , the eigenfrequencies may be directly inverted to yield the speed of sound as a function of depth.

The frequency spacing between two modes having the same ℓ and a difference of one in the number of radial nodes depends on ℓ but is only weakly dependent on the number of radial nodes, n . For $\ell = 100$, the mean frequency spacing is 1.8 times the mean spacing between modes with $\ell = 0$ and for $\ell = 700$, the mean frequency spacing is five times the mean spacing for $\ell = 0$. Thus, in a given frequency interval, the density of modes decreases with increasing degree.

For $\ell \ll n$, there is a useful asymptotic expansion for eigenfrequency $\omega_{n,\ell}$:

$$\omega_{n,\ell} = \delta\omega(n + 1/2 + \epsilon) + A[\ell(\ell + 1) + \delta]\delta\omega^2/\omega_{n,\ell} . \quad (1)$$

Here, $\delta\omega = [2 \int dr/c]^{-1}$, and ϵ , δ , and A are constant integrals of solar model. Grec (1981) found values of $A \simeq 0.267$, $\delta \simeq -17$ and $\epsilon \simeq 1$. We see from the above equation that the frequency of the mode (n, ℓ) is approximately equal to the frequency of mode $(n + 1, \ell - 2)$. In the opposite limit, for $\ell \gg n$, the asymptotic eigenfrequency is given by:

$$\omega_{n,\ell}^2 \simeq -2(n + \epsilon) \frac{dc^2}{dr} \sqrt{\ell(\ell + 1)}/R_{\odot}^2 , \quad (2)$$

where dc^2/dr is related to the gravitational acceleration and $\sqrt{\ell(\ell + 1)}/R_{\odot}$ is the horizontal wavenumber. For a fixed number of radial nodes n , the above equation describes parabolas in the $k_h - \omega$ plane which correspond to the ridges seen in the $k - \omega$ diagram.

In order to determine the energy in a mode, we need to multiply what is called the mass in the mode with the square of its observed surface velocity. The mass in a mode, M_q , is defined as the energy in the mode when the mean surface velocity (the surface is place where line used for the observation is formed) is unity; M_q is determined from the velocity eigenfunction. The mass in a mode depends on ω , ℓ , and the line used for the observation of the velocity field. The dependence of M_q on the optical depth occurs because the density in the photosphere decreases more rapidly than the energy density in the mode. Hence, the velocity increases upwards. Now, according to the definition of M_q , we have to divide the energy in the mode by the square of the velocity at the place of observation. Thus M_q decreases with decreasing optical depth. Moreover, this dependence on the optical depth is not independent of the frequency of the mode. That is, if we take the ratio of the masses in different modes, this ratio also has an optical depth dependence; although for fixed frequency and variable ℓ this ratio is independent of optical depth. What this all means is that in converting the velocity of the mode to the energy in the mode one must properly take into account the depth of formation of the line used in the observation. At a fixed optical depth, M_q is a strong function of ω but weak function of ℓ . For the modes of same frequency but different degree, $M_q \propto 1/\sqrt{\ell}$ when $\ell > 100$. Moreover, for $\ell = 100$ M_q is about 1/2 the M_q at $\ell = 0$ (valid for modes of same frequency only). For fixed ℓ , M_q decreases rapidly with increasing ω , (fig. 1).

So far we have ignored solar rotation. In this limit, all modes with the same n and ℓ but different m have the same frequency because there is no preferred direction or axis. Because the sun is rotating, modes of the same ℓ but different m do not have quite the same frequency; the degeneracy is lifted by the rotation just as a magnetic field lifts the energy degeneracy of the states of different m in an atom. Ledoux (1951) has calculated the frequency splitting for a uniformly rotating fluid body:

$$\nu_{n,\ell,m} = \nu_{n,\ell} + m(1 - C_{n\ell})\Omega/2\pi \quad -\ell \leq m \leq \ell, \quad (3)$$

where $C_{n\ell}$ is a positive constant, which depends on the equilibrium structure of the fluid body and also on the mode (n, ℓ) , and Ω is the angular velocity. For a nonuniformly rotating body, Ω must be replaced by a suitably averaged angular velocity. If Ω is a slowly varying function of r , and if large n low ℓ modes are considered, the form of mean rotational velocity that should be substituted for the rigid body rotational velocity in the above formula is given by (Gough, 1981):

$$\bar{\Omega} = \frac{\int dr \frac{\Omega(r)}{c(r)}}{\int \frac{dr}{c(r)}}, \quad (4)$$

where c is the sound speed. In the presence of latitudinal differential rotation, if the centrifugal effects can be ignored, the rotational splitting can be approximated by (Cuypers 1980)

$$\nu_{n,\ell,m} - \nu_{n,\ell,0} = -m \frac{\int_{-1}^1 d \cos \theta \bar{\Omega}(\theta) [P_{\ell}^m(\cos \theta)]^2}{\int_{-1}^1 d \cos \theta [P_{\ell}^m(\cos \theta)]^2}, \quad (5)$$

where θ is the colatitude, $\bar{\Omega}$ is a suitable depth average, and P_{ℓ}^m is the associated Legendre function. If the sun rotates uniformly with the observed surface rotational velocity, the $\Delta m=1$ frequency splitting would be about $0.4 \mu\text{Hz}$.

Broadly speaking, the theoretical problems associated with solar oscillations can be classified in two categories. The first involves modeling the frequencies and the second involves the explanation of the amplitudes and linewidths of the modes. The first category involves determining the internal structure of the sun including the abundance of elements, the depth of the convection zone, the rotation and other large scale motions, large scale magnetic fields, and any other parameter which might affect the speed of wave propagation. If one is only interested in learning about the internal composition of the sun, she may ignore the information

contained in the amplitudes and linewidths of the modes. However, by retaining the later, one can learn about the mechanisms which excite and damp the oscillations, which in turn would be very useful in providing guidelines for which stars to look at for similar oscillations.

In the next section I describe the main observational results obtained so far on the frequency, amplitude and linewidth of different modes. Section III contains the results of attempts to fit the observed frequencies with a solar model. Finally, in section IV I outline the status of our understanding of solar p -mode excitation.

2. Observational Results and Their Implication for Solar Structure

Short period solar pressure oscillations with periods around five minutes have been observed in the Doppler shift measurement of line of sight velocity as well as by photometric intensity measurements. The discussion of the principal observational results which follows has been divided into two parts. First, the results for low degree modes ($\ell \leq 5$), which are obtained by whole disk integration of either the velocity signal or the intensity fluctuations, are presented. Next, the results for intermediate ($5 < \ell < 200$) and high degree ($\ell > 200$) modes obtained from two or three dimensional data (one or two spatial dimensions, respectively) are discussed.

2.1. Observational results for low degree modes ($\ell < 5$)

The first observations of low degree modes were published by Claverie *et al.* (1979). The observations were obtained with a full disk resonance cell in the absorption line of neutral potassium at 769.9 nm over a total of 627 hours during the three years from 1976–1978. The mean line of sight velocity was determined every 42 seconds. Because the light from the whole disk of the sun was integrated, only low degree modes survived cancellation. Claverie *et al.* identified the strongest peaks in the spectrum as p -modes having between 17 and 29 radial velocity nodes

and degrees 0 and 1. The power spectrum showed a pronounced peak at 5.4 minutes (3.1 mHz) and no modes were visible outside the 2-4 mHz interval. The agreement between power spectra obtained simultaneously at Izana and at Pic Du Midi, which are separated by 2300 km, confirmed the solar origin of the oscillations. The mean frequency spacing between modes with the same ℓ was found to be $135.6 \pm 0.3 \mu\text{Hz}$. Furthermore, the modes were found to be coherent for more than three days ($Q > 800$).

The frequencies of modes with (n, ℓ) and $(n - 1, \ell + 2)$ are nearly coincident (the separation being about $10 \mu\text{Hz}$ for even ℓ and $15 \mu\text{Hz}$ for odd ℓ), and were not resolved by Claverie *et al.* (1979). The individual modes were first separated by Grec *et al.* (1980, 1983) using data obtained in a continuous five day run at the south pole with a total duration of 200 hours observation during the austral summer in December–January of 1979–80. Grec *et al.* used a sodium resonance cell to obtain full disk integrated velocity measurements in the 589.6 nm Na D1 line. The resultant spectrum from 120 hours of continuous observations had significantly better resolution ($2 \mu\text{Hz}$) than that of Claverie *et al.* (1979). Grec *et al.* , found the mean separation between the peaks to be $68 \mu\text{Hz}$, corresponding to $136 \mu\text{Hz}$ separation for modes with the same ℓ . They divided the spectrum into segments of $136 \mu\text{Hz}$ length and averaged the segments together. This process, called superposed frequency analysis, enabled them to identify all modes between degree 0 and 3. The widths of the peaks gave mean damping times of 2 days or Q 's of about 600. Grec *et al.* also looked for the reported 160 minute oscillation using superposed epoch analysis and found it to be consistent in amplitude and extrapolated phase with that reported by Crimea group (Severny *et al.* 1976) and the Stanford groups (Delache and Scherrer 1983). Kuhn *et al.* (1986) do not find any evidence for this or any long period mode in their diameter oscillation measurements. In a second paper, Grec *et al.* (1983) present more complete results from their south pole observations. By using an echelle diagram, they identified the radial order, n , of the modes. The

echelle diagram is obtained by folding the frequency line (modes are attached to the line like beads). A uniform frequency spacing between modes gives a straight line in this diagram. For the sun, the frequency spacing is not quite uniform so they get a curve in the echelle diagram and are able to identify the order of the modes. Their identification agrees with those made by Christensen-Dalsgard *et al.* (1981). By analyzing the time variation of the total power in the five minute range, the authors argue that the modes are randomly and independently excited.

The Birmingham group (Claverie *et al.* 1981b) published the results of their 271 hour data set taken at the Teide observatory on Tenerife using optical resonance scattering in the potassium line. The spectrum shows clearly separated double peaks corresponding to modes of degrees 0 and 2. By superposed frequency spectrum analysis, Claverie *et al.* determined the splitting between different m modes to be $0.75 \mu\text{Hz}$ and interpreted it as due to rotation. As the rotational axis of the sun is nearly perpendicular to the line of sight, in whole disk integrated data like that of Claverie *et al.* (1981b), we expect to see only those modes which correspond to even $(l + m)$, because spherical harmonics of odd $(l + m)$ have odd parity and very nearly cancel out in whole disk integrations. However, Claverie *et al.* saw the $\ell = 2$ peak split into five components and the $\ell = 1$ peak into three components in their superposed frequency analysis, instead of the expected three and two, respectively. Isaak (1982) speculated that the extra components are due to the intense magnetic field in the core which is not aligned with the surface rotation axis (oblique magnetic rotator). He estimates the field strength to be few mega gauss and the rotational period of the core to be about 12 days as had been postulated by Dicke (1979) to account for the 12.2 day periodic component in the Princeton oblateness data (1967,1976). However, Gough (1982) claims that even if the magnetic core exists, it could not explain the observed splitting reported by Claverie *et al.* (1981b) unless some extraordinary coincidences are invoked. Furthermore, Gough pointed out that, until the fine structure seen in the splitting is explained, one cannot be sure

of its rotational origin. Isaak (1986), in his 88 days of data, finds the splitting for $\ell = 1$ mode to be $0.75\mu\text{Hz}$, consistent with his earlier claim (Claverie *et al.* 1981b). But now he finds the $n=16$, $\ell = 1$ mode split into two components rather than the three previously seen and he admits the uncertainty of the triplet structure. The splitting of the low degree modes is very important in determining the rotation in the core. The splitting of $0.75\mu\text{Hz}$ reported by Claverie *et al.* (1981b) and Isaak (1986), implies that the solar core is rotating at twice or more the speed of the surface. However this conclusion cannot be taken as established due to the problems surrounding the structure of the splitting

The first observations of low degree solar oscillations in the total solar irradiance were reported by Woodard and Hudson (1983). Observations were obtained with the Active Cavity Radiometer Irradiance Monitor (ACRIM) onboard the solar maximum satellite for a total of 290 days, from the middle of Feb 1980 until the loss of spacecraft fine pointing control in December, 1980. The strongest p -mode signals amount to variations of a few parts per million in the total irradiance. Woodard and Hudson identify modes of degrees 0, 1, and 2 having between 18 and 24 radial nodes. Superposed frequency analysis did not reveal rotational splitting of the $\ell = 1$ and 2 lines, although they are broader than the $\ell = 0$ line (the resolution of the data is about $0.23 \mu\text{Hz}$). Woodard *et al.* find a systematic frequency difference between their data and that of Claverie *et al.* (1981a,b) and Grec *et al.* (1983). On average, the Birmingham group's frequencies tend to be smaller by $1 \mu\text{Hz}$ and the Nice group's frequencies $1 \mu\text{Hz}$ higher than the ACRIM frequencies. In a second paper, Woodard and Hudson (1984) calculate the frequency splitting for modes of degree 1 and 2 based on the ACRIM data and infers it to be $0.5(+0.2,-0.5) \mu\text{Hz}$.

Scherrer *et al.* (1982,1983) has detected five minute modes with degrees 3 to 5 in the frequency range 2.4–4.3 mHz by subtracting Doppler signals from an inner disk and outer annulus of the solar image. The frequencies of the octupole modes are in good agreement with those obtained from whole disk measurements at the

south pole by Grec *et al.* (1983).

There is some preliminary evidence for a change of the p -mode frequencies with solar cycle phase. In full disk velocity measurements, Van der Raay (1984) finds a decrease in the frequency of the $\ell = 1$ modes by $0.9\mu\text{Hz}$ between 1981 and 1983, and an increase in the frequency of the $\ell = 0$ modes by $1\mu\text{Hz}$ but no change for $\ell = 1$ modes between 1980 and 1981. Woodard and Noyes (1985), using the full disk intensity data from the SMM satellite, find the frequencies of the $\ell = 0$ and $\ell = 1$ modes to decrease by about $0.42\mu\text{Hz}$ from 1981 to 1984. Duvall *et al.* (1987b), compare the frequencies of the low degree modes determined from south pole data with those determined from data taken at Big Bear observatory $3\frac{1}{2}$ years later. The former are systematically lower than the later by about $0.1\mu\text{Hz}$. It is not certain if any of these reported frequency variations are real or whether they result from some artifact of the data analysis. More work is required before a definite conclusion can be drawn.

I conclude this section by summarizing the main observational results for low degree p -modes.

1. The mean frequency separations (mean over the radial order n) between adjacent $\ell = 0$ modes has been reported to be $135.2\pm 0.19\mu\text{Hz}$ by Claverie *et al.* (1981a,b), 135.9 by Grec *et al.* (1983) and $135.05 \pm 0.19\mu\text{Hz}$ by Woodard *et al.* (1983).
2. The frequency differences $\Delta_1 \equiv \nu_{n,0} - \nu_{n-1,2}$ and $\Delta_2 \equiv \nu_{n,1} - \nu_{n-1,3}$ have been measured by several groups and constrain the average second derivative of the sound speed with radius in the solar core (Gough 1983). The mean value of Δ_1 is reported to be $8.3 \pm 0.3\mu\text{Hz}$ by Claverie *et al.* (1981a,b), $9.4\mu\text{Hz}$ by Grec *et al.* (1983) and $9.0 \pm 0.26\mu\text{Hz}$ by Woodard *et al.* (1983). For Δ_2 , we have $15.3\mu\text{Hz}$ by Grec *et al.* (1983) and $15.0\mu\text{Hz}$ by Harvey *et al.* (1984).
3. The rms surface velocity of individual modes at the peak of the power spectrum is about 20 cm/sec and their energies are about 10^{28} ergs (Libbrecht *et al.* 1986).

4. The linewidth is a rapidly increasing function of frequency, being about 30 times greater at 4mHz than 2mHz (Isaak 1986); the Q of modes is 600 or greater.

Observations of Intermediate and High Degree Modes

In 1975 Deubner published the first observations which showed concentrations of power at low wavenumber ($k_h < 1 \text{ Mm}^{-1}$) and thus implied that a substantial part of the solar interior was participating in the oscillations. Deubner also found that the power in the $k-\omega$ diagram was concentrated along ridges which correspond to trapped modes.

Deubner, Ulrich, and Rhodes (1979) observed the p -modes with improved resolution in wavenumber and frequency. Their data was obtained at Sac Peak using the diode array system of the vacuum tower. The solar surface was scanned parallel to the equator from W to E once every 100 seconds. The resultant three dimensional data are averaged along the E–W slit, so only modes with $m = 0$ contributed to the resultant power spectra. Deubner *et al.* made an estimate of large scale, subphotospheric, horizontal velocities from the power spectra. They claimed that, even within a relatively shallow layer of about 20,000 km below the photosphere, the angular speed of solar rotation is not uniform. At a level of $\sim 11,000$ km to 15,000 km below the photosphere, the linear velocity of rotation is 80 ms^{-1} higher than the observed surface velocity. To my knowledge, this result has not been verified by any other group. Measurements of rotational splittings by several groups indicate that the interior angular velocity, Ω , is not very different from the surface value. If anything, there seems to be some decrease in Ω just below the surface.

Duvall and Harvey (1983) published results of low and intermediate degree oscillations observed in the NiI line at 631.4668 nm. They performed E–W averaging but retained spatial information in N–S direction which was covered by 200 pixels. Their observations were taken at a rate of one recording per minute. They were able to identify individual modes in the range of $0 \leq \ell \leq 139$. In the past, the

identification of the radial order, n , for the modes of low degree (the high degree individual modes were not isolated in the past) had been based on a comparison with calculated frequencies. Duvall and Harvey, by clearly identifying ridges in the $k - \omega$ diagram corresponding to oscillations of radial order 2 to 24, could assign a radial order to modes purely on observational grounds. It turned out that their assignments confirmed previous choices for the low degree modes. Duvall and Harvey also confirmed the previous conclusions of Claverie *et al.* (1981a), Woodard and Hudson (1983), and Grec *et al.* (1983), that the low degree modes are coherent for at least 2 days and further report the same coherence for modes of degree at least up to 70.

Several groups have measured rotational splittings for modes ranging in degree from 0 to 200. I summarize below the major efforts in this direction and particularly emphasize the points of disagreement.

Duvall *et al.* (1984a,b) determined the frequency splittings of modes with degrees in the range 0–100 and used this to estimate the internal rotation of the sun. The observations were carried out at Kitt Peak over a seven day period using the same technique described in their 1983 paper, except in this case they averaged the image of the sun in the N–S direction, instead of the E–W, thus retaining only harmonics with $m = \pm\ell$. There is a contribution to the power spectrum from other modes, but it falls off rapidly with increasing $|\ell - |m||$. Using the CLEAN algorithm, Duvall and Harvey identified modes with degrees between 0 to 200 and $m = \pm\ell$ and they calculated the frequency splitting, $\Delta\nu_{nl} = (\nu_{n,l,-l} - \nu_{n,l,l})/2l$. In the final analysis, they discarded two thirds of the modes because their widths were several times larger than the frequency resolution of $0.7 \mu\text{Hz}$ and it was hard to measure their average frequencies accurately. They conclude that at a degree of about 100, the rotational splitting is slightly larger than the equatorial rotational frequency at the surface. At lower degrees, the splitting decreases except in the range of 11–12 where there is a slight increase. Finally, for $\ell < 4$, there is a sharp rise in the

rotational splitting which is accompanied by an equally sharp rise in the error, so the results in this range are very uncertain. The $\ell < 4$ modes penetrate deep in the sun, but, due to the large error associated with their splitting's, it is not clear if the rotation in the core is faster than that at the surface.

In their second paper, Duvall *et al.* (1984b) use three different methods of inverting the frequency splitting reported in Duvall *et al.* (1984a). They conclude that the rotational velocity is essentially constant for $0.6 < r/R_{\odot} < 0.9$, that there is a slight decrease for $0.4 < r/R_{\odot} < 0.6$, and for $0.3 > r/R_{\odot} > 0.09$, the errors are large and the rotation rates are uncertain.

Since $m = \pm\ell$ modes are concentrated near the equator, their frequency splittings are sensitive to the equatorial rotation speed. In order to assess the latitude dependence of the rotation velocity, the frequencies of all $2\ell+1$ modes for each ℓ need to be determined. The result of such a measurement is expressed most conveniently in the terms of the coefficient of either the power series in m , a_{ℓ} , or Legendre polynomial expansion, b_{ℓ} , averaged over the radial order n . Note from equation (5) that the coefficient of the even powers of m or even degree Legendre polynomial must be zero if the internal structure of the sun is independent of the latitude. From the two days continuous data obtained at the south pole Duvall *et al.* (1986) find $b_{\ell}^{(2)}$ to be significantly positive (between 18 to 4 nHz) in the entire range of $20 \leq \ell \leq 98$. The centrifugal distortion of the sun is expected to produce negative value for $b_{\ell}^{(2)}$ (Gough and Taylor, 1984). Duvall *et al.* attribute the positive value of $b_{\ell}^{(2)}$ to differences between the structure of convection zone at the pole and at the equator. Since the magnitude of $b_{\ell}^{(2)}$ is about a thousandth of the intrinsic resolution of the 2 days data (about $5 \mu\text{Hz}$), one might expect, at least naively, that small systematic or non-gaussian errors could easily have introduced uncertainties of order greater than several nHz. The observational results of Brown (1985) from a 5 day run, and Brown and Morrow (1987) from 15 days of data, yield a value for $b_{\ell}^{(2)}$ at most one third that of Duvall *et al.* for $15 \leq \ell \leq 99$.

The $b_\ell^{(3)}$ also contain information on the latitudinal differential rotation. For an angular rotational speed which is constant on spheres, $b_\ell^{(3)}$ and all the higher order coefficients are zero. Duvall *et al.* (1986) find $b_\ell^{(3)}$ to be approximately independent of degree, suggesting that the surface differential rotation persists over the outer half of the sun (modes of $\ell = 20$ and greater penetrate about half the solar radius or less). By contrast, Brown (1985) finds $a_\ell^{(3)}$ decreasing with decreasing ℓ , ($15 \leq \ell \leq 40$), indicating that latitudinal differential rotation is decreasing with increasing depth. Brown and Morrow (1987) find a value for $b_\ell^{(3)}$ between that obtained by Duvall *et al.* (1986) and Brown (1985). Both Duvall *et al.* and Brown *et al.* agree on the qualitative behaviour of $b_\ell^{(1)}$, in other words, on the average behaviour of the rotation speed as a function of depth. Libbrecht's (1986) splitting results are in general agreement with those of Brown (1985), except for the large splitting at $\ell = 11$ found by Brown.

There are very few papers on the observations of the amplitudes and linewidths of modes in spite of their great importance in determining the excitation and damping mechanisms. Libbrecht *et al.* (1986) find the power in the modes to be approximately independent of degree, at least up to $\ell = 100$. Duvall *et al.* (1987a) find the linewidths increasing and the power decreasing with increasing degree.

I conclude this subsection by mentioning a large data base on modal frequencies made available recently by the joint work of the Pasadena and Tucson groups, Duvall *et al.* (1987b). The observations were made at the south pole and the Big Bear Solar Observatory in southern California. This data base contains over a thousand frequencies accurate to 1 part in 10^4 in the range of $5 \leq \ell \leq 99$, making it the best of its kind.

3. Determining Solar Structure from the Observed Frequencies

Prior to the observation of solar oscillations the radius, mass, luminosity and

age of the sun were the only observational constraints on theoretical solar models. The determination of more than a thousand p-mode frequencies to an accuracy of 0.1% has provided many more constraints from which we hope to learn about the solar interior. Towards this end I have already described the results obtained on the internal solar rotation from the m dependent frequency splittings.

There are two basic approaches followed in deducing solar structure from the observed frequencies. The first, based on trial and error, is also known as the forward method. The idea is to determine the effects of changes in various solar parameters or physics such as the elemental abundances, the depth of convection zone, corrections to the equation of state, the outer boundary condition, the poorly known structure of the chromosphere and corona, the interaction of the modes with turbulence or magnetic fields. The second approach, the so called inverse method, starts with the observed frequencies and inverts them to get the solar model or, perhaps more precisely, the sound speed in the solar interior. This method, although very attractive, has not been much used because the inherently incomplete and imperfect data make it very hard to implement. I am familiar only with the attempt of Christensen-Dalsgaard *et al.* (1985) to invert the observed frequencies to obtain the sound speed in the solar interior. This will be discussed later. In what follows, I briefly summarise the effects that various changes in the solar model have on the p-mode eigenfrequencies.

Christensen-Dalsgaard and Gough (1981) compared eigenfrequencies (efs) of low ℓ modes computed for solar models having three different values of Z with the observationally determined frequencies of Claverie *et al.* (1980), Grec *et al.* (1980), and Deubner (1981). They conclude that the observed frequencies are best matched by a solar model having a higher than normal Z ($Z > 0.02$). They find the rms difference between their calculated frequencies and the observed ones (Grec *et al.* 1980) to be $6 \mu\text{Hz}$ for the model with $Z = 0.02$. Moreover, the discrepancy varies systematically with frequency, the theoretical frequencies being too low at low frequency and too

high at high frequency.

Rhodes *et al.* (1981) compared theoretical efs with those measured by Claverie *et al.* (1979) and by Grec *et al.* (1980). Their standard solar model frequencies gave the best fit, although the calculated frequencies were systematically lower than the observed frequencies. Frequencies computed from their low Z solar model fell still farther below the observed frequencies.

Berthomieu *et al.* (1980) calculated solar models with various thicknesses for the convection zone and found good agreement with the observed ridges of Deubner (1975) and Deubner *et al.* (1979) for the computed eigenfrequencies of high degree p -modes from a solar model which has a convection zone depth of 34% of the solar radius. They also conclude that the efs are most strongly influenced by the mixing length while being little influenced by the changes in the atmospheric structure.

Scuflaire, Gabriel, and Noels (1981) also computed a sequence of standard solar envelope models having convection zones of differing thickness and then computed low degree p -mode efs. They found that the mean frequency separation between p -modes of low degree depended on the thickness of the convection zone. By comparing both the mean frequency separation and the absolute frequency with the observations of Claverie *et al.* (1979,1980), they conclude that the convection zone depth of $0.34 R_{\odot}$ provides the best fit. They further add that comparison with the observationally determined frequencies of high degree modes confirms the necessity of a deep convection zone.

Shibahashi and Osaki (1983) report that the calculated efs for low degree modes of a standard solar model are lower by about 5–20 μHz than the observations of Claverie *et al.* (1980), and Grec *et al.* (1983) indicates. For high ℓ 's, the calculated ridges lie slightly above the observed ridges in the $k - w$ diagram. They think that this is due to the shallow convection zone in their standard solar model.

Lubow, Rhodes, and Ulrich (1980) discuss the effect of including Coulomb

corrections to the equation of state, and of including the chromosphere and lower corona in their model and find both these changes act to lower the eigenfrequencies by $\sim 0.5\%$. Changing the outer boundary conditions to include an outgoing wave produces less than a 0.1% change in the frequencies.

Christensen-Dalsgard (1982) reports efs for low degree p and g modes for five different solar models generated with his new stellar evolution code. He calculates the sensitivity of these efs to various uncertainties in the model and concludes that, with the exception of uncertainties introduced by changing the opacity tables he used in computing the models, the uncertainty in the theoretically computed frequencies is less than 0.2% or $5 \mu\text{Hz}$. Changes in the opacity table introduce changes in the frequencies on the order of 0.4% for the high order p -modes.

Ulrich and Rhodes (1983) claim that uncertainty in the efs due to the uncertainties in the interior physics including nuclear cross sections, the equation of state and opacities is about $1 \mu\text{Hz}$. However, they claim that uncertainties in the outer boundary condition, in the physics of the superadiabatic layer of the convection zone and in the structure of solar chromosphere and corona, could cause changes in the frequencies by as much as $10 \mu\text{Hz}$ or 0.3% . They further add that such changes will also change the spacings between the frequencies of successive eigenmodes. Thus, errors in modeling the outer layers could produce agreement for one mode only; the remaining modes would disagree by more than the observational uncertainty of $1 \mu\text{Hz}$. Ulrich and Rhodes also compared the observed low ℓ efs (Claverie *et al.* 1980, Grec *et al.* 1980, Woodard *et al.* 1983) with those computed from their standard solar model and four nonstandard models and conclude that none of them match the observed frequencies. The high Z model improves the frequency agreement but only at the expense of drastically increasing the predicted neutrino count rate to about 15 SNU.

Shibahashi, Noels, and Gabriel (1983) use the interpolated opacity coefficient from the Los Alamos opacity library and also take electrostatic corrections into

account in computing an equilibrium solar model. They find the electrostatic corrections to have a significant effect on the eigenfrequencies of the modes such that the low and high degree efs calculated from their model with $Z \simeq 0.02$ agree considerably better with the observations. The rms discrepancy with the Birmingham frequencies is about $3.18 \mu\text{Hz}$ and with the south pole frequencies about $3.89 \mu\text{Hz}$. For high ℓ , Shibahashi *et al.* find that a model having a deeper convection zone of $2.02 \times 10^5 \text{ km}$, $0.3R_{\odot}$, gives a better fit to the observations. Finally, they conclude that there is still some discrepancy between theory and observation. For low ℓ , the theoretical frequencies of oscillation are slightly lower than the observed ones, while for high ℓ , they are slightly higher.

Noels, Scuflaire, and Gabriel (1984), like Shibahashi *et al.* (1983), include electrostatic corrections in the equation of state, but they find the frequency match to be much worse than claimed earlier by Shibahashi *et al.* (1983). Noels *et al.* find the calculated efs in the 5 minute range to be too small by 5–10 μHz for $\ell \leq 3$ and to be too large by 10–20 μHz for higher ℓ ($\ell = 10$ and 20). The only difference in the above two investigations appears to be in the use of partition functions to calculate electrostatic corrections. Shibahashi *et al.* used the Planck–Larkin partition function whereas Noels *et al.*’s partition function is based on Debye shielding. Noels *et al.* compare their results with those of other groups and claim that differences between numerical codes does not account for more than a 2 μHz frequency change. It is not clear what the reason is for the differences in the frequencies reported in the two papers. Noels *et al.* imply that the difference is due to the partition function. Ulrich (private communication) thinks that the partition function can not cause the reported difference. Instead, he thinks that Shibahashi *et al.* may have problems with their treatment of radiative transfer.

Duvall (1982) argued that, since the position of the upper reflection point is relatively insensitive to the mode and the lower reflection occurs where $\omega = c * k_h$ (c and k_h are local sound speed and horizontal wavenumber respectively), modes

with similar values of ω/k_h will be confined in similar cavities. For all the modes in a given cavity, $n\pi/\omega$, which is approximately the sound travel time across the cavity, should be the same. Thus n/ω should be a function of ω/k_h i.e. $n/\omega = f(\omega/k_h)$. Due to the uncertain outer boundary condition, the above relation is not quite satisfied. Instead, a slightly modified relation of the form $(n+\alpha)/\omega = f(\omega/k_h)$ for $\alpha = 3/2$ is very nearly satisfied for all the modes Duvall observed. Furthermore, modes trapped in the same cavity give essentially the same information. So, all the information contained in the $k-\omega$ diagram is also contained in the curve $(n+1.5)/\omega = f(\omega/k_h)$. This idea was used by Christensen-Dalsgard *et al.* (1985) to determine the sound speed in the solar interior directly from the observed frequencies. They find that, between a radius of 0.4 to $0.9R_\odot$, the difference between the sound speed computed by this technique from the theoretically determined efs and that read off the solar model is less than 1.2%. Probably, the most significant outcome of the inversion of the observed frequencies was the discovery of a change in the curvature of the sound speed at a distance of $0.7R_\odot$. The authors associate this with the bottom of the convection zone and hence conclude that the thickness of the solar convection zone is $0.3R_\odot$.

4. Excitation and Damping of Solar p-modes

Perhaps appropriately, most of the theoretical work on the solar oscillations has been devoted to the understanding of modal frequencies, and the literature on the excitation of the modes is quite sparse. There have been two main mechanisms proposed for the excitation of solar p -modes, the modes are self excited or overstable, or the modes are excited as a result of acoustic emission by turbulent convection.

Several authors have explored the linear stability of the solar p -modes, (Ando and Osaki 1975, Goldreich and Keeley 1977a, Christensen-Dalsgard and Frandsen 1983, Kidman and Cox 1984 and Antia *et al.* 1986). The result seems to depend sensitively on the treatment of the interaction of the oscillation with convection

and radiation. Ando *et al.* and Goldreich *et al.* find the modes to be destabilized by κ mechanism. However, when dissipation of energy due to turbulent viscosity is taken into account (Goldreich and Keeley 1975a), all the modes are found to be stable. Christensen-Dalsgard *et al.* and Kidman *et al.* find the modes to be stable even without inclusion of their interactions with convection. However, Antia *et al.* find modes to be overstable due to a combined destabilizing effect of the κ and convective Cowling mechanisms. So the question of the linear stability of the p -modes is still an open one.

If the oscillations are self excited, their amplitudes will grow exponentially in time until they are choked by some nonlinear process. In the sun, the surface velocity amplitudes of the individual modes are very small, of order 20 cm sec^{-1} near the peak of the power spectrum, compared to the speed of sound which is about 8 km/sec . Therefore, it is reasonable to assume that the nonlinear mechanism which limits the modes amplitudes depends not on the amplitudes of the individual modes but, instead, on the combined amplitudes of all the modes, which is about 0.5 km sec^{-1} . Such a nonlinear process must involve, in some form, the coupling of overstable modes to either stable or propagating waves. The lowest order interactions involve 3-mode couplings. We have carried out detailed calculations of 3-mode couplings in a plane parallel, stratified, isentropic atmosphere. Using the observed energy spectrum, we have calculated the characteristic time for energy transfer due to mode couplings. There is some uncertainty in the final result due to the unknown energies of modes with period ~ 3.5 minutes. But the fundamental mode is found to be damped as a result of mode coupling and hence requires excitation by a mechanism other than the overstability.

The second mechanism of mode excitation is sound emission from turbulent convection (Goldreich and Keeley 1975b). These authors find that, if a mode is excited and damped by quadrupole interactions with turbulent convection, its energy should be approximately equal to the kinetic energy in a resonant eddy at the top

of the convection zone. In a recent investigation Goldreich *et al.* (1987) find that the presence of gravitational field causes the turbulent convection to emit dipole radiation without enhancing its absorption, thus resulting in energy per mode equal to the thermal energy in a resonant eddy. This explains the observed energy in the solar 5-min oscillations.

References

- Ando, H. and Osaki, Y., 1975 *Publ. Astro. Soc. Japan*, **27**, 518.
- Antia, H.M., Chitre, S.M., and Narashima, D., 1986, *Astrophysics and Space Sciences*, **118**, 169.
- Berthomieu, G., Cooper, A.J., Gough, D.O., Osaki, Y., Provost, J., and Rocca, A., 1980, *Lecture Notes in Physics*, Springer Verlag, Berlin, eds. Hill, H.A. and Dziembowski, W., 307.
- Brooks, J.R., Isaak, G.R., and Van der Raay, H.B., 1976, *Nature*, **259**, 92.
- Brown, T.M. and Harrison, R.L., 1980 *Ap. J. Lett.* **236**, L169.
- Brown, T.M., 1985, *Nature*, **317**, 591.
- Brown, T.M., Mihalas, B.W. and Rhodes, E.J., 1986, *Physics of the Sun*, Vol. I, P.A. Sturrock, T.E. Holzer, D.M. Mihalas and R.K. Ulrich (eds.).
- Brown, T.M., Morrow, C.A., 1987, *Ap J.*, **314**, L21.
- Christensen-Dalsgard, J., 1982, *MNRAS* **199**, 735.
- Christensen-Dalsgard, J., 1984, in *Theoretical Problems in Stellar Stability and Pulsations*, M. Gabriel and A. Noels, eds.
- Christensen-Dalsgard, J., Duvall, T.L. Jr., Gough, D.O., Harvey, J.W., and Rhodes, E.J. Jr., 1985, *Nature* **315**, 378.
- Christensen-Dalsgard, J. and Frandsen, S., 1983, *Solar Physics* **82**, 469.
- Christensen-Dalsgard, J. and Gough, D.O., 1981, *AA* **104**, 173.
- Christensen-Dalsgard, J. and Gough, D.O., 1982, *MNRAS* **198**, 141.
- Christensen-Dalsgard, J., Gough, D.O., and Morgan, J.G., 1979, *AA* **73**, 121.
- Christensen-Dalsgard, J., Gough, D.O., Toomre, J., 1985, *Science* **229**, 923.
- Claverie, A., Isaak, G.R., McLeod, C.P., and Van del Raay, H.B., 1979, *Nature* **282**, 591.

- Claverie, A., Isaak, G.R., McLeod, C.P., Van del Raay, H.B., and Roca Cortes, T., 1980, *AA* **91**, L9.
- Claverie, A., Isaak, G.R., McLeod, C.P., Van del Raay, H.B., and Roca Cortes, T., 1981a, *Sol. Phys* **74**, 51.
- Claverie, A., Isaak, G.R., McLeod, C.P., Van del Raay, H.B., and Roca Cortes, T., 1981b, *Nature* **293**, 443.
- Cuypers, J., 1980, *Astron. Astrophys.* **89**, 207.
- Delache, P. and Scherrer, P.H., 1983, *Nature*, **306**, 651.
- Deubner, F.L., 1975, *AA* **44**, 371.
- Deubner, F.L., Ulrich, R.K., and Rhodes, E.J. Jr., 1979, *AA* **72**, 177.
- Deubner, F.L., 1981, *Nature* **290**, 682.
- Deubner, F.L. and Gough, D.O., 1984, *Ann. Rev. Astron. Astrophys.* **22**, 593.
- Dicke, R.H., 1976, *Sol. Phys.* **47**, 475.
- Dicke, R.H., 1979, *New Scientist* **83**, 12.
- Dicke, R.H. and Goldenberg, H.M., 1967, *Phys. Rev. Lett.* **18**, 313.
- Duvall, T.L. Jr., 1982, *Nature* **300**, 242.
- Duvall, T.L. Jr. and Harvey, J.W., 1983, *Nature* **302**, 24.
- Duvall, T.L. Jr. and Harvey, J.W., 1984a, *Nature* **310**, 19.
- Duvall, T.L. Jr., Dziembowski, W.A., Goode, P.R., Gough, D.O., Harvey, J.W., and Leibacher, J.W., 1984b, *Nature* **310**, 22.
- Duvall, T.M., Harvey, J.W. and Pomerantz, M.A. 1986, *Nature*, **321**, 500.
- Duvall, T.M., Harvey, J.W. and Pomerantz, M.A. 1987a, *Proc. of IAU Symposium number 123*, (in press).
- Duvall, T.M., Harvey, J.W., Libbrecht, K.G., Popp, B.D. and Pomerantz, M.A.,

1987b, *BBSO preprint#*, 0270.

- Evans, J.W. and Michard, R., 1962, *Ap. J.* **136**, 493.
- Goldreich, P. and Keeley, D.K., 1977a, *Astrophys. J.* **211**, 934.
- Goldreich, P. and Keeley, D.K., 1977b, *Astrophys. J.* **212**, 243.
- Goldreich, P. and Keeley, D.K., 1977c, *Comm. Astrophys.*, **7**, 35.
- Gough, D.O., 1981, *MNRAS* **196**, 731.
- Gough, D.O., 1982, *Nature* **298**, 350.
- Gough, D.O., 1982, *Pulsation in Classical and Cataclysmic Variable Stars*, eds. Cox, J.P. and Hansen, C.J., 117.
- Gough, D.O., 1983, *Phys. Bull.*, **34**, 502.
- Gough, D.O. and Taylor, P.P., 1984, *Men. Soc. Astron. Ital.*, **55**, 215.
- Grec, G., Fossat, E. and Pomerantz, M., 1980, *Nature* **288**, 541.
- Grec, G., Fossat, E. and Pomerantz, M., 1983, *Sol. Phys.* **82**, 55.
- Grec, G., 1981, These de doctorat, Universite de Nice.
- Harvey, J.W., and Duvall, T.L. Jr., 1984, in *Solar Seismology from Space*, R.K. Ulrich (ed.), 161.
- Isaak, G.R., 1982, *Nature* **296**, 130.
- Isaak, G.R., 1986, in *Seismology of the Sun and the distant stars*, D.O. Gough (ed.), 223.
- Kidman, R.B., and Cox, A.N., 1984, in *Solar Seismology from Space*, R.K. Ulrich (ed.), 317.
- Kuhn, J., Libbrecht, K.G. and Dicke, R.H., 1986, *Nature*, **319**, 128.
- Ledoux, P., 1951, *Ap. J.* **114**, 373.
- Leibacher, J.W. and Stein, R.F., 1971, *Astrophys. Lett.*, **7**, 191.

- Leighton, R.B., Noyes, R.W., and Simon, G.W., 1961, *Ap. J.* **135**, 474.
- Libbrecht, K.G., 1986, *Nature* **319**, 753.
- Libbrecht, K.G., Popp, B.D., Kaufman, J.M. and Penn, M.J., 1986, *Nature* **323**,
235.
- Lubow, S.L., Rhodes, E.J. Jr., and Ulrich, R.K., 1980, In *Lecture Notes in Physics*,
Springer Verlag, Berlin, P300, eds. Hill, H.A. and Dziembowski, W.
- Noels, A., Scufflaire, R., and Gabriel, M., 1984, *AA* **130**, 389.
- Rhodes, E.J. Jr., Ulrich, R.K., and Simon, G.W., 1977, *Ap. J.* **218**, 901.
- Rhodes, E.J. Jr., Ulrich, R.K., Harvey, J.W., and Duvall, T.L. Jr., 1981, *Solar
Instrumentation: What Is Next?*, ed. Dunn, R.B., P37.
- Scherrer, P.H., Wilcox, J.M., Christensen-Dalsgard, J., and Gough, D.O., 1982,
Nature **297**, 312.
- Scherrer, P.H., Wilcox, J.M., Christensen-Dalsgard, J., and Gough, D.O., 1983, *Sol.
Phys.* **82**, 75.
- Scherrer, P.H., 1984, in *Solar Seismology from Space*, R.K. Ulrich (ed.).
- Scufflaire, R., Gabriel, M. and Noels, A., 1981, *AA* **99**, 39.
- Severny, A.B., Kotov, V.A., and Tsap, T.T., 1976, *Nature* **259**, 87.
- Shibahashi, H. and Osaki, Y., 1983, *Sol. Phys.* **82**, 231.
- Shibahashi, H., Noels, A., and Gabriel, M., 1983, *AA* **123**, 283.
- Stein, R.F., and Leibacher, J.W., 1974, *Ann. Rev. Astron. Astrophys.* **12**, 407.
- Ulrich, R.K. and Rhodes, E.J., 1983, *Ap. J.* **265**, 551.
- Ulrich, R.K., 1970, *Ap. J.* **162**, 993.
- Van der Raay, H.B., 1984, in *Theoretical problems in stellar stability and oscillations*,
University of Liege, 215.

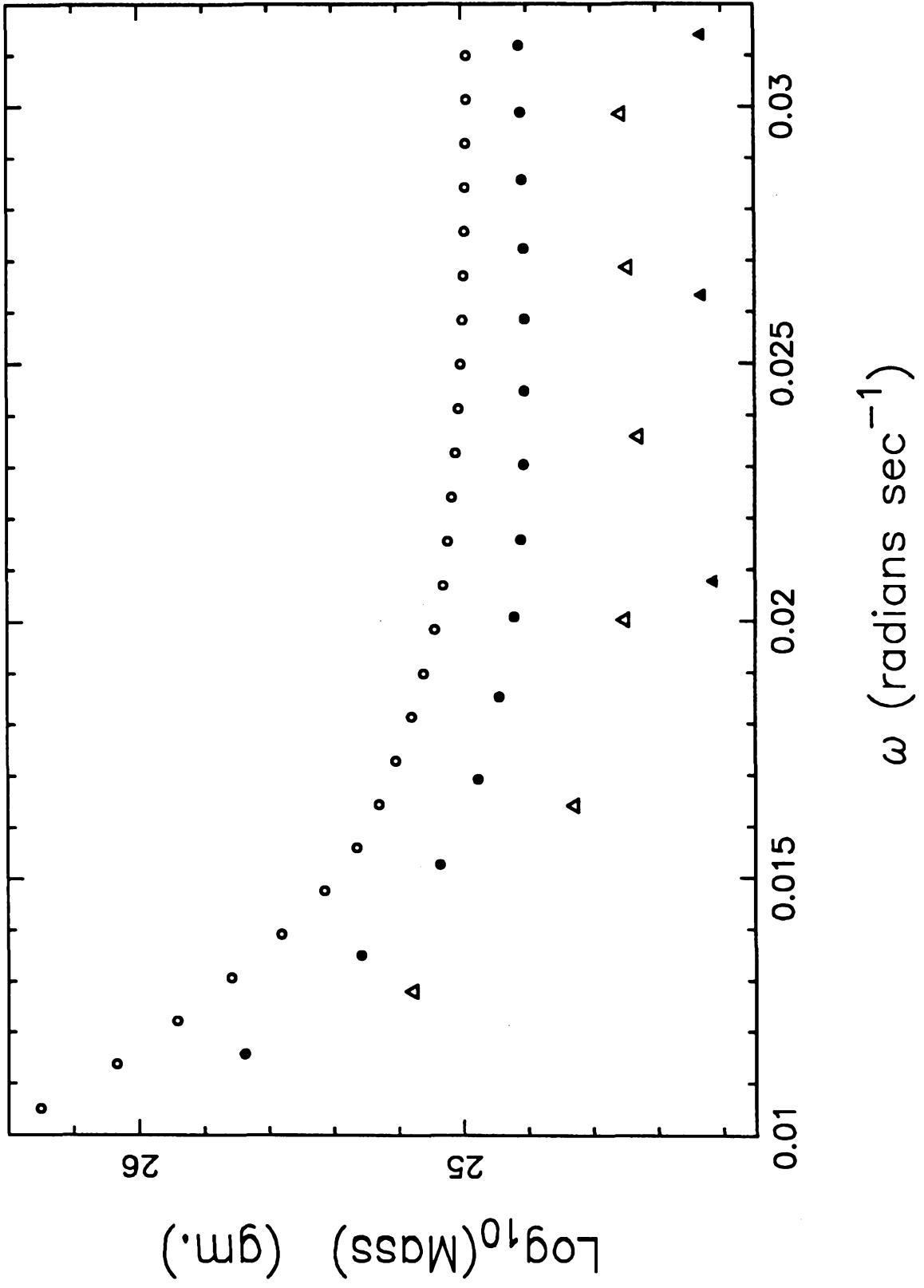
Woodard, M. and Hudson, H.S., 1983, *Nature* **305**, 589.

Woodard, M. and Hudson, H.S., 1984, *Nature* **309**, 530.

Woodard, M. and Noyes, R.W., 1985, *Nature* **318**, 449.

Figure Caption

The logarithmic mass of p-modes in the sun is plotted as a function of their frequencies for four different values of ℓ . The open circle is for $\ell = 0$, the dark circle for $\ell = 100$, the open triangle for $\ell = 400$ and the dark triangle for $\ell = 1000$. All the masses have been calculated at the optical depth $\tau_{5000}=0.05$.



CHAPTER 2

The Interaction of Acoustic Radiation with Turbulence

Submitted to the **Astrophysical Journal**

The Interaction of Acoustic Radiation with Turbulence

Peter Goldreich and Pawan Kumar

California Institute Of Technology, Pasadena California

ABSTRACT

We derive expressions for the spectral emissivity and absorptivity of acoustic radiation by low Mach number, $M \ll 1$, turbulent fluids. The emissivity and absorptivity depend on the manner in which the turbulence is excited. We consider three types of turbulence. The first is free turbulence, that is, turbulence which is not subject to external forces. The second and third examples are special cases of forced turbulence, turbulence maintained by stirring with spoons and turbulent pseudo-convection. Acoustic quadrupoles are the lowest order acoustic multipoles present in free turbulence and they control both its emissivity and absorptivity. Acoustic dipoles are created in forced turbulence and they enhance the acoustic emissivity by M^{-2} compared to that of free turbulence. The acoustic absorptivity of forced turbulence is quite subtle. The absorptivity of turbulence which is maintained by stirring is dominated by acoustic dipoles and exceeds that of free turbulence by M^{-2} . The dipole absorptivity of turbulent pseudo-convection is reduced by M^2 below that of turbulence maintained by stirring. Thus, the absorptivity of turbulent pseudo-convection is no larger than that of free turbulence.

We apply our results to estimate the equilibrium energies of the acoustic modes in a box filled with fluid some of which is turbulent. For both free turbulence and turbulence maintained by stirring, the most highly excited acoustic modes attain energies $E \sim \mathcal{M}v^2$, where \mathcal{M} and v are the typical mass and velocity of an energy bearing eddy. The quality factors, or Q 's, of the modes are larger by M^{-2} in the former case than in the latter. For pseudo-convection, the most energetic acoustic modes have equilibrium energies $E \sim \mathcal{M}c^2$, where c is the sound speed. Their Q 's are comparable to those of modes in equilibrium with free turbulence.

We evaluate the scattering of acoustic radiation by turbulent fluids. For all types of turbulence, the scattering opacity is smaller by M^3 than the absorptive opacity for frequencies near the peak of the acoustic spectrum. Radiation scattered by free turbulence and turbulent pseudo-convection suffers frequency shifts $\Delta\omega \sim \omega$. The frequency shifts are much smaller, $\Delta\omega \sim M\omega$, for radiation scattered by turbulence maintained by stirring.

We investigate the rate at which nonlinear interactions transfer energy among the acoustic modes. If all of the fluid in the box is turbulent, this rate is slower, by M^3 for free turbulence, by M^5 for turbulence maintained by stirring and by M for turbulent pseudo-convection, than the rate at which the individual acoustic modes exchange energy with the turbulence. If only a small portion of the fluid is turbulent, the nonlinear mode interactions can be significant, especially for modes in equilibrium with turbulent pseudo-convection.

Our results have potential applications to the acoustic radiation in regions of extended turbulence which often arise in nature. In particular, they should prove useful in understanding the excitation of solar oscillations.

I. INTRODUCTION

We evaluate all of the important interactions which acoustic radiation has with a turbulent fluid. These include the emission, absorption and scattering of the radiation. Previous theoretical work along these lines has been dominated by the seminal papers of Lighthill (1952, 1954) which focus on the emission of radiation by free turbulence. An excellent review is presented by Crighton (1975).

Our ultimate goal is to relate the excitation of the Sun’s acoustic modes to the turbulence in the solar convection zone. We take a first step in this direction and estimate the excitation of the acoustic modes in a box filled with fluid some of which is turbulent. Existing theory is inadequate for attaining even this more limited objective. It must be extended to include the effects of the forces which maintain the turbulence and to account for the reabsorption of the emitted radiation.

The plan of this paper is as follows. Section II is devoted to a discussion of some preliminary issues which must be addressed before we can proceed to develop formulae for the acoustic emissivity and absorptivity in Sections III and IV. In Section V, we apply these formulae to estimate the equilibrium energies and quality factors of the acoustic modes in a box which contains turbulent fluid. The scattering of acoustic radiation by the turbulent velocity and pressure fluctuations is treated in Section VI. In Section VII, we evaluate the rate at which nonlinear interactions transfer energy among the acoustic modes. There are a number of subtle points involved in determining the acoustic emissivity, and especially the acoustic absorptivity, of a turbulent fluid. We buttress our heuristic arguments on these points by appeal to more rigorous calculations which can be performed on analogous electrodynamic systems in Section VIII. The final Section IX contains a discussion and generalization of our principal results. Detailed calculations of acoustic absorption are relegated to the Appendix.

Our aim is to provide a collection of convenient formulae for later applications.

Accordingly, our calculations are often rather crude and factors of order unity, or even 4π , are ruthlessly discarded.

II. Preliminaries

Description of Turbulence

We adopt a naive picture of homogeneous, isotropic turbulence as a hierarchy of critically damped eddies. The largest, or energy bearing, eddies have linear sizes $\sim H$, velocity magnitudes $\sim v_H$, and lifetimes $\tau_H \sim H/v_H$. For smaller eddies of size $h \lesssim H$, the Kolmogoroff scaling implies $v_h \sim (h/H)^{1/3}v_H$ and $\tau_h \sim (h/H)^{2/3}\tau_H$. The Mach number of the eddies is $M_h \sim v_h/c$, where c is the adiabatic sound speed. We consider subsonic turbulence, $M \equiv M_H \ll 1$. The Reynolds number which characterizes the eddies is $Re_h \sim v_h h/\nu$, where ν is the kinematic molecular viscosity. We assume that $Re \equiv Re_H \gg 1$ so that the effects of viscous dissipation on the acoustic modes may be neglected. The size of the smallest eddies, $h_v \sim H/Re^{3/4}$, which is set by the viscous cutoff to the inertial range, is not pertinent here. The pressure fluctuations associated with eddies of size h have magnitudes $\sim \rho_0 v_h^2$ and vary on a timescale τ_h . The pressure fluctuations are accompanied by small density fluctuations whose magnitudes $\sim \rho_0 M_h^2$. Thus, eddies of size $\sim h$ are strongly coupled to acoustic modes with wavelengths $\lambda \gtrsim h/M_h$.

The picture given above is incomplete since it does not identify the manner in which the turbulence is maintained. We distinguish two general classes of turbulence, free turbulence and forced turbulence.

Free Turbulence

Free turbulence is turbulence which is unaffected by external forces. An isentropic turbulent jet provides an example of free turbulence. Energy is transferred from the bulk motion of the jet to the turbulent eddies by Kelvin-Helmholtz instabilities. The lowest order acoustic multipoles present in free turbulence are quadrupoles (Lighthill 1952).

Forced Turbulence

Our interest is principally in turbulence which is locally maintained by fluctuat-

ing external forces. We are particularly concerned with the external forces that are applied to the fluid since these are responsible for the creation of acoustic dipoles. Next we describe two types of forced turbulence in some detail.

Turbulence Maintained by Stirring

Turbulence may be excited by stirring a fluid with a spoon. The size and velocity of the spoon sets the characteristic size and velocity of the largest eddies. A single spoon would excite at most a few energy bearing eddies. Many spoons, with typical spacing H , would be required to maintain an extended region of homogeneous fluid turbulence. For the moment, we assume that the velocity of each spoon is prescribed. We avoid addressing the practical question of how the spoons' movements are coordinated so as to avoid collisions.

The force exerted on the fluid by each spoon has magnitude $\sim \rho_0 H^2 v_H^2$ and fluctuates on timescale $\sim \tau_H$. In addition, there are smaller, more rapidly fluctuating, components of the force which arise from the spoon's interactions with eddies of size $h \lesssim H$. A typical eddy of size $M^{3/2} H \lesssim h \leq H$ feels a force of magnitude

$$f_h \sim \rho_0 \frac{h^3}{H} v_h^2, \quad (1)$$

which fluctuates on timescale $\sim \tau_h$ (Davies 1970). Equation (1) is easy to derive. We approximate the closest spoon by a planar surface and replace the eddy by a quadrupole source located a distance $d \lesssim H$ from it. In the limit that the planar surface is infinite in extent, the velocity potential follows immediately from the method of images. A simple integration of the perturbation pressure associated with the quadrupole source proves that the net force on the surface vanishes. For a surface of finite horizontal extent $\sim H$, the cancellation of the integrated pressure is incomplete and results in the force given by equation (1). The lower limit, $M^{3/2} H \lesssim h$, insures that the closest spoon to each eddy is in its near field. The forces exerted by spoons on smaller, $h \lesssim M^{3/2} H$, eddies depend on the distances of the eddies

from the nearest spoon. However, these forces are not important for the interaction of the fluid with acoustic radiation and consequently, we ignore them.

Note that f_h is smaller, by a factor $\sim h/H$, than the force associated with the Reynolds stress on eddies of size $\sim h$. Thus, the spoons do not affect the energy cascade in the inertial range and the Kolmogoroff scaling applies to this type of forced turbulence.

Turbulent Pseudo-Convection

Turbulent convection is another type of forced turbulence. The coupling of gravity to the entropy fluctuations within the fluid gives rise to a fluctuating buoyancy force. Turbulent convection is anisotropic, at least on the scale of the energy bearing eddies, since the direction of the gravitational field is singled out. Furthermore, the gravitational field couples to the total density and not just to its fluctuations about the mean. This produces both pressure and density gradients in the fluid. In order to restrict our investigation to the simpler case of homogeneous isotropic turbulence, we imagine a slightly modified version of turbulent convection which we call turbulent pseudo-convection.

The excitation of turbulent pseudo-convection results from the coupling of a spatially uniform external vector field to the concentration of a non-diffusing, scalar contaminant which is randomly added and removed from the fluid on spatial scale $\sim H$ and timescale $\sim \tau_H$. To assure isotropy, the direction of the external force field is also assumed to vary randomly on timescale $\sim \tau_H$. In an obvious analogy with the notation for ordinary convection, we denote the external vector field by $\mathbf{g}(t)$ and the fluctuating component of the concentration of the scalar contaminant by s . The buoyancy force acting on an eddy of size $\sim h$ has a magnitude $\sim g\rho_0 h^3 s_h / c_v$, where c_v would be the specific heat per unit mass at constant volume for true convection. The appropriate scaling law for a scalar contaminant is $s_h \sim (h/H)^{1/3} s_H$ (Tennekes and Lumley 1972). In order to maintain the turbulence, the magnitude of the external force which acts on an energy bearing eddy must be $\sim \rho_0 H^2 v_H^2$. Thus,

$s_H \sim c_v v_H^2 / (gH)$. The scaling relations for v_h and s_h imply that the external force felt by an eddy of size h is

$$f_h \sim \rho_0 \frac{h^{8/3}}{H^{2/3}} v_h^2, \quad (2)$$

which is smaller, by a factor $\sim (h/H)^{2/3}$, than the force due to the Reynolds stress. Thus, the Kolmogoroff scaling applies to turbulent pseudo-convection (Ledoux, Schwarzschild and Spiegel 1961, Goldreich and Keeley 1977a).

Separation of Turbulent and Acoustic Velocity Fields

Both the turbulence and the acoustic radiation are associated with pressure and velocity fields which vary randomly in time and space. The velocity field can be decomposed, globally and uniquely, into a divergence free and a curl free part which we refer to as the shear and the compressive parts of the velocity field. The local values of the shear and compressive components of the velocity field may be expressed in terms of integrals over the distributions of the curl of the vorticity and the divergence of the velocity, respectively (Kraichnan 1953). In the vector Fourier expansion of the velocity field, the shear and compressive parts arise from the components of $\mathbf{v}(\mathbf{k})$ which are perpendicular and parallel to \mathbf{k} .

The turbulent and acoustic parts of the velocity field are included within the shear and compressive parts, respectively; there are shear flows which are not turbulent and compressive flows which not composed of acoustic waves. The turbulent power is spread out over a wide range of k at fixed ω whereas the acoustic power is concentrated at $\omega = ck$. We assume that the energy density in the acoustic radiation is small compared to that in the turbulence. This assumption is justified in Section V.

Acoustic Emissivity and Absorptivity

The emission and absorption of acoustic radiation by a turbulent fluid is expressed in terms of the spectral emissivity, $\epsilon(\omega)$, and absorptivity, $\alpha(\omega)$. The former

is energy emission rate, per unit volume, per unit frequency. The latter is the coefficient which relates the energy absorption rate, per unit volume, per unit frequency, to the spectral energy density.

Classical calculations of emissivity are easier than those of absorptivity because the latter involve the response of the radiator to incident waves. From a quantum mechanical perspective this might, at first, seem paradoxical. After all, given the value of the coefficient of spontaneous emission, the value of the coefficient of stimulated emission follows immediately from the Bose nature of the quanta. Furthermore, once the coefficient of stimulated emission is known, the absorption coefficient is determined by the invariance of the laws of mechanics under time reversal. The paradox is resolved by noting that classical absorption is net absorption, the difference between true absorption and stimulated emission. To calculate the net absorption, we must know how the quantum states of the system are populated. This is obvious for systems which are in thermodynamic equilibrium. However, turbulent fluids are definitely not in thermodynamic equilibrium although they may be in statistically steady states. Turbulence is inherently dissipative and requires a continuous supply of mechanical energy to be kept from decaying.

In our calculations of acoustic emissivity and absorptivity, we treat eddies of size h as though they are particles. Then v_h provides a measure of the relative velocities of neighboring particles of size h . Of course, these particles are advected by the energy bearing eddies so their total velocities are of order v_H .

Electrodynamic Analogues

The interaction of acoustic radiation with a turbulent fluid has many similarities to the interaction of electromagnetic radiation with a system of charged particles. We exploit these analogies to clarify subtle points in Section VIII. We have identified eddies as the basic excitations in a turbulent fluid. Their electrodynamic analogues are charged particles in motion. The sound speed plays a role similar to that of the velocity of light. We use the same symbol, c , for both speeds.

Turbulent pressure fluctuations are to be associated with fluctuating electrostatic fields. The counterpart of acoustic radiation is electromagnetic radiation.

Quadrupoles are the lowest order acoustic multipoles present in free turbulence of a homogeneous fluid; as consequence of the fluid's homogeneity, all eddies behave as though they have the same effective acoustic charge to mass ratios. Thus, the analogous charged particles must all have identical charge to mass ratios. We assume that overall charge neutrality is maintained by a uniform background of opposite sign charge.

Radiative interactions are often easier to analyze in the analogous electrodynamic system than in the original turbulent one. The properties of a charged particle are conceptually simpler than those of an eddy. Moreover, there is a cleaner separation between the radiators and the medium through which the radiation propagates in electrodynamics than in acoustics.

The Acoustic Wave Equation

Following Lighthill (1952), we manipulate the continuity equation and the inviscid momentum equation to yield

$$\left(\frac{\partial^2}{\partial x_i^2} - \frac{1}{c^2} \frac{\partial^2}{\partial t^2} \right) \rho = \frac{1}{c^2} \left(\frac{\partial F_i}{\partial x_i} - \frac{\partial^2 T_{ij}}{\partial x_i \partial x_j} \right), \quad (3)$$

where F_i is the external force per unit volume and

$$T_{ij} \equiv \rho v_i v_j + (p - c^2 \rho) \delta_{ij}. \quad (4)$$

We adopt the adiabatic equation of state $p = \kappa \rho^\gamma$. Thus $c^2 \equiv \gamma p_0 / \rho_0$ and

$$p - c^2 \rho \approx p_0 - c^2 \rho_0 + (\gamma - 1) c^2 \frac{(\rho - \rho_0)^2}{\rho_0}. \quad (5)$$

With different choices for the terms on the right hand side, the wave equation(3) is used to evaluate the emission, the scattering and the 3-mode couplings of acoustic

waves in the Sections which follow.

III. EMISSIVITY

The starting point for the calculation of emissivity is the wave equation (3). For the moment, we do not specify the form of F_i since it depends upon the type of turbulence under consideration. In this application, the velocities which appear in the first term of the tensor T_{ij} come from the turbulent part of the total velocity field. The fluctuations of the second term in T_{ij} are much smaller than those of the first since the fractional density fluctuations are of order M^2 . This allows us to make an immediate simplification and set

$$T_{ij} \approx \rho v_i v_j. \quad (6)$$

We refer to T_{ij} as the Reynolds stress tensor.

The radiation field, $r \gg H/M$, density perturbation produced by the eddies located near the coordinate origin is

$$\rho_{ff}(\mathbf{r}, t) \approx \frac{1}{4\pi c^2 r} \int d\mathbf{x} \left(\frac{n_i}{c} \frac{\partial F_i}{\partial t}(\mathbf{x}, t - r/c) + \frac{n_i n_j}{c^2} \frac{\partial^2 T_{ij}}{\partial t^2}(\mathbf{x}, t - r/c) \right), \quad (7)$$

where $\mathbf{n} = \mathbf{r}/r$. From the angular dependences of the terms in equation (7), we see that the external force and the Reynolds stress are sources of dipole and quadrupole radiation, respectively.

It follows from elementary fluid mechanics that the total radiated acoustic power is

$$P^T \sim \frac{c^3 r^2 \rho_{ff}^2}{\rho_0}. \quad (8)$$

Since different eddies are uncorrelated, their contributions to ρ_{ff} add incoherently and their contributions to P^T simply sum. We separate the contributions to P^T according to eddy size, h . The total power radiated per unit volume by eddies of size $\sim h$, in other words, their emissivity

$$\epsilon_h^T \sim \frac{v_h^2 h F_h^2}{\rho_0 c^3} + \frac{\rho_0 v_h^8}{h c^5}. \quad (9)$$

In writing equation (9), we substitute F_h for the magnitude of F_i and set the magnitude of $T_{ij} \sim \rho_0 v_h^2$.

In all of our examples, the spectral emissivity associated with eddies of size $\sim h$ has a power law dependence on frequency, $\epsilon_h(\omega) \propto \omega^n$, below a cutoff at $\omega \tau_h \sim 1$. Thus, we relate $\epsilon_h(\omega)$ to ϵ_h^T by

$$\epsilon_h(\omega) \sim (\omega \tau_h)^n \tau_h \epsilon_h^T \quad \text{for } \omega \tau_h \lesssim 1. \quad (10)$$

The emissivity of a turbulent fluid is obtained by summing the contributions from eddies in the size range $h_v \lesssim h \lesssim H$. Hence

$$\epsilon(\omega) \sim \int_{h_v}^H \frac{dh}{h} \epsilon_h(\omega), \quad (11)$$

We are now in a position to explicitly evaluate the spectral emissivity of specific types of turbulent fluids.

Free Turbulence

As discussed previously, in the absence of external forces, the emissivity is entirely due to the acoustic quadrupoles associated with the Reynolds stress. We identify two kinds of acoustic quadrupoles. They are easily characterized in limiting cases.

Time dependent, longitudinal quadrupoles, with associated $T_{ii} \sim \rho_0 h^2 v_h^2 f_i(t)$, result from head on collisions between fluid particles moving along coordinate axis i . During a collision the particles' relative velocities reverse on a timescale $\sim \tau_h$. Thus, $f_i(t)$, which is a constant of order unity both before and after the collision, drops to zero within a time interval $\sim \tau_h$ around impact.

Time dependent, lateral quadrupoles, with associated $T_{ij} \sim \rho_0 h^3 v_h^2 f_{ij}(t)$, arise

from deflections suffered in glancing collisions between particles moving in the ij plane. During a collision the directions of the particles' motions change. Hence, the components of $f_{ij}(t)$ have the character of step functions of approximately unit magnitude spread out over time intervals $\sim \tau_h$.

The second time derivative of T_{ij} is the source of the quadrupole radiation field. Thus, the contributions from the longitudinal and lateral quadrupoles to $\epsilon_h(\omega)$ vary as ω^4 and ω^2 below a cutoff at $\omega\tau_h \sim 1$. Since the two kinds of acoustic quadrupoles make comparable contributions to the total emissivity, we take $\epsilon_h(\omega) \propto \omega^2$ for $\omega\tau_h \lesssim 1$. Now, we combine equations (9) and (10) and find

$$\epsilon_h(\omega) \sim \frac{\rho_0 h^2 v_h^5 \omega^2}{c^5}. \quad (12)$$

To evaluate $\epsilon(\omega)$, we substitute the expression for $\epsilon_h(\omega)$ given in equation (12) into equation (11) and use the Kolmogoroff scaling for v_h . This procedure yields

$$\begin{aligned} \epsilon(\omega) &\sim \rho_0 v_H^2 M^5 (\omega\tau_H)^2 \quad \text{for } \omega\tau_H \lesssim 1, \\ \epsilon(\omega) &\sim \rho_0 v_H^2 M^5 (\omega\tau_H)^{-7/2} \quad \text{for } 1 \lesssim \omega\tau_H \lesssim Re^{3/4}, \\ \epsilon(\omega) &\sim 0 \quad \text{for } Re^{3/4} \lesssim \omega\tau_H. \end{aligned} \quad (13)$$

The acoustic efficiency, η , the ratio of the total radiated power to the total power dissipated by the fluid, is given by

$$\eta \sim \frac{H \epsilon^T}{\rho_0 v_H^3} \sim M^5. \quad (14)$$

Forced Turbulence

For both types of forced turbulence, the contribution to the external force per unit volume, F_i , associated with eddies of size $\sim h$ may be approximated by a sequence of independent pulses. Each pulse has magnitude $\sim F_h$, duration $\sim \tau_h$ and spatial correlation length $\sim h$. Since the first time derivative of F_i is the source

of the dipole radiation field, the dipole emissivity must be proportional to ω^2 up to a cutoff at $\omega\tau_h \sim 1$.

Turbulence Maintained by Stirring

We obtain the external force per unit volume, F_h , by dividing the external force per eddy, f_h , given in equation (1) by the eddy volume, h^3 . Thus

$$F_h \sim \frac{\rho_0 v h^2}{H}. \quad (15)$$

for $M^{3/2}H \lesssim h \lesssim H$.

The emissivity due to eddies of size $\sim h$ follows from combining equations (9), (10) and (15). It reads

$$\epsilon_h(\omega) \sim \frac{\rho_0 h^4 v h^3 \omega^2}{H^2 c^3} + \frac{\rho_0 h^2 v h^5 \omega^2}{c^5}. \quad (16)$$

The above expressions reveals that the dipole emission dominates for eddies with $h \gtrsim M^{3/2}H$.

We obtain the spectral emissivity, $\epsilon(\omega)$, by substituting equation (16) into equation (11).

$$\begin{aligned} \epsilon(\omega) &\sim \rho_0 v H^2 M^3 (\omega\tau_H)^2 \quad \text{for } \omega\tau_H \lesssim 1, \\ \epsilon(\omega) &\sim \rho_0 v H^2 M^3 (\omega\tau_H)^{-11/2} \quad \text{for } 1 \lesssim \omega\tau_H \lesssim M^{-1}, \\ \epsilon(\omega) &\sim \rho_0 v H^2 M^5 (\omega\tau_H)^{-7/2} \quad \text{for } M^{-1} \lesssim \omega\tau_H \lesssim Re^{3/4}, \\ \epsilon(\omega) &\sim 0 \quad \text{for } Re^{3/4} \lesssim \omega\tau_H. \end{aligned} \quad (17)$$

The energy bearing eddies are the principal contributors to the emissivity at the low frequency, $\omega\tau_H \lesssim 1$, end of the spectrum. The emissivity is dominated by dipole emission for $\omega\tau_H \lesssim M^{-1}$ and by quadrupole emission at higher frequencies.

The acoustic efficiency is given by

$$\eta \sim \frac{H\epsilon^T}{\rho_0 v_H^3} \sim M^3. \quad (18)$$

It is larger, by a factor $M^{-2} \gg 1$, than that for free turbulence.

Turbulent Pseudo-Convection

The emissivity of this type of forced turbulence differs only slightly from that of the former case. The difference arises because the magnitude of the external force density,

$$F_h \sim \frac{\rho_0 v_h^2}{h^{1/3} H^{2/3}}, \quad (19)$$

obtained by dividing f_h given in equation (2) by h^3 , is larger, by a factor $(H/h)^{1/3}$, than that in the previous case. Allowing for this minor difference, the emissivity of a fluid undergoing turbulent pseudo-convection is obtained by a small modification of equation (17). It reads

$$\begin{aligned} \epsilon(\omega) &\sim \rho_0 v_H^2 M^3 (\omega \tau_H)^2 \quad \text{for } \omega \tau_H \lesssim 1, \\ \epsilon(\omega) &\sim \rho_0 v_H^2 M^3 (\omega \tau_H)^{-9/2} \quad \text{for } 1 \lesssim \omega \tau_H \lesssim M^{-2}, \\ \epsilon(\omega) &\sim \rho_0 v_H^2 M^5 (\omega \tau_H)^{-7/2} \quad \text{for } M^{-2} \lesssim \omega \tau_H \lesssim Re^{3/4}, \\ \epsilon(\omega) &\sim 0 \quad \text{for } Re^{3/4} \lesssim \omega \tau_H. \end{aligned} \quad (20)$$

The stronger dipole emission of the inertial range eddies leads to a shallower drop off of $\epsilon(\omega)$ on the high frequency side of its peak than that given by equation (17) for turbulence maintained by stirring.

The acoustic efficiency,

$$\eta \sim M^3, \quad (21)$$

is the same as that for turbulence maintained by mixing.

IV. ABSORPTIVITY

The time reversal invariance of the laws of mechanics guarantees that turbulent fluids have absorption processes which are the inverses of their emission processes. However, as discussed in Section II, we are concerned with the net absorption rate, the difference between the rates of true absorption and stimulated emission. Even estimating the order of magnitude of this quantity requires considerable care since it depends in subtle ways upon the manner in which the turbulence is excited.

We consider heuristic models for acoustic absorption in free and forced turbulence. More detailed calculations, both classical and quantum mechanical, are presented in the Appendix. We identify three distinct absorption mechanisms. The first mechanism involves quadrupole absorption and operates in all types of turbulence both free and forced. The other two mechanisms involve dipole absorption and act only in the presence of an appropriate external force. Each of our examples of forced turbulence illustrates one of these dipole mechanisms.

As a first step, we concentrate on estimating the spectral absorptivity, $\alpha_h(\omega)$, due to eddies of a particular size, $\sim h$. Then we sum the contributions from eddies of all sizes to obtain the acoustic absorptivity, $\alpha(\omega)$, appropriate to each type of turbulence.

$$\alpha(\omega) \sim \int_{h_v}^H \frac{dh}{h} \alpha_h(\omega). \quad (22)$$

Free Turbulence

To obtain an intuitive understanding of the quadrupole absorption of acoustic radiation, we consider the elastic scattering of two fluid particles of size $\sim h$ in the presence of an acoustic wave. The wave, with pressure amplitude, p_w , frequency, ω , and wave vector, \mathbf{k} , forces a periodic oscillation of the velocity of each particle,

$$\mathbf{v}_w = \frac{\mathbf{k} p_w}{(\omega - \mathbf{k} \cdot \mathbf{v}) \rho_0}, \quad (23)$$

which is superposed on the mean velocity, \mathbf{v} . We view the scattering in the frame which corresponds to the center of mass computed using the colliding particles' mean velocities. At the moment of impact, each particle's velocity will differ from its mean value because of the perturbation by the wave. To a first approximation, at impact, the velocity perturbations of the two particles are equal because, at that time, their spacing is much smaller than one wavelength.

The quadrupole absorption is attributable to the small differential velocity perturbation, $\Delta\mathbf{v}_w$, at the moment of impact which has two separate causes. The mass centers of the particles are separated by a distance $\sim h$ at impact. This accounts for a differential velocity perturbation $\sim (\mathbf{k} \cdot \mathbf{h})\mathbf{v}_w$. Prior to impact, the particles are moving at a mean relative velocity $\Delta\mathbf{v}$, where $|\Delta\mathbf{v}| \sim v_h$. If $\mathbf{k} \cdot \Delta\mathbf{v} \neq 0$, they see the wave at different Doppler shifted frequencies. This gives rise to a differential velocity perturbation $\sim (\mathbf{k} \cdot \Delta\mathbf{v})\mathbf{v}_w/\omega$.

The differential velocity perturbation at impact results in an increase of the mean energy of the particles following impact. The increase comes at the expense of the acoustic wave. This is the physical basis for quadrupole absorption. Part of the energy increase is associated with a random walk of the relative mean velocity with step size $\sim |\Delta\mathbf{v}_w|$. An additional and comparable contribution arises because the instantaneous relative velocity at impact is slightly larger, by an amount $\sim |\Delta\mathbf{v}_w|^2/|\Delta\mathbf{v}|$, than the mean relative velocity; the particles are more likely to collide when the differential velocity perturbation increases their velocity of approach. On average, the mean energy of the particles increases by $\Delta E_a \sim \rho_0 h^3 |\Delta\mathbf{v}_w|^2$ per scattering.

The duration of a collision is $\sim \tau_h$. For $\omega\tau_h \gtrsim 1$, the acoustic absorption is severely diminished because it depends upon the differential velocity perturbation averaged over the finite time of the collision. This implies that the absorption of acoustic energy is substantial only for $\omega\tau_h \lesssim 1$.

We have identified two components of the differential velocity perturbation at

impact, the first due to the separation of the particles and the second to their relative mean velocity. The ratio of the magnitude of the first component to that of the second is $\sim \omega\tau_h$ ¹. Thus, except at the very top of the frequency range $\omega\tau_h \lesssim 1$, it is the mean relative velocity of the colliding fluid particles rather than their separation which is responsible for the major share of the absorptivity. Accordingly, we set $|\Delta\mathbf{v}_w| \sim M_h|\mathbf{v}_w|$ and determine that the absorption of wave energy,

$$\Delta E_a \sim \rho_0 h^3 |\Delta\mathbf{v}_w|^2 \sim \frac{h^3 p_w^2 v_h^2}{\rho_0 c^4}, \quad (24)$$

per scattering. It is then a simple matter to verify that the absorptivity

$$\alpha_h \sim M_h^2 \frac{v_h}{h}, \quad (25)$$

for $\omega\tau_h \lesssim 1$.

The quadrupole contribution to the spectral absorptivity is obtained from equations (22) and (25). It reads,

$$\begin{aligned} \alpha(\omega) &\sim \frac{M^2}{\tau_H} \quad \text{for } \omega\tau_H \lesssim Re^{3/4}, \\ \alpha(\omega) &\sim 0 \quad \text{for } Re^{3/4} \lesssim \omega\tau_H. \end{aligned} \quad (26)$$

Forced Turbulence

Turbulence Maintained by Stirring

The simplest type of absorption is that which occurs during the interaction of turbulent fluid with a spoon. We can understand the absorption process intuitively by analyzing the multiple elastic scattering of a fluid particle by stationary spoons

¹ The two components of the differential velocity perturbation give rise to two components of absorptivity, the first proportional to ω^2 and the second independent of ω . These absorptivity components are intimately related to the two emissivity components identified with longitudinal and lateral quadrupoles in Section III.

in the presence of an acoustic wave. The restriction to stationary spoons is a convenience to assure that all changes in the particle's energy are attributable to the wave.

A single scattering of a particle which represents an eddy of size $\sim h$ lasts for a time $\sim \tau_h$, the lifetime of the eddy. Thus, the absorption of energy from the wave cuts off for $\omega\tau_h \gtrsim 1$. Furthermore, from the force, f_h , that the spoons exert on the eddy (cf. eqn. [1]), it follows that the momentum transfer in a single scattering is limited to a fraction $\sim h/H$ of the eddies typical momentum.

During each scattering, the particle suffers an impulse which partially reverses the component of its incident momentum along \mathbf{s} , the unit normal to the plane of the spoon. Consequently, the magnitude of the particle's mean velocity changes by an amount $\sim (h/H)|\mathbf{s} \cdot \mathbf{v}_w|$, the precise value depending upon the phase of the wave at the time of the scattering. Multiple scatterings lead to a random walk of the particle's mean velocity with an associated increase, per scattering, in the mean kinetic energy. An additional and comparable increase in the mean kinetic energy per scattering arises because, on average, the instantaneous normal component of the velocity at impact exceeds the mean normal velocity. Thus, the average energy absorbed by an eddy during a single scattering is

$$\Delta E_a \sim \frac{h^5 p_w^2}{H^2 \rho_0 c^2}. \quad (27)$$

The angular dependence, $\propto (\mathbf{s} \cdot \mathbf{k})^2$, of the absorbed energy makes manifest the dipole nature of the absorption process. The dipole absorptivity due to eddies of size $\sim h$ then turns out to be

$$\alpha_h(\omega) \sim \frac{\rho_0 c^2 \Delta E_a}{\tau_h h^3 p_w^2} \sim \left(\frac{h}{H}\right)^2 \frac{1}{\tau_h}, \quad (28)$$

for $\omega\tau_h \lesssim 1$ and $h \gtrsim M^{3/2}H$.

The dipole absorptivity due to eddies for which $h \gtrsim M^{3/2}H$ is obtained by

combining equations (22) and (28). Adding this to the quadrupole absorptivity given by equation (26), we arrive at the total absorptivity of turbulence which is maintained by stirring.

$$\begin{aligned}
 \alpha(\omega) &\sim \frac{1}{\tau_H} \quad \text{for } \omega\tau_H \lesssim 1, \\
 \alpha(\omega) &\sim \frac{1}{\omega^2\tau_H^3} \quad \text{for } 1 \lesssim \omega\tau_H \lesssim M^{-1}, \\
 \alpha(\omega) &\sim \frac{M^2}{\tau_H} \quad \text{for } M^{-1} \lesssim \omega\tau_H \lesssim Re^{3/4}, \\
 \alpha(\omega) &\sim 0 \quad \text{for } Re^{3/4} \lesssim \omega\tau_H.
 \end{aligned} \tag{29}$$

The dipole absorption is dominant at low frequencies and the quadrupole absorption at high frequencies. They are of comparable importance for $\omega\tau_H \sim M^{-1}$.

Turbulent Pseudo-Convection

To investigate the nature of the acoustic absorption process in turbulent pseudo convection, we consider the motion of a particle under the combined influence of an acoustic wave and the fluctuating external force. Acting alone, the acoustic wave produces a periodic perturbation velocity, \mathbf{v}_w , given by equation (23). The external force effects random changes of magnitude $|\Delta\mathbf{v}| \sim v_h(h/H)^{2/3}$ in the mean velocity over timescales $\sim \tau_h$. These translate into random variations, $\sim (h/H)^{2/3}M_h\omega$, of the Doppler shifted frequency at which the particle feels the wave. If $\omega\tau_h \gg 1$, the particle's oscillation in the acoustic wave responds adiabatically to the changing Doppler shifted frequency and there is no net acoustic energy absorbed from the wave. However, for $\omega\tau_h \lesssim 1$, the random variations of the Doppler shift result in a random walk of the particle's velocity with step size $\sim (h/H)^{2/3}v_h|\mathbf{v}_w|/c$ ². The average amount of wave energy absorbed by the eddy per impulse is

$$\Delta E_a \sim \rho_0 h^3 |\Delta\mathbf{v}_w|^2 \left(\frac{h}{H}\right)^{4/3} \sim \frac{h^3 p_w^2 v_h^2}{\rho_0 c^4} \left(\frac{h}{H}\right)^{4/3}. \tag{30}$$

² This contribution to the random walk of the velocity is a small addition to that produced directly by the external force.

The magnitude of ΔE_a given by equation (30) is smaller, by the factor $(h/H)^{4/3}$, than ΔE_a given by equation (24) which results from the interactions among eddies. Also, interactions among eddies produce quadrupole absorption whereas the present case involves dipole absorption as indicated by the proportionality of the velocity step to $\mathbf{k} \cdot \Delta \mathbf{v}$.

The preceding argument proves that the dipole absorptivity of eddies is small compared to their quadrupole absorptivity except for the energy bearing eddies where it is comparable. Thus, at all frequencies, the absorptivity of turbulent pseudo-convection is comparable to that of free turbulence and is given by

$$\begin{aligned} \alpha(\omega) &\sim \frac{M^2}{\tau_H} \quad \text{for } \omega\tau_H \lesssim Re^{3/4}, \\ \alpha(\omega) &\sim 0 \quad \text{for } Re^{3/4} \lesssim \omega\tau_H. \end{aligned} \tag{31}$$

Discussion Of Acoustic Absorption

We compare the results of the model calculations of acoustic absorption carried out in the Appendix with the heuristic results deduced in this section in order to better understand the net absorption in the two types of forced turbulence. In the interest of brevity, we focus the discussion on the energy bearing eddies. To connect the calculations carried out in the Appendix to those done in the main body of the text, we associate the particle mass with the eddy mass,

$$m \sim \rho_0 H^3, \tag{32}$$

the plane wave potential with the acoustic wave pressure perturbation divided by the unperturbed density,

$$\Phi \sim \frac{p_w}{\rho_0}, \tag{33}$$

and the magnitude of the impulsive velocity change with the typical velocity of the energy bearing eddies,

$$|\Delta \mathbf{v}| \sim v_H. \quad (34)$$

Classical Calculations

Turbulence Maintained by Stirring

The average wave energy absorbed, ΔE_a , during the reflection of a particle by a wall is given by equation (A10). With the relations expressed in equations (32) and (33), ΔE_a converts to

$$\Delta E_a \sim \frac{H^3 p_w^2}{\rho_0 c^2}, \quad (35)$$

which agrees with equation (27) for $h = H$.

Turbulent Pseudo-Convection

The average wave energy absorbed due to the impulsive acceleration of a particle is given by equation (A24). Here, ΔE_a contains a pair of terms, one of which is proportional to the first, and the other to the second, power of $\mathbf{k} \cdot \Delta \mathbf{v}$. Since the direction of $\Delta \mathbf{v}$ is random, only the latter term is relevant. Applying the conversion relations expressed in equations (32)-(34), we find

$$\Delta E_a \sim \frac{H^3 p_w^2 v_H^2}{\rho_0 c^4}, \quad (36)$$

which is equivalent to equation (30) for $h = H$.

Quantum Mechanical Calculations

We have emphasized that quantum mechanical calculations hold the key to understanding the difference of a factor v_H^2/c^2 between ΔE_a given by equations (27) and (30). This point is amplified further below.

Turbulence Maintained by Stirring

The probability of absorption or stimulated emission during a scattering is given by equation (A36). Application of the conversion factors yields

$$\mathcal{P}_{\pm} \sim \left(\frac{H^3 p_w v_H}{\hbar \omega c} \right)^2 \left(1 \pm \frac{\hbar \omega}{\rho_0 H^3 v_H^2} \right). \quad (37)$$

Turbulent Pseudo-Convection

The absorption and stimulated emission probabilities during an impulse are given by equation (A49). Once again, this equation contains terms which are proportional to both the first and second powers of $\mathbf{k} \cdot \Delta \mathbf{v}$. Dropping the former, since the direction of $\Delta \mathbf{v}$ is random, and applying the conversion factors yields

$$\mathcal{P}_{\pm} \sim \left(\frac{H^3 p_w v_H}{\hbar \omega c} \right)^2 \left(1 \pm \frac{\hbar \omega}{\rho_0 H^3 c^2} \right). \quad (38)$$

Comparison of Transition Probabilities

The absorption and stimulated emission transition probabilities for turbulence maintained by stirring and for turbulent pseudo-convection are given by equations (37) and (38). They are identical except for their second factors which express the fractional differences between the probabilities for absorption and stimulated emission. For macroscopic systems, these fractional differences are extremely small for both types of forced turbulence. However, the fractional difference is larger, by a factor c^2/v_H^2 , for turbulence maintained by stirring than for turbulent pseudo-convection. This accounts for factor c^2/v_H^2 by which the net dipole absorption of the former type of turbulence exceeds that of the latter.

V. AMPLITUDES AND QUALITY FACTORS OF ACOUSTIC MODES

We are concerned with the excitation of the acoustic modes in a rigid box of volume V which is filled with a homogeneous, isentropic fluid. The fluid in a patch of volume fV , $f \leq 1$, is maintained in a steady-state of homogeneous, isotropic turbulence. We assume that the acoustic wavelength at the peak of the acoustic spectrum, $\sim H/M_H$, is smaller than $V^{1/3}$. Thus, even the largest eddies interact with many modes. Also, the energy density of a mode with $\omega\tau_H \gtrsim 1$ has the same average value in the turbulent region as it does in the box as a whole. The mode density, or number of modes per unit frequency interval, is given by

$$\frac{dN}{d\omega} \sim \frac{\omega^2}{c^3} V. \quad (39)$$

The energy in each acoustic mode is determined from

$$E(\omega) \sim \frac{c^3 \epsilon(\omega)}{\omega^2 \alpha(\omega)}, \quad (40)$$

and its quality factor is defined by

$$Q(\omega) \sim \frac{\omega}{\alpha(\omega) f}. \quad (41)$$

Another quantity of interest is the ratio, $R(\omega)$, of the spectral energy density in acoustic part of velocity field to that in the turbulent part. Of course, this ratio is meaningful only in the region where the fluid is turbulent. Using the Kolmogoroff scaling, which implies $v_h(\omega) \sim (\omega\tau_H)^{-1/2} v_H$, it is straightforward to show that

$$R(\omega) \sim \frac{\omega^2 \tau_H \epsilon(\omega)}{\rho_0 v_H^2 \alpha(\omega)} \sim \frac{\omega^4 \tau_H}{c^3 \rho_0 v_H^2} E(\omega). \quad (42)$$

To evaluate $E(\omega)$, $Q(\omega)$ and $R(\omega)$, we apply the expressions deduced in Sections III and IV for $\epsilon(\omega)$ and $\alpha(\omega)$.

Free Turbulence

$$\begin{aligned} E(\omega) &\sim \rho_0 H^3 v_H^2 \quad \text{for } \omega\tau_H \lesssim 1, \\ E(\omega) &\sim \frac{\rho_0 H^3 v_H^2}{(\omega\tau_H)^{11/2}} \quad \text{for } 1 \lesssim \omega\tau_H \lesssim Re^{3/4}. \end{aligned} \quad (43)$$

Equation (43) states that modes with $\omega\tau_H \lesssim 1$ have energies equal to the kinetic energies of the energy bearing eddies and that modes with $1 \lesssim \omega\tau_H \lesssim Re^{3/4}$ have energies equal to the kinetic energies of the eddies with which they resonate.

$$Q(\omega) \sim \frac{\omega\tau_H}{M^2 f} \quad \text{for } \omega\tau_H \lesssim Re^{3/4}. \quad (44)$$

$$R(\omega) \sim \left(\frac{\omega H}{c}\right)^3 \frac{(\omega\tau_H)}{1 + (\omega\tau_H)^{11/2}} \quad \text{for } \omega\tau_H \lesssim Re^{3/4}. \quad (45)$$

Note that the peak value of $R(\omega)$ occurs at $\omega\tau_H \sim 1$ and has magnitude $\sim M^3$.

Forced Turbulence

Turbulence Maintained by Stirring

$$\begin{aligned} E(\omega) &\sim \rho_0 H^3 v_H^2 \quad \text{for } \omega\tau_H \lesssim 1, \\ E(\omega) &\sim \frac{\rho_0 H^3 v_H^2}{(\omega\tau_H)^{11/2}} \quad \text{for } 1 \lesssim \omega\tau_H \lesssim Re^{3/4}. \end{aligned} \quad (46)$$

The energies of acoustic modes in equilibrium with turbulence maintained by stirring are identical to those of modes in equilibrium with free turbulence.

$$\begin{aligned} Q(\omega) &\sim \frac{\omega\tau_H}{f} \quad \text{for } \omega\tau_H \lesssim 1, \\ Q(\omega) &\sim \frac{(\omega\tau_H)^3}{f} \quad \text{for } 1 \lesssim \omega\tau_H \lesssim M^{-1}, \\ Q(\omega) &\sim \frac{\omega\tau_H}{M^2 f} \quad \text{for } M^{-1} \lesssim \omega\tau_H \lesssim Re^{3/4}. \end{aligned} \quad (47)$$

Note that for acoustic modes in equilibrium with turbulence maintained by mixing and $\omega\tau_H \lesssim M^{-1}$, $Q(\omega)$ is lower than it is for free turbulence by the factor $[1 + (\omega\tau_H)^2]M^2 \lesssim 1$.

$$R(\omega) \sim \left(\frac{\omega H}{c}\right)^3 \frac{(\omega \tau_H)}{1 + (\omega \tau_H)^{11/2}} \quad \text{for } \omega \tau_H \lesssim Re^{3/4}. \quad (48)$$

We see that $R(\omega)$ is identical to that for free turbulence.

Turbulent Pseudo-Convection

$$\begin{aligned} E(\omega) &\sim \rho_0 H^3 c^2 \quad \text{for } \omega \tau_H \lesssim 1, \\ E(\omega) &\sim \frac{\rho_0 H^3 c^2}{(\omega \tau_H)^{13/2}} \quad \text{for } 1 \lesssim \omega \tau_H \lesssim M^{-2}, \\ E(\omega) &\sim \frac{\rho_0 H^3 v_H^2}{(\omega \tau_H)^{11/2}} \quad \text{for } M^{-2} \lesssim \omega \tau_H \lesssim Re^{3/4}. \end{aligned} \quad (49)$$

Equation (49) states that the equilibrium energies of modes with $\omega \tau_H \lesssim 1$ are equal to the thermal energies of the largest eddies rather than to their kinetic energies as was the case for free turbulence and turbulence maintained by mixing. The enhancement of mode energy persists up to $\omega \tau_H \sim M^{-2}$.

$$Q(\omega) \sim \frac{\omega \tau_H}{M^2 f} \quad \text{for } \omega \tau_H \lesssim Re^{3/4}. \quad (50)$$

The value of $Q(\omega)$ for modes in equilibrium with turbulent pseudo-convection is identical to that for modes in equilibrium with free turbulence.

$$\begin{aligned} R(\omega) &\sim \frac{M(\omega \tau_H)^4}{1 + (\omega \tau_H)^{13/2}} \quad \text{for } \omega \tau_H \lesssim M^{-2}, \\ R(\omega) &\sim \left(\frac{\omega H}{c}\right)^3 \frac{1}{(\omega \tau_H)^{9/2}} \quad \text{for } M^{-2} \lesssim \omega \tau_H \lesssim Re^{3/4}. \end{aligned} \quad (51)$$

The maximum value attained by $R(\omega) \sim M$ at $\omega \tau_H \sim 1$. This value is larger, by a factor M^{-2} , than that for either free turbulence or for turbulence maintained by mixing. However, even in this case, the equilibrium spectral energy density of the acoustic part of the velocity field is smaller than that of the turbulent part.

Comparison with Previous Results

The literature on the energies of acoustic modes in equilibrium with turbulence is very sparse. We are aware of two earlier contributions. Crow (1967) estimated

the acoustic absorptivity by modeling a turbulent fluid as a viscoelastic medium. He computed the emissivity from Lighthill's theory for free turbulence and reached the conclusion that the equilibrium acoustic energy density is equal to $\sim M^3$ times the turbulent kinetic energy density. Goldreich and Keeley (1977b) considered the excitation of the acoustic modes of the Sun by turbulence in the solar convection zone. They assumed an absorptivity due to turbulent viscosity which they modeled using mixing length theory. These authors failed to recognize the enhanced emissivity of turbulent convection and used Lighthill's emissivity. Consequently, they underestimated the equilibrium mode energies by a factor M^2 .

VI. SCATTERING OF ACOUSTIC WAVES BY TURBULENCE

As acoustic waves propagate through turbulent fluids they are scattered by inhomogeneities associated with velocity and pressure fluctuations. These interactions are described by the acoustic wave equation (3) with the nonlinear source term, S , on the right hand side cast in the form

$$S = -\frac{1}{c^2} \nabla \cdot \left[2\rho_0 \nabla \cdot (\mathbf{v}_w \mathbf{v}) + \nabla \cdot (\rho_w \mathbf{v} \mathbf{v}) + \frac{(\gamma - 1)c^2}{\rho_0} \nabla [\rho_w (\rho - \rho_0)] \right]. \quad (52)$$

We have retained only those source terms which are linear in the acoustic field since we are treating the wave propagation as a perturbation with negligible back reaction. Quantities associated with the acoustic wave are given the subscript w . Because the turbulence is assumed to be of low Mach number and $|\mathbf{v}|/c = O(M)$, $(\rho - \rho_0)/\rho_0 = O(M^2)$, the largest contribution to the scattering is made by the source term which is linear in \mathbf{v} .

The inhomogeneous wave equation is transformed into an integral equation for the scattered density field, $\rho_s(\mathbf{x}, t)$, using the free space Green's function.

$$\rho_s(\mathbf{x}, t) = \frac{1}{4\pi} \int d\mathbf{x}_1 dt_1 \frac{S(\mathbf{x}_1, t_1)}{|\mathbf{x} - \mathbf{x}_1|} \delta \left(t_1 - t + \frac{|\mathbf{x} - \mathbf{x}_1|}{c} \right). \quad (53)$$

The first order scattering is evaluated by substituting for ρ_w and \mathbf{v}_w in S the fields corresponding to the incoming plane wave,

$$\begin{aligned} \rho_w &= \rho_{w_0} \exp(i\mathbf{k} \cdot \mathbf{x} - \omega t), \\ \mathbf{v}_w &= \frac{kc^2}{\rho_0 \omega} \rho_{w_0} \exp(i\mathbf{k} \cdot \mathbf{x} - \omega t). \end{aligned} \quad (54)$$

This procedure yields

$$\rho_s(\mathbf{x}, t) \approx -\frac{\rho_{w_0} \exp(i|\mathbf{k}||\mathbf{x}|)}{2\pi|\mathbf{x}|c^2} \frac{\partial^2}{\partial t^2} \int d\mathbf{x}_1 \left(\frac{\mathbf{n} \cdot \mathbf{k}}{\omega} \right) \mathbf{n} \cdot \mathbf{v} \left(\mathbf{x}_1, t - \frac{|\mathbf{x} - \mathbf{x}_1|}{c} \right) \exp[-i\omega t + i\mathbf{k}' \cdot \mathbf{x}_1], \quad (55)$$

for the largest source terms where

$$\mathbf{k}' \equiv \mathbf{k} - k\mathbf{n} \quad \text{and} \quad \mathbf{n} \equiv \frac{\mathbf{x} - \mathbf{x}_1}{|\mathbf{x} - \mathbf{x}_1|}. \quad (56)$$

We express the scattering efficiency of the turbulent fluid in terms of the scattering cross section associated with a single eddy. Since different eddies are uncorrelated, their scattered waves add incoherently. We restrict our investigation to waves for which $kH \ll 1$. This includes the main portion of the acoustic spectrum associated with the turbulent fluid. For these waves, the scattering is dominated by the velocity fields of the energy bearing eddies. Accordingly, we calculate the scattering by an eddy of size H . Since $kH \ll 1$, the term $\exp(i\mathbf{k}' \cdot \mathbf{x}_1)$ in the integrand is effectively a constant. Therefore, the scattering cross section is

$$\sigma = \int d\Omega \frac{|\mathbf{x}|^2 \langle \rho_s^2 \rangle}{|\rho_w|^2} \sim M^6 H^2 [1 + (\omega\tau_H)^4], \quad (57)$$

where the angular brackets denote an expectation value with respect to the turbulent fluctuations. The scattered flux has a broad angular distribution. The scattering is not elastic but involves a frequency shift, $\Delta\omega \sim v_H/H$, which arises from the finite lifetime of the eddies. While not explicitly stated, the scattering cross section given by equation (57) follows from the detailed treatments of the scattering of sound by turbulence in Kraichnan (1953) and Lighthill (1953).

The scattering length associated with σ is

$$L_s(\omega) \sim \frac{H^3}{\sigma} \sim \frac{H}{M^6 [1 + (\omega\tau_H)^4]}, \quad (58)$$

and holds for $\omega\tau_H \lesssim M^{-1}$. A comparison of L_s from equation (58) with the absorption length, $L_a \equiv c/\alpha(\omega)$, for frequencies near the peak of the acoustic spectrum of turbulent fluids reveals that $L_s \gg L_a$ for all types of turbulence. However, at much higher frequencies the scattering opacity exceeds the absorptive opacity. The

precise frequency at which the two opacities are equal depends upon the type of turbulence.

The scattering length given by equation (58) applies to both free turbulence and turbulent pseudo-convection. For turbulence which is maintained by stirring, the spoons are the dominant scatterers. A standard calculation shows that, in this case,

$$L_s \sim \left(\frac{c}{\omega H} \right)^4 H \sim \frac{H}{(M\omega\tau_H)^4}, \quad (59)$$

which is shorter, by a factor $M^2[1 + (\omega\tau_H)^4]$, than L_s given in equation (58). Moreover, the scattering by spoons is nearly elastic, $\Delta\omega \sim M\omega$.

VII. 3-MODE COUPLINGS

In addition to interacting with the turbulence, the acoustic modes interact with each other. These interactions are described by the nonlinear terms on the right hand side of the acoustic wave equation (3). The forms of these terms imply that the lowest order nonlinear interactions involve triplets of modes. The frequencies and wave vectors of the 3-modes involved in each interaction must satisfy the constraints

$$\omega_a \approx \omega_b + \omega_c \quad \text{and} \quad \mathbf{k}_a = \mathbf{k}_b + \mathbf{k}_c, \quad (60)$$

where we have arbitrarily chosen ω_a to be the highest frequency. These constraints express the conservation of energy and momentum. The frequency matching condition is only approximate since the modes have finite linewidths as a consequence of their interactions with the turbulence and with each other. Taken together, equations (60) imply that the 3-modes must be nearly collinear, a consequence of the homogeneity of the fluid.

The density eigenfunctions of the acoustic modes in a box of volume V are

$$\frac{\rho_{\mathbf{k}}}{\rho_0} = \frac{A(t)}{(2V)^{1/2}} \exp(i\mathbf{k} \cdot \mathbf{x} - i\omega t) + c.c., \quad (61)$$

The velocity eigenfunction, $\mathbf{v}_{\mathbf{k}}/c = \hat{\mathbf{k}}(\rho_{\mathbf{k}}/\rho_0)$. The energy contained in a mode is related to its amplitude by

$$E(\omega) = \rho_0 c^2 |A|^2. \quad (62)$$

To calculate the time evolution of A_a , we substitute the eigenfunctions into the wave equation (3) and use the approximate collinearity of the modes when evaluating the nonlinear terms. We obtain

$$\frac{dA_a}{dt} = \frac{-i\omega_a(\gamma + 1)}{2(2V)^{1/2}} A_b A_c \exp(i\Delta\omega t), \quad (63)$$

where $\Delta\omega = \omega_a - \omega_b - \omega_c$. Similar equations hold for dA_b/dt and dA_c/dt . In arriving at equation (63), we have discarded the second time derivative of A_a which is valid for $\Delta\omega \ll \omega$.

We solve equation (63) perturbatively. The zeroth order amplitude is taken to be the actual amplitude at some arbitrarily chosen time t , $A_a^{(0)} \equiv A_a(t)$. The correction of order n to A_a at time $t + \tau$, $A_a^{(n)}$, is computed with the right hand side of the equation evaluated to order $n - 1$. This procedure yields first and second order corrections at time $t + \tau$:

$$A_a^{(1)} = -\frac{(\gamma + 1)}{2(2V)^{1/2}} \frac{\omega_a}{\Delta\omega} [\exp(i\Delta\omega\tau) - 1] A_b^{(0)} A_c^{(0)} \exp(i\Delta\omega t), \quad (64)$$

$$A_a^{(2)} = \frac{(\gamma + 1)^2}{8V} \frac{\omega_a}{(\Delta\omega)^2} \{[\exp(-i\Delta\omega\tau) - 1] + i\Delta\omega\tau\} A_a^{(0)} \times \left[\omega_b |A_c^{(0)}|^2 + \omega_c |A_b^{(0)}|^2 \right]. \quad (65)$$

We wish to determine the rate of change of the energy, or equivalently, the absolute square amplitude, $|A_a|^2$, in mode a . To this end, we calculate

$$|A_a(t + \tau)|^2 - |A_a(t)|^2 = A_a^{*(0)} A_a^{(1)} + A_a^{(0)} A_a^{*(1)} + |A_a^{(1)}|^2 + A_a^{*(0)} A_a^{(2)} + A_a^{(0)} A_a^{*(2)}. \quad (66)$$

Taking the expectation value (denoted by angular brackets) of the preceding equation yields

$$\langle |A_a(t + \tau)|^2 - |A_a(t)|^2 \rangle = \frac{(\gamma + 1)^2}{2V} \frac{\omega_a}{(\Delta\omega)^2} \sin^2 \left(\frac{\Delta\omega\tau}{2} \right) \left[\omega_a |A_b^{(0)}|^2 |A_c^{(0)}|^2 - \omega_b |A_a^{(0)}|^2 |A_c^{(0)}|^2 - \omega_c |A_a^{(0)}|^2 |A_b^{(0)}|^2 \right]. \quad (67)$$

The first order terms do not contribute to equation (67) since they have zero expectation values. Similar relations govern the evolution of $|A_b|^2$ and $|A_c|^2$.

It is easy to verify that 3-mode couplings imply

$$\langle |A_a(t+\tau)|^2 + |A_b(t+\tau)|^2 + |A_c(t+\tau)|^2 - |A_a(t)|^2 - |A_b(t)|^2 - |A_c(t)|^2 \rangle = 0, \quad (68)$$

and

$$\begin{aligned} \frac{\langle |A_a(t+\tau)|^2 - |A_a(t)|^2 \rangle}{\omega_a} &= - \frac{\langle |A_b(t+\tau)|^2 - |A_b(t)|^2 \rangle}{\omega_b} \\ &= - \frac{\langle |A_c(t+\tau)|^2 - |A_c(t)|^2 \rangle}{\omega_c}. \end{aligned} \quad (69)$$

The former relation expresses energy conservation and the latter states that one phonon of mode a may convert into, or be created from, one phonon from each of modes b and c .

We are now in a position to determine $\langle d|A_{\mathbf{k}}|^2/dt \rangle$ for a mode which is coupled to a continuum of other modes. To do so, we make a number of modifications to equation (67). We replace a, b, c by $\mathbf{k}, \mathbf{k}', \mathbf{k} - \mathbf{k}'$. Then we multiply by the density of states, $V/(2\pi)^3$, and integrate over $d^3\mathbf{k}'$. We take the integral over $k' \equiv |\mathbf{k}'|$ to go from $k/2$ to k to avoid double counting the pairs which interact with mode \mathbf{k} . Since $\sin^2(x)/x^2$ is sharply peaked at $x = 0$, most of the contribution to the integral arises from triplets for which $\Delta\omega \lesssim \pi/\tau$. Taking into account that $\int_{-\infty}^{\infty} dx x^{-2} \sin^2 x = \pi$, we make the replacement

$$\frac{1}{(\Delta\omega)^2} \sin^2 \left(\frac{\Delta\omega\tau}{2} \right) \approx \frac{\pi\tau}{2} \delta(\Delta\omega), \quad (70)$$

where $\Delta\omega \equiv \omega_{\mathbf{k}} - \omega_{\mathbf{k}'} - \omega_{\mathbf{k}-\mathbf{k}'}$. Finally, we integrate over solid angle and eliminate the delta function. These operations determine the portion of $\langle d|A_{\mathbf{k}}|^2/dt \rangle$ which arises from pairs of modes that satisfy $\mathbf{k} = \mathbf{k}' + \mathbf{k}''$. With a few minor changes, we can add the contributions from pairs which satisfy $\mathbf{k} = \mathbf{k}' - \mathbf{k}''$. The resulting expression for $\langle d|A_{\mathbf{k}}|^2/dt \rangle$ reads

$$\begin{aligned} \left\langle \frac{d|A_{\mathbf{k}}|^2}{dt} \right\rangle &= \frac{(\gamma+1)^2 c}{16\pi} \left\{ \int_{k/2}^{\infty} dk' k' |k' - k| [k|A_{k'}|^2 |A_{|k'-k|}|^2 \right. \\ &\quad \left. - k'|A_k|^2 |A_{|k'-k|}|^2 + (k' - k)|A_k|^2 |A_{k'}|^2] \right\}. \end{aligned} \quad (71)$$

The 3-mode couplings tend to equalize the energies of the modes. In all of our examples, the equilibrium modal energies are independent of ω for $\omega\tau_H \lesssim 1$ and decline steeply with ω for $\omega\tau_H \gtrsim 1$. Thus, the nonlinear interactions transfer energy from the lower to the higher frequency modes. To assess the importance of this process, we compare the timescale, τ_{NL} , over which it depletes the energy of a mode having $\omega\tau_H \sim 1$ to $\tau_H Q(\tau_H^{-1})$, where Q given in Section V is associated with turbulent absorption. From equation (71) we obtain

$$\frac{\tau_{NL}}{\tau_H} \sim \frac{\rho_0 H^3 c^2}{M^3 E(\tau_H^{-1})}. \quad (72)$$

Thus, $(\tau_H/\tau_{NL})Q \sim M^3/f$, M^5/f , M^1/f , for free turbulence, turbulence maintained by stirring and turbulent pseudo-convection, respectively. If the fluid is turbulent throughout most of the box, the nonlinear interactions do not play a decisive role in determining the equilibrium mode energies. However, they could be important if the turbulence is confined to a small fraction of the volume. This is particularly so for turbulent pseudo-convection.

VIII. GEDANKAN EXPERIMENTS AND THEIR ELECTRODYNAMIC ANALOGUES

We have taken several uncertain steps in arriving at our conclusions. Perhaps the most serious is our literal acceptance of the simple picture of turbulent fluid motion as a hierarchy of critically damped eddies which obey the Kolmogoroff scaling. To a great extent these oversimplifications are unavoidable since there is no fundamental theory of turbulence on which to base an investigation of the interaction of turbulence with acoustic radiation. For this reason, as much as we believe the validity of our results, they must be regarded as tentative.

Below we describe three gedanken experiments which could, at least in principle, serve to test the theoretical conclusions which we have reached. Some day these experiments may be simulated by hydrodynamical computations performed with the aid of a supercomputer. However, this day is probably well in the future. Meanwhile, these gedanken experiments serve a very useful purpose. For each, we can propose an electrodynamic analogue which can be subjected to detailed analysis. The more rigorous analysis of the analogue electrodynamic experiment serves to enhance the plausibility of our hydrodynamical conclusions. Actually, we never really bother to carry through the analysis of these electrodynamic experiments. Rather, we assume that the results we state for each of them are sufficiently obvious that the reader needs no further demonstration of their validity.

In all our electrodynamic experiments, electrons play the role of turbulent eddies. Where needed, it is implicitly assumed that there is a smooth background of positive charge to maintain overall charge neutrality. For simplicity, we treat only the energy bearing eddies and neglect the smaller eddies of the inertial range. Eddies are critically damped in the Kolmogoroff picture of turbulence. Therefore, we assume that there is of order one electron per Debye sphere so that the electron-electron collision time is comparable to the time an electron takes to move the interparticle distance. Moreover, we imagine that collisions between electrons are

substantially inelastic. In this manner, we simulate the inelastic interactions among eddies which are responsible for the turbulent cascade. The condition that the interelectron distance be of order the Debye length leads to a relation between the mass, m , the charge, e , the number density, n , and the mean square velocity, v^2 , of the electrons which we write in the form

$$e^2 \sim \frac{mv^2}{n^{1/3}}. \quad (73)$$

This relation is used to simplify the formulae which pertain to the analogue electrodynamic experiments.

There is one detail in which the properties of the acoustic and the electrodynamic radiators differ. Each multipole radiation field is proportional to one order higher time derivative of the relevant multipole moment in the acoustic case than in the electrodynamic case. Thus, at low frequency, the acoustic emissivity is proportional to ω^2 whereas the electrodynamic emissivity is independent of ω . By restricting our comparisons of spectral emissivity and absorptivity and energy per mode to frequencies near the peak of the equilibrium spectra, we avoid the complications introduced by this detail.

Free Turbulence

A region of turbulent fluid is maintained in an interaction region where laminar jets which enter through several small holes in the sides of the box intersect and become turbulent. The jets have diameters of order H and speeds of order v_H . The return flow exits through many other holes in the box at speeds $\ll v_H$. For modes whose wavelengths are large compared to the hole diameters, the loss of acoustic energy due to the holes is negligible and may be ignored. It is important that the interaction region of turbulent fluid be confined to the interior of the box since otherwise acoustic dipoles would be created by the forces exerted on eddies by the walls.

In the electrodynamic analogue experiment, electron beams replace the laminar jets. The electrons suffer Coulomb scatterings in the interaction region and, when doing so, emit and absorb electromagnetic radiation by the quadrupole process. We assume that each electron is flushed out of the box after making at most a few collisions. A little thought convinces one that the electromagnetic modes come into equipartition with the electrons. That is, at equilibrium, the energy per mode $\sim mv^2$.

Application of the standard expressions for the emission and absorption of quadrupole radiation during electron-electron collisions yields

$$\epsilon(\omega_p) \sim n^{4/3} e^2 \left(\frac{v}{c}\right)^5 \sim nmv^2 \left(\frac{v}{c}\right)^5. \quad (74)$$

$$\alpha(\omega_p) \sim \frac{n^{2/3} e^2 v}{mc^2} \sim n^{1/3} v \left(\frac{v}{c}\right)^2. \quad (75)$$

We use equation (73) to obtain the final forms of the expressions for $\epsilon(\omega_p)$ and $\alpha(\omega_p)$. With the replacement of $n^{1/3}$ by H^{-1} , these reduce to the corresponding acoustic results given in equations (13) and (26).

Forced Turbulence

Turbulence Maintained by Stirring

Here the turbulence is excited by stirring with spoons which transmit velocity dependent impulses to the fluid. In a statistically steady state, the energy put into the fluid by the spoons balances that which is dissipated into heat at the bottom end of the turbulent cascade.

In the electrodynamic analogue experiment, the spoons are replaced by heavy, positively charged, particles, for example, protons. The protons transmit velocity dependent impulses to the electrons they scatter. Since each spoon is represented by a proton, there must be of order one proton per Debye sphere. Thus the proton density is equal to the electron density. We imagine that the protons maintain a

constant temperature by interacting with some external heat bath. Since collisions between electrons are assumed to be inelastic³, the electron temperature is lower than the proton temperature. We assume that the protons are so heavy that they do not couple significantly to the electromagnetic radiation. The electrons emit and absorb electromagnetic radiation during their collisions with the protons principally by the dipole process. The quadrupole emission and absorption which accompanies electron-electron collisions is less important and may be neglected in comparison. It is clear that the equilibrium energies of the electromagnetic modes must again be $\sim mv^2$. However, energy is transferred between the electrons and the electromagnetic modes more rapidly in this case than in the previous one.

The calculation of $\epsilon(\omega_p)$ and $\alpha(\omega_p)$ again follows from standard formulae. We find

$$\epsilon(\omega_p) \sim n^{4/3} e^2 \left(\frac{v}{c}\right)^3 \sim nmv^2 \left(\frac{v}{c}\right)^3. \quad (76)$$

$$\alpha(\omega_p) \sim \frac{n^{2/3} e^2}{mv} \sim n^{1/3} v. \quad (77)$$

Once again, the final versions of the formulae for $\epsilon(\omega_p)$ and $\alpha(\omega_p)$ are in accord with their acoustic counterparts, here given by equations (17) and (29).

Turbulent Pseudo-Convection

In this case, the energy input to the turbulence comes from the external field which couples to a scalar contaminant whose concentration fluctuates in both space and time. In true convection, the external field has a fixed direction. We have chosen to restrict our attention to isotropic turbulence. Hence, we take the direction of the external field to vary in time. The crucial difference between this example and the previous one is that here the impulses transmitted by the external force are independent of the fluid velocity.

³ We assume that proton-proton and proton-electron collisions are elastic

The electrodynamic analogue experiment involves a box within which there is a region filled with electrons and a smooth compensating positive charge. It is assumed that each electron carries some scalar contaminant which is randomly added and removed from it on timescale τ . The scalar contaminant couples to an spatially uniform but temporarily varying external field resulting in the impulsive acceleration of the electrons. The external field supplies energy to the system which is dissipated by the inelastic electron-electron collisions. The electrons emit and absorb electromagnetic radiation by the dipole process while they are being accelerated by the external field. This emission is much greater than the quadrupole emission which occurs during collisions between electrons. However, the net dipole absorption which takes place during the acceleration is only comparable to the quadrupole absorption during electron-electron collisions. This is the result of the near cancellation of the true dipole absorption by stimulated dipole emission. Thus, in this case, the equilibrium energies of the electromagnetic modes are $\sim mc^2$ instead of $\sim mv^2$ as in the previous two examples.

Once again, the calculation of $\epsilon(\omega_p)$ is straightforward. The only new twist is that the external force must have magnitude $\sim n^{1/3}mv^2/e \sim n^{1/2}m^{1/2}v$ so that it can maintain the energies of the electrons against the losses suffered during inelastic collisions. The determination of $\alpha(\omega_p)$ is more difficult. It requires calculations comparable to those presented in the Appendix for the analogous acoustic case. We have carried out both classical and quantum mechanical calculations to satisfy ourselves that the electrodynamic derivations do indeed resemble the acoustic ones. In fact, the only small differences are attributable to relativistic effects in the electrodynamic calculations. The upshot is that

$$\epsilon(\omega_p) \sim n^{4/3}e^2 \left(\frac{v}{c}\right)^5 \sim nmv^2 \left(\frac{v}{c}\right)^5. \quad (78)$$

$$\alpha(\omega_p) \sim \frac{n^{2/3}e^2}{mv} \sim n^{1/3}v. \quad (79)$$

A comparison of equations (78) and (79) with equations (20) and (31) confirms the agreement between the electrodynamic and the acoustic results.

IX. DISCUSSION

Our main results are the expressions for the energies of acoustic modes in equilibrium with turbulence of different kinds. For free turbulence and turbulence maintained by stirring, the most highly excited modes come into equipartition with the energy bearing turbulent eddies. The mode energies are of order

$$E \sim \mathcal{M}v^2, \quad (80)$$

where $\mathcal{M} \sim \rho_0 H^3$ is the mass associated with an energy bearing eddy. For turbulent pseudo-convection, and by extension for turbulent convection, the most highly excited modes have energies comparable to the thermal energies contained in a volume equal to that of an energy bearing eddy. Thus

$$E \sim \mathcal{M}c^2. \quad (81)$$

The latter is our most surprising and important result. At first sight, it appears to imply that, for turbulent pseudo-convection, the equilibrium energy of the most energetic modes is independent of the magnitude of the turbulent velocity. This is a false impression. For a given mode, that is, for fixed ω_p , the equilibrium energy per mode is proportional to v_H^3 since $\mathcal{M} \sim \rho_0(v_H/\omega_p)^3$. In making this statement, we are comparing a sequence of experiments for which τ_H is constant and v_H and hence H varies.

We have identified eddies as the basic excitations of turbulent fluids. Turbulence must be continuously excited or else it will decay. The energy supplied to the energy bearing eddies cascades to smaller eddies and is ultimately dissipated into heat by molecular viscosity. The kinetic energy per eddy is $E_h \sim \rho_0 h^3 v_h^2$ and, accordingly to the Kolmogoroff scaling, varies with h as $h^{11/3}$. Thus, there is no equipartition of energy between eddies of different sizes. However, in equilibrium, acoustic modes which interact with either free turbulence or turbulence maintained

by stirring do reach equipartition of energy with the eddies to which they couple most strongly. This conclusion does not hold for acoustic modes in equilibrium with turbulent pseudo-convection. How are these results to be understood?

The conclusions regarding modes in equilibrium with either free turbulence or turbulence maintained by stirring are an unavoidable consequence of our model of eddies. They are taken to be particles which scatter each other in free turbulence and are scattered by spoons in turbulence maintained by stirring. The scattering events are treated as elastic. Elementary thermodynamic considerations then demand that

$$\frac{\epsilon_h(\omega)}{\alpha_h(\omega)} \sim \rho_0 h^3 v_h^2 \frac{\omega^2}{c^3} \quad \text{for } \omega\tau_h \lesssim 1. \quad (82)$$

This relation states that acoustic modes in equilibrium with eddies of size $\sim h$ have a Rayleigh-Jeans spectrum with energy per mode equal to the kinetic energy of the eddies. It is easy to verify that the expressions for $\epsilon_h(\omega)$ and $\alpha_h(\omega)$ given in Sections III and IV for free turbulence and turbulence maintained by mixing do satisfy equation (82). We believe that the model we have adopted for the eddies captures the essence of their radiative interactions so that the conclusions regarding equipartition are not only an inevitable consequence of it but are also correct.

The preceding discussion serves to highlight the special character of the interaction of acoustic modes with turbulent pseudo-convection. In this case, the equilibrium mode energies exceed the equipartition values, at least near the peak of the acoustic spectrum. The calculations in the Section IV and the Appendix show that acoustic dipoles created by the external force enhance the emissivity but not the absorptivity of turbulent pseudo-convection relative to that of free turbulence. The quantum mechanical calculations provide additional insights. They establish that both the true absorption and the stimulated emission rates for turbulent pseudo-convection are nearly the same as those for turbulence maintained by

mixing. However, the small fractional differences between the rates of true absorption and stimulated emission are of order $\hbar\omega/(\rho_0 H^3 c^2)$ in the former case compared to $\hbar\omega/(\rho_0 H^3 v_H^2)$ in the latter. This subtle difference accounts for the reduction, by a factor M^2 , of the dipole absorptivity of turbulent pseudo-convection with respect to that of turbulence maintained by stirring.

The higher than equipartition equilibrium energies of acoustic modes which interact with turbulent pseudo-convection does not signal a conflict with thermodynamics. The external force acting on the eddies tends, on average, to increase their kinetic energies. Thus, we cannot appeal to thermodynamic arguments to relate the absorptivity to the emissivity. However, this is not quite the entire story. In turbulence maintained by mixing, the spoons also do net work on the eddies and, in this case, the equilibrium mode energies correspond to equipartition. The crucial distinction may be traced to the *explicit* position dependence of the external force.

In turbulence maintained by mixing, the external force which acts on a fluid particle depends on its position with respect to the spoons. In scattering a particle, a spoon transmits an impulse which depends upon the particle's velocity. In the presence of an acoustic wave, the impulse depends upon the velocity perturbation forced by the wave. The *explicit* position dependence of the external force gives rise to the velocity dependence of the impulse which is responsible for the dipole absorption of the wave energy as described heuristically in Section IV.

In turbulent pseudo-convection, the external force which acts on a fluid particle is a function of the instantaneous value of the scalar contaminant which it carries. There is no explicit position dependence of the external force. The impulses received by the particle are independent of its velocity. Thus, the principal mechanism responsible for the dipole absorption of wave energy in turbulence maintained by mixing is absent. All that remains is the reduced dipole absorption associated with changes in the Doppler shifted wave frequency as discussed in Section IV.

Acknowledgments

Some of the research reported in this paper was done while P.G. held visiting appointments at the Canadian Institute for Theoretical Astronomy in Toronto and at the Institute for Theoretical Physics in Santa Barabara. He thanks the directors and their staffs for making these visits so pleasant. Financial support was provided by the NSF through grant AST-861299.

REFERENCES

- Crighton, D.G., 1975, *Prog. Aerospace Sci.*, **16**, 31.
- Crow, S.C., 1967, *Phys. Fluids*, **10**, 1587.
- Davies, H.G., 1970, *J. Fluid Mechanics*, **43**, 597.
- Goldreich, P. and Keeley, D.K., 1977a, *Ap. J.*, **211**, 934.
- Goldreich, P. and Keeley, D.K., 1977b, *Ap. J.*, **212**, 243.
- Kraichnan, R.H., 1953, *J. Acoust. Soc. Amer.*, **25**, 1096.
- Ledoux, P., Schwarzschild, M. and Spiegel, E.A., 1961, *Ap. J.*, **133**, 184.
- Lighthill, M.J., 1952, *Proc. Roy. Soc.*, A **211**, 564.
- Lighthill, M.J., 1953, *Proc. Camb. Phil. Soc.*, **49**, 531.
- Lighthill, M.J., 1954, *Proc. Roy. Soc.*, A **222**, 1.
- Tennekes, H. and Lumley, J.L., 1972, *A First Course In Turbulence* (Cambridge: MIT Press).

APPENDIX

CLASSICAL CALCULATIONS OF ACOUSTIC ABSORPTION

Case A. Turbulence Maintained by Stirring

To model the absorption of acoustic radiation due to the interaction of an eddy with a spoon, we consider the motion of a particle of mass m under the influence of a plane wave potential $\Phi = \Phi_0 \sin(\omega t - \mathbf{k} \cdot \mathbf{x})$ in the presence of a stationary wall. The particle and wall represent the eddy and spoon. The choice of a stationary wall implies that our calculations are made in the rest frame of the spoon. The z axis is taken to be perpendicular to the wall. We assume that the particle is specularly reflected by the wall.

We denote the particle's position at time $t = 0$ by \mathbf{x}_0 and the collision time by $t = \tau$, where $\omega\tau \gg 1$. For $t \neq \tau$, the equation of motion reads

$$\frac{d^2\mathbf{x}}{dt^2} = \mathbf{k}\Phi_0 \cos(\omega t - \mathbf{k} \cdot \mathbf{x}). \quad (\text{A1})$$

The time dependent potential, Φ , induces a periodic variation of the particle's energy. We define the mean energy to be the time average of the instantaneous energy over one wave cycle. Since the wall is stationary, it does no work on the particle. Thus, the change in the mean energy upon reflection is equal to the energy absorbed from the wave.

We solve equation (A1) perturbatively to first order with respect to the parameter $\Phi_0/c^2 \ll 1$, where $c \equiv \omega/k$. The mean velocity jumps from \mathbf{v}_- before $t = \tau$ to \mathbf{v}_+ after $t = \tau$. We determine this jump by applying the reflection condition, $v_z(\tau_+) = -v_z(\tau_-)$, to the instantaneous velocity just before and just after $t = \tau$.

The first order change in velocity, \mathbf{v}_1 , is obtained by integrating the equation of motion with \mathbf{x} in the wave potential set equal to $\mathbf{x}(t) = \mathbf{x}_0 + \mathbf{v}_-t$ for $t < \tau$ and $\mathbf{x}(t) = \mathbf{x}_0 + \mathbf{v}_-\tau + \mathbf{v}_+(t - \tau)$ for $t > \tau$. This procedure yields

$$\mathbf{v}_1 = \frac{\mathbf{k}\Phi_0}{\omega_-} \sin \theta_-, \quad (\text{A2})$$

for $t < \tau$ and

$$\mathbf{v}_1 = \frac{\mathbf{k}\Phi_0}{\omega_+} \sin \theta_+, \quad (\text{A3})$$

for $t > \tau$. Here we have defined the shorthand notation

$$\theta_0 \equiv -\mathbf{k} \cdot \mathbf{x}_0, \quad \theta_- \equiv \omega_- t + \theta_0, \quad (\text{A4})$$

$$\theta_\tau \equiv \omega_- \tau + \theta_0, \quad \theta_+ \equiv \theta_\tau + \omega_+(t - \tau),$$

with

$$\omega_\pm \equiv \omega - \mathbf{k} \cdot \mathbf{v}_\pm. \quad (\text{A5})$$

The velocity matching condition at $t = \tau$ is expressed by

$$\mathbf{v}_+ + \frac{\mathbf{k}\Phi_0}{\omega_+} \sin \theta_\tau = (1 - 2\hat{\mathbf{z}}\hat{\mathbf{z}} \cdot) \left(\mathbf{v}_- + \frac{\mathbf{k}\Phi_0}{\omega_-} \sin \theta_\tau \right). \quad (\text{A6})$$

To lowest order in v/c , this yields

$$\mathbf{v}_+ = \mathbf{v}_- - 2\hat{\mathbf{z}}\hat{\mathbf{z}} \cdot \left(\mathbf{v}_- + \frac{\mathbf{k}\Phi_0}{\omega} \sin \theta_\tau \right). \quad (\text{A7})$$

Note that \mathbf{v}_+ depends upon the value of the wave's phase at the instant of reflection. This implies that the change in mean energy, and hence, the energy absorbed from the wave, also depends on θ_τ . Our interest is in the average energy absorbed per collision. To obtain this quantity, we must average the absorbed energy over z_0 , or equivalently, over θ_τ . The appropriate probability density to use in the latter average is

$$\frac{dP(\theta_\tau)}{d\theta_\tau} = \frac{1}{2\pi} \left(1 + \frac{k_z \Phi_0}{\omega |\hat{\mathbf{z}} \cdot \mathbf{v}_-|} \sin \theta_\tau \right), \quad (\text{A8})$$

because, per unit time, the collision probability is proportional to the instantaneous value of velocity component along the direction of the wall's normal. We denote these averages by angular brackets. To lowest order in Φ_0 , we have

$$\langle \sin \theta_\tau \rangle = \frac{k_z \Phi_0}{2\omega v_z} \quad \text{and} \quad \langle \sin^2 \theta_\tau \rangle = \frac{1}{2}. \quad (\text{A9})$$

Armed with these averages, it is a simple matter to determine the average change in the particle's mean energy and thus the average wave energy absorbed per collision, ΔE_a . We find

$$\Delta E_a = \frac{2mk_z^2 \Phi_0^2}{\omega^2}. \quad (\text{A10})$$

Only the change in kinetic energy contributes to ΔE_a . The change in potential energy is of higher order in $v/c \ll 1$.

Case B. Pseudo-Convection

To model the absorption of acoustic radiation, we again consider particle motion in the plane wave potential Φ . However, in this case, the particle is acted upon by a position independent impulsive external acceleration $\mathbf{a}(t) = \Delta \mathbf{v} \delta(t - \tau)$, where $\Delta \mathbf{v}$ is constant in both space and in time. The new equation of motion reads,

$$\frac{d^2 \mathbf{x}}{dt^2} = \mathbf{k} \Phi_0 \cos(\omega t - \mathbf{k} \cdot \mathbf{x}) + \Delta \mathbf{v} \delta(t - \tau), \quad (\text{A11})$$

where, here and throughout this subsection, we adopt the notation defined in the previous subsection. We solve equation (A11) perturbatively to second order with respect to the parameter $\Phi_0/c^2 \ll 1$. We choose $\omega\tau \gg 1$ and denote the particle's position at time $t = 0$ by \mathbf{x}_0 . To simplify the algebra, we set the mean velocity $\mathbf{v}_- = 0$. Following the impulse at $t = \tau$, the mean velocity changes to \mathbf{v}_+ . We apply the jump condition to the instantaneous velocity just before and just after

$t = \tau$ and then solve for the mean velocity \mathbf{v}_+ . Once this task is completed, it is a straightforward matter to compute the absorption of wave energy by the particle.

For $t < \tau$, the first order variations in velocity, \mathbf{v}_1 , and displacement, \mathbf{x}_1 , are obtained by successive integrations of the equation of motion with \mathbf{x} set to \mathbf{x}_0 in the wave potential. We find

$$\mathbf{v}_1 = \frac{\mathbf{k}\Phi_0}{\omega} \sin \theta_-, \quad (\text{A12})$$

$$\mathbf{x}_1 = -\frac{\mathbf{k}\Phi_0}{\omega^2} [\cos \theta_- - \cos \theta_0]. \quad (\text{A13})$$

The second order velocity follows from integrating equation (A11) after expanding the wave potential to second order with the aid of \mathbf{x}_1 given by equation (A13). It reads

$$\mathbf{v}_2 = \frac{\mathbf{k}\Phi_0^2}{4c^2\omega} (\cos 2\theta_- - 4 \cos \theta_- \cos \theta_0). \quad (\text{A14})$$

For $t > \tau$, a similar procedure yields

$$\mathbf{v}_1 = \frac{\mathbf{k}\Phi_0}{\omega_+} \sin \theta_+, \quad (\text{A15})$$

$$\mathbf{x}_1 = -\frac{\mathbf{k}\Phi_0}{\omega_+^2} [\cos \theta_+ - \cos \theta_\tau] - \frac{\mathbf{k}\Phi_0}{\omega^2} [\cos \theta_\tau - \cos \theta_0], \quad (\text{A16})$$

$$\mathbf{v}_2 = \frac{\mathbf{k}\Phi_0^2}{4c^2\omega_+} \left[\frac{\omega^2}{\omega_+^2} (\cos 2\theta_+ - 4 \cos \theta_+ \cos \theta_\tau) + 4 \cos \theta_+ (\cos \theta_\tau - \cos \theta_0) \right]. \quad (\text{A17})$$

The velocity matching condition at $t = \tau$ takes the form

$$\mathbf{v}_+ + \mathbf{v}_1(\tau_+) + \mathbf{v}_2(\tau_+) = \Delta \mathbf{v} + \mathbf{v}_1(\tau_-) + \mathbf{v}_2(\tau_-). \quad (\text{A18})$$

We substitute the expressions given by equations (A12), (A14), (A15) and (A17) for the first and second order velocities in the above equation. After a little rearrangement, we arrive at

$$\begin{aligned} \mathbf{v}_+ = \Delta \mathbf{v} - \frac{\mathbf{k}\Phi_0(\mathbf{k} \cdot \mathbf{v}_+) \sin \theta_\tau}{\omega\omega_+} + \frac{\mathbf{k}\Phi_0^2(\mathbf{k} \cdot \mathbf{v}_+)}{c^2\omega\omega_+} \cos \theta_\tau \cos \theta_0 \\ + \frac{\mathbf{k}\Phi_0^2\omega(\mathbf{k} \cdot \mathbf{v}_+)}{4c^2\omega_+^3} \left[2 \cos^2 \theta_\tau + 3 + \frac{\mathbf{k} \cdot \mathbf{v}_+}{\omega} (2 \cos^2 \theta_\tau - 3) \right]. \end{aligned} \quad (\text{A19})$$

We solve equation (A19) recursively for \mathbf{v}_+ retaining terms up to second order in Φ_0/c^2 and $\mathbf{f}/(mc)$. Thus,

$$\begin{aligned} \mathbf{v}_+ = \Delta \mathbf{v} - \frac{\mathbf{k}\Phi_0(\mathbf{k} \cdot \Delta \mathbf{v})}{\omega^2} \sin \theta_\tau + \frac{\mathbf{k}\Phi_0^2(\mathbf{k} \cdot \Delta \mathbf{v})}{4c^2\omega^2} [2 \sin^2 \theta_\tau + 5] \\ - \frac{\mathbf{k}\Phi_0(\mathbf{k} \cdot \Delta \mathbf{v})^2}{\omega^3} \sin \theta_\tau + \frac{\mathbf{k}\Phi_0^2(\mathbf{k} \cdot \Delta \mathbf{v})}{c^2\omega^2} \cos \theta_\tau \cos \theta_0 \\ + \frac{\mathbf{k}\Phi_0^2(\mathbf{k} \cdot \Delta \mathbf{v})^2}{4c^2\omega^3} [24 \cos \theta_\tau \cos \theta_0 + 11]. \end{aligned} \quad (\text{A20})$$

The changes in the particle's mean kinetic and mean potential energies and the work done by the external force all depend on θ_τ , the value of the wave's phase at the position of the particle when the impulse occurs. Accordingly, we average these quantities over the initial position \mathbf{x}_0 or, equivalently, over θ_τ . Since the impulse occurs at a random time, the probability distribution for θ_τ is constant. To obtain the average wave energy absorbed by the particle per impulse, we add the average change in the mean kinetic energy,

$$\Delta K = \frac{m(\Delta \mathbf{v})^2}{2} + \frac{m\Phi_0^2(\mathbf{k} \cdot \Delta \mathbf{v})}{2c^2\omega} + \frac{5m\Phi_0^2(\mathbf{k} \cdot \Delta \mathbf{v})^2}{2c^2\omega^2}, \quad (\text{A21})$$

to the average change in the mean potential energy,

$$\Delta P = \frac{m\Phi_0^2(\mathbf{k} \cdot \Delta \mathbf{v})}{c^2\omega} + \frac{3m\Phi_0^2(\mathbf{k} \cdot \Delta \mathbf{v})^2}{2c^2\omega^2}, \quad (\text{A22})$$

and then subtract the average work done by the external force,

$$W = \frac{m(\Delta \mathbf{v})^2}{2}. \quad (\text{A23})$$

These steps lead to

$$\Delta E_a = \frac{3m\Phi_0^2(\mathbf{k} \cdot \Delta \mathbf{v})}{2c^2\omega} + \frac{4m\Phi_0^2(\mathbf{k} \cdot \Delta \mathbf{v})^2}{c^2\omega^2}, \quad (\text{A24})$$

for the average wave energy absorbed per impulse.

Quantum Mechanical Calculations of Acoustic Absorption

Here we redo the absorption calculations from a quantum mechanical perspective. The quantum mechanical calculations emphasize that the classical absorption is a net absorption, that is, the difference between the true absorption and the stimulated emission. Furthermore, they illustrate, in a way which the classical calculations cannot, why the acoustic absorption is so sensitive to the mechanism by which the turbulence is maintained.

Case A. Turbulence Maintained by Stirring With Spoons

We consider a particle of mass m which is confined to the half-space $z \geq 0$ and moves under the influence of a plane wave potential $\Phi = \Phi_0 \sin(\omega t - \mathbf{k} \cdot \mathbf{x})$. The evolution of the particle's wave function is governed by Schrödinger's equation which reads

$$i\hbar \frac{\partial \Psi}{\partial t} = \left[-\frac{\hbar^2}{2m} \nabla^2 + m\Phi \right] \Psi. \quad (\text{A25})$$

We separate the Hamiltonian into a zeroth and a first order piece,

$$H_0 = -\frac{\hbar^2}{2m} \nabla^2, \quad (\text{A26})$$

and

$$H_1 = m\Phi = m[\Phi^{(+)} + \Phi^{(-)}] = \frac{im\Phi_0}{2} \{ \exp[-i(\omega t - \mathbf{k} \cdot \mathbf{x})] - \exp[+i(\omega t - \mathbf{k} \cdot \mathbf{x})] \}. \quad (\text{A27})$$

We assume that the wave amplitude, Φ_0 , decays smoothly to 0 at large z .

The eigenfunctions of H_0 ,

$$\Psi_{\mathbf{p}} = \frac{2}{(2\pi\hbar)^{3/2}} \exp \left[\frac{i}{\hbar} (\mathbf{p}_{\perp} \cdot \mathbf{x} - E_{\mathbf{p}} t) \right] \sin \left(\frac{p_z z}{\hbar} \right), \quad (\text{A28})$$

are normalized such that

$$\int d\mathbf{x} \Psi_{\mathbf{p}}^* \Psi_{\mathbf{q}} = \delta^3(\mathbf{p} - \mathbf{q}). \quad (\text{A29})$$

Here $p_z > 0$ and \mathbf{p}_{\perp} are the components of the momentum parallel and perpendicular to the z -axis and $E_{\mathbf{p}} \equiv (\mathbf{p}_{\perp}^2 + p_z^2)/2m$. Each eigenfunction can be decomposed into two plane waves one of which may be viewed as incident upon and the other reflected from the wall at $z = 0$.

The wave potential, Φ , modifies the solutions of Schrödinger's equation. However, there are still simple solutions for which the incident wave is that associated with one of the eigenfunctions of H_0 . As $z \rightarrow \infty$, the outgoing part of each solution decomposes into three pieces, the reflected part of the unperturbed eigenfunction and two additional waves, $\Psi'_{\mathbf{p}\pm}$, which determine the amplitudes for absorption and stimulated emission. The latter satisfy the following inhomogeneous equation,

$$\frac{\hbar^2}{2m} \nabla^2 \Psi'_{\mathbf{p}\pm} + i\hbar \frac{\partial \Psi'_{\mathbf{p}\pm}}{\partial t} = m\Phi^{(\pm)} \Psi_{\mathbf{p}}. \quad (\text{A30})$$

It is obvious from equation (A30) that the energy and the x and y components of the momentum of $\Psi'_{\mathbf{p}\pm}$ must be the sum of the corresponding quantities for the incident particle and the plane wave potential. This reduces the equation to the inhomogeneous, one dimensional, Helmholtz equation,

$$\frac{d^2\Psi'_{\mathbf{p}\pm}}{dz^2} + \kappa_{\mathbf{p}\pm}^2\Psi'_{\mathbf{p}\pm} = \pm \frac{2im^2\Phi_0}{\hbar^2(2\pi\hbar)^{3/2}} \exp(\pm ik_z z) \sin\left(\frac{p_z z}{\hbar}\right), \quad (\text{A31})$$

where

$$\kappa_{\mathbf{p}\pm} = \frac{1}{\hbar} \sqrt{p_z^2 - \hbar^2|\mathbf{k}_\perp|^2 \mp 2\hbar\mathbf{p}_\perp \cdot \mathbf{k}_\perp \pm 2m\hbar\omega} \approx \frac{p_z}{\hbar} \left[1 \pm \frac{m\hbar\omega}{p_z^2} - \frac{1}{2} \left(\frac{m\hbar\omega}{p_z^2} \right)^2 \right]. \quad (\text{A32})$$

The Green's function for equation (A31) which vanishes at $z = 0$ and reduces to an outgoing wave at large z is given by

$$G(z, z') = \begin{cases} -\frac{\sin \kappa_{\mathbf{p}\pm} z \exp(i\kappa_{\mathbf{p}\pm} z')}{\kappa_{\mathbf{p}\pm}} & z < z' \\ -\frac{\sin \kappa_{\mathbf{p}\pm} z' \exp(i\kappa_{\mathbf{p}\pm} z)}{\kappa_{\mathbf{p}\pm}} & z > z' \end{cases} \quad (\text{A33})$$

Using (A33), we write $\Psi'_{\mathbf{p}\pm}$ at large z as

$$\Psi'_{\mathbf{p}\pm}(z) = \mp \frac{2im^2\Phi_0}{\hbar^2(2\pi\hbar)^{3/2}\kappa_{\mathbf{p}\pm}} \int_0^\infty dz' \exp(i\kappa_{\mathbf{p}\pm} z \pm ik_z z') \sin \kappa_{\mathbf{p}\pm} z' \sin\left(\frac{p_z z'}{\hbar}\right),$$

which reduces to

$$\Psi'_{\mathbf{p}\pm}(z) \approx -\frac{k_z p_z \Phi_0 \exp(i\kappa_{\mathbf{p}\pm} z)}{(2\pi\hbar)^{3/2}\hbar\omega^2}, \quad (\text{A34})$$

where, in the last step, we have used $\int_0^\infty dz \sin qz = 1/q$ for $q \neq 0$.

Next, we calculate the flux, $F_{\mathbf{p}\pm}$, associated with $\Psi'_{\mathbf{p}\pm}(z)$ from

$$F_{\mathbf{p}\pm} \equiv \frac{\hbar}{2im} \left[\Psi'_{\mathbf{p}\pm}{}^* \nabla \Psi'_{\mathbf{p}\pm} - \Psi'_{\mathbf{p}\pm} \nabla \Psi'_{\mathbf{p}\pm}{}^* \right] = (\hbar\kappa_{\mathbf{p}\pm} \hat{\mathbf{z}} + \mathbf{p}_\perp + \pm \hbar\mathbf{k}_\perp) \frac{k_z^2 \Phi_0^2 p_z^2}{(2\pi\hbar)^3 \hbar^2 m \omega^4}. \quad (\text{A35})$$

The probability of absorption or stimulated emission per scattering, \mathcal{P}_\pm , is evaluated by dividing $\hat{\mathbf{z}} \cdot F_{\mathbf{p}\pm}$ by $p_z / [(2\pi\hbar^3)m]$, the z component of the incident flux. We obtain,

$$\mathcal{P}_{\pm} = \left(\frac{k_z p_z \Phi_0}{\hbar \omega^2} \right)^2 \left(1 \pm \frac{m \hbar \omega}{p_z^2} \right). \quad (\text{A36})$$

The net energy absorbed per scattering is given by

$$\Delta E_a \equiv \hbar \omega (\mathcal{P}_+ - \mathcal{P}_-) = \frac{2m k_z^2 \Phi_0^2}{\omega^2}. \quad (\text{A37})$$

This expression is identical to that derived classically and given in equation (A10).

Case B. Pseudo-Convection

We consider the behavior of a particle of mass m which is subject to the combined influence of a plane wave potential, $\Phi = \Phi_0 \sin(\omega t - \mathbf{k} \cdot \mathbf{x})$, and the potential associated with an impulsive external acceleration, $U(\mathbf{x}, t) = -m\mathbf{x} \cdot \mathbf{a}(t) = -m\mathbf{x} \cdot \Delta \mathbf{v} \delta(t - \tau)$. With these potentials, Schrödinger's equation reads

$$i\hbar \frac{\partial \Psi}{\partial t} = \left[-\frac{\hbar^2}{2m} \nabla^2 - m\Delta \mathbf{v} \cdot \mathbf{x} + m\Phi \right] \Psi. \quad (\text{A38})$$

We separate the Hamiltonian into a zeroth and a first order piece,

$$H_0 = -\frac{\hbar^2}{2m} \nabla^2 - m\Delta \mathbf{v} \cdot \mathbf{x} \delta(t - \tau), \quad (\text{A39})$$

and

$$H_1 = m\Phi = m[\Phi^{(+)} + \Phi^{(-)}] = \frac{im\Phi_0}{2} \{ \exp[-i(\omega t - \mathbf{k} \cdot \mathbf{x})] - \exp[+i(\omega t - \mathbf{k} \cdot \mathbf{x})] \}. \quad (\text{A40})$$

The normalized plane wave solutions of H_0 are given by

$$\Psi_{\mathbf{p}} = \frac{1}{(2\pi\hbar)^{3/2}} \exp \left[\frac{i}{\hbar} \left(\mathbf{P} \cdot \mathbf{x} - \int^t dt' \frac{P^2}{2m} \right) \right], \quad (\text{A41})$$

where

$$\mathbf{P}(t) = \mathbf{p} + m \int_0^t dt' \Delta \mathbf{v} \delta(t' - \tau) = \mathbf{p} + m\Delta \mathbf{v} \theta(t - \tau). \quad (\text{A42})$$

Note that $\mathbf{p} \equiv \mathbf{P}(0)$ is used to label the plane wave solutions of H_0 .

We solve for the transition amplitude,

$$\mathcal{A}_{\pm}(t) = \frac{1}{i\hbar} \int_0^t dt' \int d\mathbf{x} \Psi_{\mathbf{p}_f}^* H_{1\pm} \Psi_{\mathbf{p}_i}, \quad (\text{A43})$$

from an initial state \mathbf{p}_i to a final state \mathbf{p}_f using time dependent perturbation theory. The amplitudes for absorption and emission come from the positive and negative frequency parts of the wave potential. The integrand in equation (A43) is evaluated with the aid of equations (A40) and (A41). The transition amplitudes for absorption and emission are easily shown to be

$$\begin{aligned} \mathcal{A}_{\pm}(t > \tau) = & \pm \frac{m\Phi_0}{2\hbar} \int_0^t dt' \delta^3(\mathbf{p}_f - \mathbf{p}_i \mp \hbar\mathbf{k}) \\ & \exp \left[i \left(\mp \omega t' + \frac{p_f^2 - p_i^2}{2\hbar m} t' + \frac{\Delta\mathbf{v} \cdot (\mathbf{p}_f - \mathbf{p}_i)}{\hbar} (t' - \tau) \theta(t' - \tau) \right) \right]. \end{aligned} \quad (\text{A44})$$

Evaluating the above integral yields

$$\mathcal{A}_{\pm} = \frac{im\Phi_0}{2\hbar} \left(\frac{\exp(\mp i\omega_{1\pm}\tau) - 1}{\omega_{1\pm}} + \frac{\exp(\mp i\omega_{2\pm}t \mp i\mathbf{k} \cdot \Delta\mathbf{v}\tau) - \exp(\mp i\omega_{1\pm}\tau)}{\omega_{2\pm}} \right), \quad (\text{A45})$$

where

$$\omega_{1\pm} = \omega - \frac{\mathbf{k} \cdot \mathbf{p}_i}{m} \mp \frac{\hbar k^2}{2m}, \quad (\text{A46})$$

$$\omega_{2\pm} = \omega_{1\pm} - \mathbf{k} \cdot \Delta\mathbf{v}. \quad (\text{A47})$$

To determine the average absorption probability, \mathcal{P}_{\pm} , we average the absolute square of the coefficient of the δ function in the transition amplitude with respect to both τ and t and then discard the terms which are independent of the impulse $\Delta\mathbf{v}$.⁴ This procedure yields

⁴ Without this averaging and subtraction, the transition probabilities would de-

$$\mathcal{P}_{\pm} = \frac{m^2 \Phi_0^2 (\mathbf{k} \cdot \Delta \mathbf{v})}{2 \hbar^2 \omega_1 \omega_2^2}. \quad (\text{A48})$$

Expanding $1/\omega_1 \omega_2^2$ using equations (A46) and (A47), we arrive at

$$\mathcal{P}_{\pm} = \frac{m^2 \Phi_0^2 (\mathbf{k} \cdot \Delta \mathbf{v})}{2 \hbar^2 \omega_d^3} \left[1 \pm \frac{3 \hbar k^2}{2 m \omega_d} + \frac{2 \mathbf{k} \cdot \Delta \mathbf{v}}{\omega_d} \pm \frac{4 \hbar k^2 (\mathbf{k} \cdot \Delta \mathbf{v})}{m \omega_d^2} \dots \right], \quad (\text{A49})$$

where

$$\omega_d \equiv \omega - \frac{\mathbf{k} \cdot \mathbf{p}_i}{m}. \quad (\text{A50})$$

The net energy absorption, ΔE_{abs} , is just $\hbar \omega$ times the difference between the upward and downward transition probabilities from the initial state \mathbf{p}_i . Thus

$$\Delta E_a \equiv \hbar \omega (\mathcal{P}_+ - \mathcal{P}_-) = \frac{3 m \Phi_0^2 (\mathbf{k} \cdot \Delta \mathbf{v})}{2 c^2 \omega} + \frac{4 m \Phi_0^2 (\mathbf{k} \cdot \Delta \mathbf{v})^2}{c^2 \omega^2}. \quad (\text{A51})$$

We note that ΔE_a given above is in exact accord with the corresponding classical result.

pend on the value of τ and would contain terms which are independent of $\Delta \mathbf{v}$. The root of this problem is that, even for $\Delta \mathbf{v} = 0$, Φ mixes the plane wave solutions of H_0 .

CHAPTER 3

Absorption of Acoustic Waves by Sunspots

Absorption of Acoustic Waves by Sunspots

Peter Goldreich, Pawan Kumar and Ken Libbrecht

California Institute of Technology, Pasadena, California

Abstract

The discovery of acoustic absorption in regions associated with sunspots (Braun, Duvall and LaBonte 1987) is an unexpected but welcome development in the study of solar oscillations. At least for the moment, the nature of the absorption process is unknown. We show that a straightforward explanation involving a decrease of acoustic emission from sunspots due to suppression of convection cannot account for the observations of Braun *et al.* Instead, an enhanced absorption associated with sunspots is required. We propose an absorption mechanism based on the work of Goldreich and Kumar. We show that at fixed turbulent mach number, M , dynamically significant magnetic fields can increase the absorptivity of turbulent convection by up to a factor M^{-2} but they do not change its emissivity. A simple estimate of the acoustic absorptivity by turbulence in the presence of a magnetic field accounts for both the magnitude and horizontal wavenumber dependence of the sunspot absorption deduced by Braun *et al.* (1987).

Enhanced Absorption in Sunspots

The sizes of the sunspots observed by Braun *et al.* are typically 25 arc seconds and the area surrounding them is 240 arc seconds or more in diameter. The absorptivity over a horizontal wavelength range of 5 to 21 arc second is found to be between 0.6 and 0.3. Let us assume that the presence of sunspots causes no extra absorption of acoustic waves only a reduced emission. Now, if the absorption length for high degree acoustic waves is large compared to the size of the sunspots, then the fractional difference between the incoming and the outgoing flux would be approximately the ratio of sunspot area to the damping length squared or less, falling far short of the observed absorptivity. On the other hand, if we take the absorption length to be about the size of the sunspots then their presence can not be felt outside of a region few times the size of the spots. Therefore, if the area of the region observed is much greater than the sunspots, as is the case with Braun *et al.*, the difference between the incoming and outgoing flux would be small again. Thus we conclude that there must be an enhanced absorption associated with the sunspots. We present below a simple calculation estimating this extra absorption required to explain the observations.

The analytic dispersion relation

$$\omega^2 = \frac{4}{3}g k_h \left(n + \frac{3}{4} \right), \quad (1)$$

provides an adequate representation for high degree p-modes in the 5-minute band. Here, $g = 2.7 \times 10^4 \text{ cm sec}^{-2}$ is the gravitational acceleration at the solar photosphere. Each mode is characterized by its radian frequency, ω , radial order, n , and horizontal wavenumber, $k_h = \ell/R_\odot$.

The horizontal group velocity of a wave packet composed of modes of radial order n is given by

$$v_{hgp} = \frac{\partial \omega}{\partial k_h} = \frac{\omega}{2k_h}. \quad (2)$$

Thus, the time the packet takes to cross a sunspot of linear dimension L is

$$t_c = \frac{k_h L}{\pi} P, \quad (3)$$

where $P = 2\pi/\omega$ is the wave period. Braun *et al.* (1987) find significant damping of 5-minute oscillations with $k_h = 1.0 \text{ Mm}^{-1}$ for $L \approx 15 \text{ Mm}$. Inserting these parameters into equation (3), we deduce that the damping time inside sunspots is of order 5 wave periods or half an hour. This deduction comes with two caveats. We have assumed that acoustic waves penetrate sunspot umbras and that they travel inside them at the same speed as in field free regions. Both of these assumptions are likely to be invalid. Unfortunately, the manner in which acoustic waves propagate in and near sunspots depends on unknown properties of the magnetic field such as its homogeneity and depth dependence. It seems likely that spots reflect a significant fraction of the incident acoustic flux and that much of the absorption may take place outside the umbra.

The width of ridges in the $k_h - \omega$ diagram provides a lower limit on the lifetime of modes. The width of ridges at high degree ($\ell \sim 400$), at five minutes is observed to be about $20 \mu\text{Hz}$ or less, corresponding to decay time for modes of half a day or more. Thus the sunspots absorb acoustic waves at least 20 times more efficiently than the surrounding medium, which requires explanation.

The Acoustic Emissivity and Absorptivity of Turbulent Fluids

Our hypothesis for the absorption of acoustic radiation by sunspots is based on a recent investigation of the interaction of acoustic radiation with turbulence by Goldreich and Kumar (1987). These authors find that both the emission and the absorption of acoustic radiation by turbulent fluids depend upon the manner in which the turbulence is excited. For free turbulence, that is, turbulence which is not affected by external forces, both the emission and the absorption are dominated by the quadrupole process. Turbulence which is maintained by local forces, such

as provided by stirring with spoons or by buoyancy forces associated with convection, has its emissivity enhanced by a factor M^{-2} relative to that of free turbulence because the external forces create acoustic dipoles. The absorptivity of forced turbulence is quite subtle. It depends on the manner in which eddies respond to the combined radiation and external forces. When stirring with spoons, an impulse is transmitted to the eddies which depends upon its velocity. In the presence of an acoustic wave the impulse depends upon the velocity perturbation forced by the wave. This increases the absorptivity by a factor of M^{-2} relative to that of free turbulence. However, the absorptivity of turbulent convection is equal to that of free turbulence. In this case, the impulses received by eddies are independent of their velocities, and the dipole contribution to the absorptivity is reduced, by a near cancelation of the true absorption by stimulated emission, so that it is no larger than the absorptivity due to the quadrupoles.

Magnetic Enhancement of Acoustic Absorption

The turbulence which is responsible for exciting and damping the solar oscillations is driven by convection. Magnetic fields exert time dependent stresses in a turbulent, electrically conducting, fluid. In so doing they act like the spoons to which we referred in the previous section. If the magnetic fields are dynamically significant, and if the sunspots consist of magnetic tubes of cross section roughly equal to the granules, they can increase the absorptivity by up to a factor of M^{-2} relative to that in field free regions.² However, the emissivity is not significantly affected by the magnetic fields since it is enhanced, even in field free regions, by the buoyancy forces associated with the convection.

The turbulent mach number peaks at the top of the convection zone. From observations of the solar granules and from mixing length theory, we know that the turbulent velocity there is $1 - 2 \text{ km s}^{-1}$. The photospheric sound speed is 7

² This comparison is at a fixed value of the turbulent mach number.

$km\ sec^{-1}$ which yields $10^1 \lesssim M^{-2} \lesssim 10^2$. Thus, the presence of magnetic fields could reasonably be expected to increase the acoustic absorptivity by an order of magnitude or more. This would neatly account for the short damping lengths associated with sunspots.

Discussion

The central issue which remains to be resolved is whether the acoustic absorption associated with sunspots signals the existence of some new mechanism of either k_h dependent or magnetic field dependent damping.

The proportionality of t_c to k_h implies that absorption by sunspots must increase with k_h , as observed, almost independently of the absorption mechanism. Moreover, if the mechanism operates near the top of the convection zone or just above the photosphere, there would be an additional but weaker increase in the damping rate associated with the inverse variation of the mode mass, \mathcal{M} , with k_h .

The best way to distinguish between an unsuspected form of k_h dependent damping and turbulent damping enhanced by magnetic fields is to investigate the linewidths and the mean square surface velocities of high degree p-modes. In the absence of a new mechanism of k_h dependent damping, both should vary in direct proportion to \mathcal{M}^{-1} as k_h varies at fixed frequency. In order to account for the small absorption lengths deduced for sunspots, an appropriate k_h dependent damping mechanism would have to increase the damping by at least an order of magnitude for $\ell = 700$. This would imply linewidths and mean square velocity amplitudes at $\ell = 700$ which are smaller, by at least a factor of 2, than those at $\ell = 0$. On the other hand, if magnetically enhanced acoustic absorption is responsible for the Braun *et al.* (1987) observations, the linewidths and mean square velocities should be about a factor of 2 larger at $\ell = 700$ than at $\ell = 0$.

REFERENCES

Braun, D.C., Duvall, T.L. Jr. and LaBonte, B.J., 1987, Preprint.

Goldreich, P. and Kumar, P., 1987, Preprint.

CHAPTER 4

**Distribution Functions for the Time Averaged
Energies of Stochastically Excited Solar p-modes**

Submitted to the Astrophysical Journal

**Distribution Functions for the Time Averaged
Energies of Stochastically Excited Solar p-modes**

Pawan Kumar, Joel Franklin and Peter Goldreich

California Institute of Technology, Pasadena, California

ABSTRACT

We study the excitation of a damped harmonic oscillator by a random force as a model for the stochastic excitation of a solar p-mode by turbulent convection. An extended sequence of observations is required to separate different p-modes and thus determine the energies of individual modes. Therefore, the observations yield time averaged values of the energy. We apply the theory of random differential equations to calculate distribution functions for the time averaged energy of the oscillator. The instantaneous energy satisfies a Boltzmann distribution. With increasing averaging time the distribution function narrows and its peak shifts towards the mean energy. We also perform numerical integrations to generate finite sequences of time averaged energies. These are treated as simulated data from which we obtain approximate probability distributions for the time averaged energy. A comparison of our calculated distributions with those determined observationally should help to resolve whether the solar p-modes are stochastically excited. If they are, modes of the same frequency with degree $\ell \lesssim 200$ should have identical values for the products of their mean energies, linewidths and masses. If, in addition, turbulence or radiative dissipation provides the principal damping mechanism, the mean energies should be independent of angular order, ℓ .

I. INTRODUCTION

The frequency, linewidth and photospheric velocity amplitude are the primary observables associated with each p-mode. The energy in a mode is proportional to the square of its velocity amplitude. If the mode is stochastically excited, its energy, E , will fluctuate on the damping timescale. Unfortunately, observations of solar p-modes cannot determine the instantaneous energy, E , but only, E_T , the energy averaged over some interval of time, say $-T \leq t \leq T$.

A damped harmonic oscillator excited by a random force provides a simple model for the stochastic excitation of a solar p-mode by turbulent convection (Goldreich and Keeley 1977, Goldreich and Kumar 1987). The current investigation is devoted to calculating distributions for E_T appropriate to the model harmonic oscillator. It is obvious that the distribution function is a decaying exponential, or Boltzmann, distribution for $T = 0$ and that it approaches a delta function at the mean energy as $T \rightarrow \infty$. We determine distribution functions appropriate to arbitrary averaging times by applying the theory of random differential equations. In addition, we provide examples of approximate distribution functions obtained from finite strings of numerically simulated data. The latter are intended as a guide for interpreting observationally determined distribution functions of E_T for solar p-modes.

The organization of this paper is as follows. In section II we describe the model harmonic oscillator and outline the procedure for calculating distribution functions for its time averaged energy. We develop the method used to compute the eigenvalues required to determine the distribution functions in Section III. In Section IV we present our theoretical distribution functions. We solve the harmonic oscillator equation numerically in Section V to generate finite sequences of values for E_T which are treated as simulated data to determine approximate distribution functions. We briefly discuss some observational implications of our results for the solar p-modes in Section VI.

II. THE STOCHASTICALLY EXCITED OSCILLATOR

The differential equation governing the time evolution of the coordinate, q , of a damped harmonic oscillator of frequency, ω_0 , which interacts with a random force, $F(t)$, reads

$$\frac{d^2q}{dt^2} + 2\Gamma \frac{dq}{dt} + \omega_0^2 q = \frac{F(t)}{M}, \quad (1)$$

where M is the mass and Γ is a positive damping constant. We assume that $F(t)$ is a gaussian random process. This assumption is not very restrictive because the central limit theorem implies that other processes, such as the Poisson process, reduce to a gaussian process in the limit of large N .

The energy, E , consists of a kinetic and a potential part;

$$E = \frac{M}{2} \left[\left(\frac{dq}{dt} \right)^2 + \omega_0^2 q^2 \right]. \quad (2)$$

Our basic strategy is to expand $x_1 \equiv \omega_0 q$ and $x_2 \equiv dq/dt$ in terms of a set of functions which are orthonormal over the time interval $-T \leq t \leq T$. We define \mathbf{x} to be the column vector with components x_1 and x_2 . Then, we have

$$\mathbf{x}(t) = \sum_n A_n f_n \phi_n(t) \quad \text{for} \quad -T \leq t \leq T, \quad (3)$$

where the ϕ_n are two-component functions which satisfy

$$\int_{-T}^T dt \phi_m^\dagger(t) \cdot \phi_n(t) = \delta_{m,n}, \quad (4)$$

the f_n are uncorrelated, random, gaussian variables with unit variance and the A_n are constants. Equation (3) is an extension of the Karhunen-Loève expansion (Davenport and Root 1958) to two stochastic processes.

To determine $A_m f_m$, we take the dot product of both sides of equation (3) by ϕ_m^\dagger , then integrate over $-T \leq t \leq T$.¹ Next, we multiply $A_m f_m$ by $A_n^* f_n^*$ and take the expectation value of the resulting expression.² This procedure yields

$$\langle A_m A_n^* f_m f_n^* \rangle = \int_{-T}^T dt_1 \int_{-T}^T dt_2 \left[\phi_m^\dagger(t_1) \cdot \langle \mathbf{x}(t_1) \mathbf{x}^\dagger(t_2) \rangle \cdot \phi_n(t_2) \right]. \quad (5)$$

Since $\langle f_m f_n^* \rangle = \delta_{n,m}$, the ϕ_n must satisfy the integral equation

$$\int_{-T}^T dt_2 \mathcal{R}(t_1, t_2) \cdot \phi_n(t_2) = \lambda_n \phi_n(t_1), \quad (6)$$

where

$$\mathcal{R}(t_1, t_2) = \langle \mathbf{x}(t_1) \mathbf{x}^\dagger(t_2) \rangle \quad (7)$$

is a 2x2 matrix. Thus, ϕ_n is an eigenfunction of the integral operator defined by equation (6) and A_n is the square root of the corresponding eigenvalue, λ_n . We may now rewrite equation (3) as

$$\mathbf{x}(t) = \sum_n \sqrt{\lambda_n} f_n \phi_n(t). \quad (8)$$

We note that ϕ_2 is the time derivative of ϕ_1 . To prove this we multiply equation (8) by f_n^* and take the expectation value of both sides. This yields

$$\langle f_n^* \mathbf{x}(t) \rangle = \sqrt{\lambda_n} \phi_n(t) \quad \text{or} \quad (\phi_n)_1 = \langle f_n^* x_1(t) \rangle / \sqrt{\lambda_n}, \quad (\phi_n)_2 = \langle f_n^* x_2(t) \rangle / \sqrt{\lambda_n}. \quad (9)$$

But by definition $x_2 = \omega_0^{-1} dx_1/dt$. Therefore, the above equation implies that $(\phi_n)_2 = \omega_0^{-1} d(\phi_n)_1/dt$.

¹ A dagger, †, denotes the complex conjugate and transpose of a matrix.

² Angular brackets, $\langle \quad \rangle$, denote an expectation value.

The operator defined by equation (6) is easily shown to be hermitian. Thus, the eigenvalues, λ_n , are real. Furthermore, rewriting equation (5) using $|A_n|^2 = \lambda_n$ yields

$$\lambda_n = \left\langle \left| \int_{-T}^T dt_1 \phi_n^\dagger(t_1) \cdot \mathbf{x}(t_1) \right|^2 \right\rangle, \quad (10)$$

which proves that the λ_n are positive. Because the matrix \mathcal{R} is real, the eigenfunctions can be chosen to be real. Also, since \mathbf{x} is real the f_n must be real.

To evaluate the average energy, E_T , we integrate $|\mathbf{x}|^2$ using equation (8) and the orthonormality property of the ϕ_n ;

$$E_T \equiv \frac{1}{2T} \int_{-T}^T dt E = \frac{M}{4T} \int_{-T}^T dt \mathbf{x}^\dagger \cdot \mathbf{x} = \frac{M}{4T} \sum_n \lambda_n f_n^2 \equiv \sum_n y_n. \quad (11)$$

Since f_n is a gaussian random variable with unit variance and zero mean the probability distribution for y_n , $P(y_n)$, is

$$P(y_n) = \sqrt{\frac{4T}{\pi M y_n \lambda_n}} \exp\left(\frac{-4T y_n}{M \lambda_n}\right), \quad (12)$$

and the characteristic function, $\mathcal{C}_{y_n}(\omega_E)$, is

$$\mathcal{C}_{y_n}(\omega_E) = \frac{1}{\sqrt{1 - iM\omega_E \lambda_n/4T}}. \quad (13)$$

The characteristic function for E_T is just the product of the $\mathcal{C}_{y_n}(\omega_E)$.

$$\mathcal{C}_{E_T}(\omega_E) = \prod_n \frac{1}{\sqrt{1 - iM\omega_E \lambda_n/4T}}. \quad (14)$$

The inverse Fourier transform of equation (14) gives the probability distribution, $P(E_T)$, for E_T . Thus, our main task is to determine the eigenvalues of equation (6). We develop a procedure for doing this in the next section.

III. DETERMINING THE EIGENVALUES

This section is divided into three parts. In a) we calculate the correlation matrix \mathcal{R} by solving equation (1) for \mathbf{x} . Next, in b) we transform the integral equation (6) into a differential equation for ϕ . Equipped with this we write down the most general form for ϕ . Finally, in c) we substitute the general form for ϕ into the integral equation (6) and reduce the problem of finding the eigenvalues to that of finding the roots of an ordinary algebraic equation.

a) Determining The Correlation Matrix

Throughout this section we take $F(t)$ to be a gaussian, white noise, random process. The solution of equation (1) is obtained in the terms of the causal Green's function, G , for a damped harmonic oscillator.

$$q(t) = \frac{1}{M} \int_{-\infty}^t dt' G(t, t') F(t'), \quad (15)$$

where

$$G(t, t') = \frac{1}{\omega_1} \theta(t - t') \exp[-\Gamma(t - t')] \sin \omega_1(t - t'). \quad (16)$$

Here $\theta(t)$ is the Heaviside function, $\theta(t) = 0$ for $t < 0$ and $\theta(t) = 1$ for $t > 0$.

Using equations (15) and (16) we determine the correlation matrix, \mathcal{R} , defined by equation (7), to be

$$\mathcal{R}_{11} \equiv \langle x_1(t_1) x_1(t_2) \rangle = \frac{g\omega_0}{4M^2\Gamma\omega_1} \exp(-\Gamma|t_1 - t_2|) \cos(\omega_1|t_1 - t_2| - \alpha) \equiv \frac{g\omega_0}{4M^2\Gamma\omega_1} R_0, \quad (17)$$

where

$$\omega_1^2 = \omega_0^2 - \Gamma^2, \quad \cos \alpha = \frac{\omega_1}{\omega_0}, \quad \sin \alpha = \frac{\Gamma}{\omega_0}. \quad (18)$$

In deriving equation (17) we have used $\langle F(t_1) F(t_2) \rangle = g\delta(t_1 - t_2)$. The other components of \mathcal{R} may be expressed in terms of R_0 . We find

$$\mathcal{R}(t_1, t_2) = \frac{g\omega_0}{4M^2\omega_1\Gamma} \begin{pmatrix} R_0 & \frac{dR_0}{\omega_0 dt_2} \\ -\frac{dR_0}{\omega_0 dt_2} & -\frac{d^2 R_0}{\omega_0^2 dt_2^2} \end{pmatrix} \quad (19)$$

Using equation (17)

$$\begin{aligned} \mathcal{R}(t_1, t_2) &= \frac{g\omega_0}{4M^2\omega_1\Gamma} \exp(-\Gamma|t_1 - t_2|) \\ &\times \begin{pmatrix} \cos(\omega_1|t_1 - t_2| - \alpha) & \sin \omega_1(t_1 - t_2) \\ -\sin \omega_1(t_1 - t_2) & \cos(\omega_1|t_1 - t_2| + \alpha) \end{pmatrix} \end{aligned} \quad (20)$$

b) Differential Equation For Eigenvectors

In order to derive the general form of an eigenvector it is useful to convert the integral equation (6) into a differential equation. To achieve this we exploit a special property of the Fourier transform of the kernel \mathcal{R} .

Let

$$\mathcal{R}(\tau) = \frac{1}{\sqrt{2\pi}} \int_{-\infty}^{\infty} d\omega \tilde{\mathcal{R}}(\omega) \exp(i\omega\tau), \quad (21)$$

where $\tau \equiv t_1 - t_2$. Then $\tilde{\mathcal{R}}(\omega)$ is determined by taking the Fourier transform of equation (20):

$$\tilde{\mathcal{R}}(\omega) = \frac{g\omega_0^2}{\sqrt{2\pi}M^2 [\omega^4 + \omega_0^4 - 2\omega^2\omega_1^2 \cos(2\alpha)]} \begin{pmatrix} 1 & -\frac{i\omega}{\omega_0} \\ \frac{i\omega}{\omega_0} & \frac{\omega^2}{\omega_0^2} \end{pmatrix}. \quad (22)$$

We note that $\tilde{\mathcal{R}}(\omega)$ is the ratio of rational functions. This property enables us to convert the integral equation into a differential equation. Rewriting equation (6) in terms of $\tilde{\mathcal{R}}(\omega)$ we arrive at

$$\frac{1}{\sqrt{2\pi}} \int_{-T}^T dt' \int_{-\infty}^{\infty} d\omega \exp i\omega(t - t') \frac{\mathcal{P}(i\omega) \cdot \phi(t')}{Q(i\omega)} = \lambda\phi(t), \quad (23)$$

where

$$\tilde{\mathcal{R}}(\omega) \equiv \frac{\mathcal{P}(i\omega)}{Q(i\omega)}, \quad Q(i\omega) \equiv \omega^4 + \omega_0^4 - 2\omega_0^2\omega^2 \cos 2\alpha, \quad (24)$$

and $\mathcal{P}(i\omega)$ is a 2x2 matrix equal to $Q(i\omega)\tilde{\mathcal{R}}(\omega)$. Operating on equation (23) by $Q(d/dt)$ we get

$$\lambda Q\left(\frac{d}{dt}\right)\phi(t) = \sqrt{2\pi}\mathcal{P}\left(\frac{d}{dt}\right) \cdot \phi(t). \quad (25)$$

Then, combining equations (22) and (25) we obtain a pair of differential equations for the components of ϕ :

$$\begin{aligned} \lambda'Q(D)\phi_1 &= \omega_0[\omega_0\phi_1 - D\phi_2], \\ \lambda'Q(D)\phi_2 &= \omega_0D\phi_1 - D^2\phi_2, \end{aligned} \quad (26)$$

where

$$\lambda' = \lambda M^2/g, \quad D \equiv \frac{d}{dt}, \quad Q(D) = D^4 + 2\omega_0^2 \cos 2\alpha D^2 + \omega_0^4. \quad (27)$$

Substituting $\phi_2 = D\phi_1/\omega_0$ into equations (26) yields uncoupled differential equations for ϕ_1 and ϕ_2 :

$$Q_1(D)\phi_1 = 0 \quad \text{and} \quad Q_1(D)\phi_2 = 0, \quad (28)$$

where

$$Q_1(D) = \lambda'Q(D) + D^2 - \omega_0^2. \quad (29)$$

We see from equations (28) and (29) that the general form for the eigenfunctions of equation (6) is a sum of four exponentials, each of which satisfies $Q_1(D)\exp\beta_k t = 0$. Furthermore, the β_k cannot be equal to either $\Gamma \pm i\omega_1$ or $-\Gamma \pm i\omega_1$ because the four factors of the operator $Q(D)$ are $D \pm \Gamma \pm i\omega_1$. Therefore, if $Q(D)\exp(\beta_k t) = 0$, $Q_1(D)\exp(\beta_k t) = (D^2 - \omega_0^2)\exp(\beta_k t) \neq 0$, since $\omega_0^2 \neq (\Gamma \pm i\omega_1)^2$.

We conclude this subsection by summarizing the properties of the eigenfunctions.

1. $\phi = \begin{pmatrix} \phi_1 \\ D\phi_1/\omega_0 \end{pmatrix}$.
2. $\phi_1 = \sum_{k=1}^4 a_k \exp(\beta_k t)$, where β_k is solution of $Q_1(i\beta_k) = 0$. (30)
3. $\beta_k \neq \Gamma \pm i\omega_1$ and $\beta_k \neq -\Gamma \pm i\omega_1$.

c) Algebraic Equation For Eigenvalues

We substitute the general form for ϕ given by equation (30) into the integral eigenvalue equation (6). Equating the coefficients of the exponentials on both sides of the resulting equation yields a set of algebraic equations which is solved to give the eigenvalues.

The evaluation of the left side of equation (6) is simplified by noting that all of the integrals there can be expressed in terms of the integral of $R_0 \exp(\beta t)$ which is given below:

$$\begin{aligned}
 2 \int_{-T}^T dt' R_0(t, t') \exp(\beta t') &= \frac{8\Gamma\omega_0\omega_1 \exp(\beta t)}{(\beta^2 + \omega_0^2)^2 - 4\Gamma^2\beta^2} \\
 &- \frac{\exp[(t+T)(i\omega_1 - \Gamma) - \beta T - i\alpha]}{\Gamma + \beta - i\omega_1} - \frac{\exp[(T-t)(i\omega_1 - \Gamma) + \beta T - i\alpha]}{\Gamma - \beta - i\omega_1} \\
 &- \frac{\exp[-(t+T)(i\omega_1 + \Gamma) - \beta T + i\alpha]}{\Gamma + \beta + i\omega_1} - \frac{\exp[(t-T)(i\omega_1 + \Gamma) + \beta T + i\alpha]}{\Gamma - \beta + i\omega_1}.
 \end{aligned} \tag{31}$$

The denominators in this equation do not vanish because $\beta \neq \Gamma \pm i\omega_1$ and $\beta \neq -\Gamma \pm i\omega_1$.

Armed with the above expression and equation (19), we are ready to evaluate the integral in equation (6) for the general ϕ given by equation (30). The first component of equation (6) yields

$$\begin{aligned}
2 \int_{-T}^T dt' \left[R_0(t, t') \phi_1(t') + \frac{1}{\omega_0^2} \frac{dR_0}{dt'} \frac{d\phi_1}{dt'} \right] &= \sum_{k=1}^4 \frac{8\Gamma(\omega_0^2 - \beta_k^2) a_k \exp(\beta_k t) \cos \alpha}{(\beta_k^2 + \omega_0^2)^2 - 4\Gamma^2 \beta_k^2} \\
&- \sum_{k=1}^4 \frac{a_k [\omega_0^2 - \beta_k(i\omega_1 - \Gamma)]}{\omega_0^2(\Gamma + \beta_k - i\omega_1)} \exp[(t+T)(i\omega_1 - \Gamma) - \beta_k T - i\alpha] \\
&- \sum_{k=1}^4 \frac{a_k [\omega_0^2 + \beta_k(i\omega_1 - \Gamma)]}{\omega_0^2(\Gamma - \beta_k - i\omega_1)} \exp[(T-t)(i\omega_1 - \Gamma) + \beta_k T - i\alpha] \\
&- \sum_{k=1}^4 \frac{a_k [\omega_0^2 + \beta_k(i\omega_1 + \Gamma)]}{\omega_0^2(\Gamma + \beta_k + i\omega_1)} \exp[-(t+T)(i\omega_1 + \Gamma) - \beta_k T + i\alpha] \\
&- \sum_{k=1}^4 \frac{a_k [\omega_0^2 - \beta_k(i\omega_1 + \Gamma)]}{\omega_0^2(\Gamma - \beta_k + i\omega_1)} \exp[(t-T)(i\omega_1 + \Gamma) + \beta_k T + i\alpha] \\
&= \frac{8\Gamma\omega_1\lambda'}{\omega_0} \sum_{k=1}^4 a_k \exp(\beta_k t).
\end{aligned} \tag{32}$$

Comparing the coefficients of the exponential functions, $\exp \beta_k t$, on the two sides of the last equation, and recalling that $\cos \alpha = \omega_1/\omega_0$, we find

$$\lambda' = \frac{\omega_0^2 - \beta_k^2}{(\beta_k^2 + \omega_0^2)^2 - 4\Gamma^2 \beta_k^2} \quad \text{for } k = 1, 2, 3, 4. \tag{33}$$

Furthermore, the coefficients of $\exp t(\pm\Gamma \pm i\omega_1)$ must be zero because $\beta_k \neq \Gamma \pm i\omega_1$ and $\beta_k \neq -\Gamma \pm i\omega_1$. This yields four equations of constraint on the a_k :

$$\begin{aligned}
\sum_{k=1}^4 a_k \left(\frac{\Gamma + \beta_k + i\omega_1}{\Gamma + \beta_k - i\omega_1} \right) \exp -\beta_k T &= 0, \\
\sum_{k=1}^4 a_k \left(\frac{\Gamma - \beta_k + i\omega_1}{\Gamma - \beta_k - i\omega_1} \right) \exp +\beta_k T &= 0, \\
\sum_{k=1}^4 a_k \left(\frac{\Gamma + \beta_k - i\omega_1}{\Gamma + \beta_k + i\omega_1} \right) \exp -\beta_k T &= 0, \\
\sum_{k=1}^4 a_k \left(\frac{\Gamma - \beta_k - i\omega_1}{\Gamma - \beta_k + i\omega_1} \right) \exp +\beta_k T &= 0.
\end{aligned} \tag{34}$$

The existence of a non-zero solution for the a_k requires that the determinant

of the 4x4 matrix of the coefficients given by equations (34) vanish. This condition gives one equation for the β_k . Equations (33) provide 3 more independent constraints on the β_k . These four equations can be solved simultaneously to yield the four β_k . Next, we reduce the four β_k to a single unknown and also reduce the 4x4 matrix equation to 2x2 block diagonal form.

Consider two of the four β_k , say β_1 and β_2 , such that $\beta_1^2 \neq \beta_2^2$. Equation (33) is solved to provide a relation between β_1 and β_2 ,

$$\beta_1^2 + \beta_2^2 = 4\Gamma^2 - 2\omega_0^2 - 1/\lambda'. \quad (35)$$

Since $i\beta_1$ is a root of the real polynomial Q_1 , so is $-i\beta_1^*$. Thus, by taking the imaginary part of equation (35) we conclude that β_2 , and hence each of the β_k , must be either real or imaginary. We have shown in section II that the λ are positive. It follows that if $\Gamma < \omega_0/2$ equation (35) implies that at least one of the β_k must be imaginary. We name the imaginary β_k , β_1 . Since Q_1 is an even polynomial, the β_k must come in pairs of opposite sign. Thus, without loss of generality, the four β_k may be taken to be $\beta_1, \beta_2, -\beta_1$ and $-\beta_2$.

The first and second constraint equations (34) now take the form

$$\begin{aligned} \sum_{k=1}^2 \left[a_k \left(\frac{\Omega_+ + \beta_k}{\Omega_- + \beta_k} \right) \exp(-\beta_k T) + b_k \left(\frac{\Omega_+ - \beta_k}{\Omega_- - \beta_k} \right) \exp(+\beta_k T) \right] &= 0, \\ \sum_{k=1}^2 \left[a_k \left(\frac{\Omega_+ - \beta_k}{\Omega_- - \beta_k} \right) \exp(+\beta_k T) + b_k \left(\frac{\Omega_+ + \beta_k}{\Omega_- + \beta_k} \right) \exp(-\beta_k T) \right] &= 0, \end{aligned} \quad (36)$$

where $\Omega_{\pm} = \Gamma \pm i\omega_1$, $b_1 = a_3$ and $b_2 = a_4$. Adding and subtracting these two equations, we obtain

$$\begin{aligned} \sum_{k=1}^2 z_k \left[\left(\frac{\Omega_+ + \beta_k}{\Omega_- + \beta_k} \right) \exp(-\beta_k T) + \left(\frac{\Omega_+ - \beta_k}{\Omega_- - \beta_k} \right) \exp(\beta_k T) \right] &= 0, \\ \sum_{k=1}^2 z'_k \left[\left(\frac{\Omega_+ + \beta_k}{\Omega_- + \beta_k} \right) \exp(-\beta_k T) - \left(\frac{\Omega_+ - \beta_k}{\Omega_- - \beta_k} \right) \exp(\beta_k T) \right] &= 0, \end{aligned} \quad (37)$$

where

$$z_1 = a_1 + b_1, \quad z_2 = a_2 + b_2, \quad z'_1 = a_1 - b_1, \quad z'_2 = a_2 - b_2. \quad (38)$$

Two other equations in the z_k and the z'_k are obtained by interchanging Ω_+ and Ω_- in equation (37).

The advantage of these new variables over the a_k is that they reduce the 4×4 matrix which expresses the equations of constraint to 2×2 block diagonal form. For convenience, we define $\beta_j^{(1)} = \beta_j$ and $\beta_j^{(2)} = -\beta_j$ for $j=1,2$. Then, the requirement that the determinant of the 4×4 matrix vanish reduces to the vanishing of the determinant of either one of the following 2×2 matrices

$$\begin{vmatrix} \sum_{k=1}^2 \left(\frac{\Omega_+ + \beta_1^{(k)}}{\Omega_- + \beta_1^{(k)}} \right) \exp(-\beta_1^{(k)} T); & \sum_{k=1}^2 \left(\frac{\Omega_+ + \beta_2^{(k)}}{\Omega_- + \beta_2^{(k)}} \right) \exp(-\beta_2^{(k)} T) \\ \sum_{k=1}^2 \left(\frac{\Omega_- + \beta_1^{(k)}}{\Omega_+ + \beta_1^{(k)}} \right) \exp(-\beta_1^{(k)} T); & \sum_{k=1}^2 \left(\frac{\Omega_- + \beta_2^{(k)}}{\Omega_+ + \beta_2^{(k)}} \right) \exp(-\beta_2^{(k)} T) \end{vmatrix} = 0, \quad (39)$$

or

$$\begin{vmatrix} \sum_{k=1}^2 i^{2k} \left(\frac{\Omega_+ + \beta_1^{(k)}}{\Omega_- + \beta_1^{(k)}} \right) \exp(-\beta_1^{(k)} T); & \sum_{k=1}^2 i^{2k} \left(\frac{\Omega_+ + \beta_2^{(k)}}{\Omega_- + \beta_2^{(k)}} \right) \exp(-\beta_2^{(k)} T) \\ \sum_{k=1}^2 i^{2k} \left(\frac{\Omega_- + \beta_1^{(k)}}{\Omega_+ + \beta_1^{(k)}} \right) \exp(-\beta_1^{(k)} T); & \sum_{k=1}^2 i^{2k} \left(\frac{\Omega_- + \beta_2^{(k)}}{\Omega_+ + \beta_2^{(k)}} \right) \exp(-\beta_2^{(k)} T) \end{vmatrix} = 0. \quad (40)$$

Here, β_2 is determined in terms of β_1 from equation (35). This completes our reduction of the integral eigenvalue equation (6) to an algebraic equation.

IV. THE DISTRIBUTION FUNCTIONS

We solve the independent transcendental equations (39) and (40) numerically to obtain two infinite sequences of values for β_1 . Given β_1 the eigenvalue λ' is obtained from equation (33). We arrange the eigenvalues in each sequence in order of decreasing size and label them by consecutive positive and negative integers, respectively. The sum of all the eigenvalues, λ'_n , is equal to T/Γ . This result follows from equating the expectation value of the integral over $(-T, T)$ of the absolute square of equation (8) to $2T$ times the trace of $\mathcal{R}(t, t)$ obtained from equation (20). The largest eigenvalues, divided by T/Γ , are displayed in Figure 1 for several values of ΓT . Note that the width of the peak decreases with increasing ΓT and that there is approximately unit area under each curve

To obtain an accurate expression for the characteristic function \mathcal{C}_{E_T} , the sum of the eigenvalues used in equation (14) must be close to T/Γ . As equation (33) indicates, $\lambda(\beta_1)$ peaks for β_1 close to $i\omega_0$ and is independent of T . In our determinations of \mathcal{C}_{E_T} we use only the few largest λ_n for $\Gamma T \lesssim 1$ but more than a hundred for $\Gamma T \gtrsim 10$.

The probability distribution function is obtained by taking the inverse Fourier transform of \mathcal{C}_{E_T} . It is a function of two dimensionless parameters, ΓT and Γ/ω_0 . For $\Gamma/\omega_0 \ll 1$, the case of interest to us, the dependence on Γ/ω_0 is very weak and may be ignored. Figure 2 displays the distribution function for several values of ΓT . For $\Gamma T \ll 1$ the distribution function has the Boltzmann form; that is, it is a decreasing exponential. With increasing ΓT the peak of the distribution functions narrows and it shifts towards the mean energy of the oscillator. For $\Gamma T \gg 1$ the distribution function tends to a delta function. The limiting distributions can be obtained analytically from equations (6), (19) and (30).

Our calculations for the distribution functions successfully passed the following three tests. Both the integrated distribution functions and the mean energy are

independent of T and the sum of the λ'_n are equal to T/Γ . There is one additional test of our calculations. For $\Gamma T \gtrsim 1$ the orthogonal series expansion of \mathbf{x} is approximately the same as the Fourier series expansion over the interval $(-T, T)$, as expected.

V. NUMERICAL SIMULATIONS

We can model the random force $F(t)$ as a Poisson process by setting it equal to a random sequence of delta function impulses which occur at times t_n . The time intervals

$$\Delta t_n \equiv t_{n+1} - t_n \quad (41)$$

are independent random variables. The probability density for the waiting time between impulses, Δt , is given by

$$P(\Delta t) = r \exp(-r\Delta t), \quad (42)$$

where r denotes the average number of impulses per unit time. The random variable Δt may be generated from a random variable y which is uniformly distributed on the interval (0,1) by using the relation

$$\Delta t = -\frac{1}{r} \ln(y). \quad (43)$$

Between impulses $q(t)$ satisfies the homogeneous version of equation (1) and can be written in the form

$$q_n(t) = A_n \exp[-(\Gamma - i\omega_1)(t - t_n)] + A_n^* \exp[-(\Gamma + i\omega_1)(t - t_n)], \quad (44)$$

for $t_n \leq t < t_{n+1}$. Inserting $F(t) = p\delta(t - t_{n+1})$, where p is a random sign (± 1), into equation (15) we obtain

$$q_{n+1}(t) = q_n(t) + \frac{p}{M} G(t, t_{n+1}). \quad (45)$$

Substituting for the Green's function, G , from equation (16), equations (44) and (45) define a mapping from A_n and A_{n+1} , namely,

$$A_{n+1} = A_n \exp[-\Delta t_n(\Gamma - i\omega_1)] - \frac{ip}{2\omega_1}. \quad (46)$$

We define E_n to be the energy immediately following the n th impulse at $t = t_n$. With the aid of equations (2) and (44) it may be expressed as

$$E_n = M\omega_0^2 \left[4|A_n|^2 + A_n^2 + A_n^{*2} - A_n^2 \exp(2i\alpha) - A_n^{*2} \exp(-2i\alpha) \right], \quad (47)$$

where $\sin \alpha = \Gamma/\omega_0$.

We have now assembled all the ingredients needed to calculate a string of values of E_n . The initial conditions are specified by choosing a value for A_0 . The time intervals between consecutive impulses are determined from equation (43) with the values of y obtained from a uniform random number generator. The new amplitude and the energy of the oscillator immediately after an impulse are calculated using equations (46) and (47), respectively. Taking a running mean over time $2T$ of the sequence of values for E yields a sequence of values for E_T . It is then a straightforward matter to compute approximate distribution functions for E_T and to demonstrate empirically that they converge to the distribution functions derived theoretically.

A theoretically computed distribution function for E_T corresponds to an infinite data sample, whereas observations inevitably produce a finite data sample. Figure 2 illustrates how observationally determined distribution functions might appear in comparison to our theoretically predicted ones. These plots display approximate distribution functions computed from data simulated for 100 damping times, along with the theoretical distribution functions. The distribution function obtained from a simulated data of 1000 damping time is quite indistinguishable from the theoretical distribution. In addition, we show in Figure 3 a portion of the strings of values of E_T from which each of these distribution functions is obtained.

V. OBSERVATIONAL IMPLICATIONS

One of our goals is to determine, with the help of the observations, if the solar p-modes are randomly excited. So far our discussion has been rather abstract and consequently its relevance to the excitation of the solar oscillations may be a bit obscure. Here, we briefly indicate some ways in which the results of this investigation might aid in the understanding of the solar oscillations.

The most obvious application of our results would be to compare the theoretically calculated distribution functions for E_T with those determined from observations of solar p-modes. The observational determination of the distribution function requires many independent samples of E_T for a single mode. Since the lifetimes of the modes in the 5-minute band are of order days, rather lengthy data strings will be required to obtain accurate distribution functions for single modes (cf. Figure 2). A more economical approach might be to treat modes with the same n and ℓ but different m as copies of a single mode. It might be still better to further enlarge the set of similar modes to include those with a range of ℓ values at a fixed value of n . For instance, lumping together all modes with fixed n having $90 < \ell < 110$ and including all values of m gives a set of about 4,000 individual modes.

The spectral density of a random process is the expectation value of the time averaged, absolute square of the finite Fourier transform in the limit of infinite averaging time. The Wiener-Khinchin theorem (Goodman 1985) states that the spectral density is equal to the Fourier transform of the autocorrelation function. Thus, the spectral density for q , $P_q(\omega)$, is equal to $\tilde{\mathcal{R}}_{11}(\omega)/\omega_0^2$, which from equation (22) is given by

$$P_q(\omega) = \frac{g}{\sqrt{2\pi}M^2} \frac{1}{(\omega^2 - \omega_0^2)^2 + 4\omega^2\Gamma^2}. \quad (48)$$

To a very good approximation $P_q(\omega)$ is Lorentzian, with linewidth, Γ , near the peak of the power spectrum which is located at $\sqrt{\omega_0^2 - 2\Gamma^2}$. Thus, the drag force

responsible for the damping produces a small frequency shift,

$$\Delta\omega \approx -\frac{\Gamma^2}{\omega_0}. \quad (49)$$

For solar p-modes in the five minute band $\Gamma \sim 1\mu\text{Hz}$ (Libbrecht and Zirin 1986, Isaak 1986). Thus, the frequency shift caused by the decay is $\lesssim 1\text{Hz}$, which is much smaller than typical errors in the frequency measurements, $\sim 0.1\mu\text{Hz}$, and is insignificant compared to the discrepancies between the observed and theoretically computed frequencies, $\sim 15\mu\text{Hz}$.

The mean energy, \bar{E} , is equal to $M/2$ times the trace of $\mathcal{R}(t, t)$. Using equation (20) we obtain

$$\bar{E} = \frac{g}{4M\Gamma}. \quad (50)$$

We may generalize the expression for \bar{E} so that it applies to an arbitrary random force by replacing g by the spectral density of the random force evaluated at frequency ω_0 . Thus, different oscillators interacting with random forces which have the same $g(\omega_0)$ should have identical values for the products of their mean energies, linewidths and masses.

The excitation and damping of solar oscillations by turbulent convection are described by effective random forces and damping constants for which $g(\omega_0)$ and Γ are given by overlap integrals of particular combinations of modal eigenfunctions and turbulent fields (Goldreich and Keeley 1977, Goldreich and Kumar 1987). Since the excitation and damping by turbulence depend sensitively upon the turbulent Mach number, it is likely that both are dominated by contributions from the upper few scale heights of the solar convection zone.

The radial displacement dominates the horizontal displacement for p-modes in the five minute band with $\ell \lesssim 200$. Moreover, the shape of the radial displacement component of the eigenfunction in the upper convection zone depends only on fre-

quency and is independent of ℓ . Thus, we would expect modes which have the same frequencies but different values of ℓ and m to have identical values of $M\bar{E}\Gamma$ if they are stochastically excited by turbulent convection. If, in addition, either turbulent convection or radiative dissipation near the photosphere is the major source of damping, Γ should be inversely proportional to the mass of the mode.³ This would lead to a stronger prediction, namely, that all modes of a given frequency having $\ell \lesssim 200$ should have the same value of \bar{E} .

The observational results of Libbrecht *et al.* (1986) suggest that the energies of p-modes in the five minute band are approximately independent of ℓ , at least for $\ell \lesssim 100$.

Acknowledgments

The research reported in this paper was supported by NSF through grant AST-861299.

³ The mass of a mode is the ratio of its total energy to the square of its rms, photospheric, radial velocity.

REFERENCES

- Davenport, W.B. jr., and Root, W.L., 1958, *An Introduction to the Theory of Random Signals and Noise* (New York: McGraw-Hill Book Co, Inc).
- Goldreich, P. and Keeley, D., 1977, *Ap. J.*, **212**, 243.
- Goldreich, P. and Kumar, P., 1987, *in preparation*.
- Goodman, J.W., 1985, *Statistical Optics* (New York: John Wiley and Sons).
- Isaak, G.R. 1986, in *Seismology of the Sun and the Distant Stars*, ed. D.O. Gough (Dordrecht: Reidel), 223.
- Libbrecht, K.G., and Zirin, H., 1986, *Ap. J.*, **308**, 413.
- Libbrecht, K.G., Popp, B.D., Kaufman, J.M., and Penn, M.J., 1986, *Nature*, **323**, 235.

FIGURE CAPTIONS

Figure 1. Plot of the largest eigenvalues (λ') times Γ/T for the two families of eigenfunctions for three cases of averaging times. The eigenvalues have been arranged in a descending series and labeled by positive and negative integers for the two families. The solid curve is for $\Gamma T = 0.5$, the dashed curve for $\Gamma T = 4$ and the dash dot curve for $\Gamma T = 32$.

Figure 2. The dark solid curves are theoretically determined distribution functions for four different values of ΓT , and in each case are same in the range $10 \leq \omega_0/\Gamma \leq \infty$. The light solid curves are distribution functions obtained from a string of simulated data 100 damping times long, with r equal to five hits per period and $\omega/\Gamma = 10^3$.

Figure 3. A sample of the average energy as a function of time for the four averaging times considered above.

Figure 1

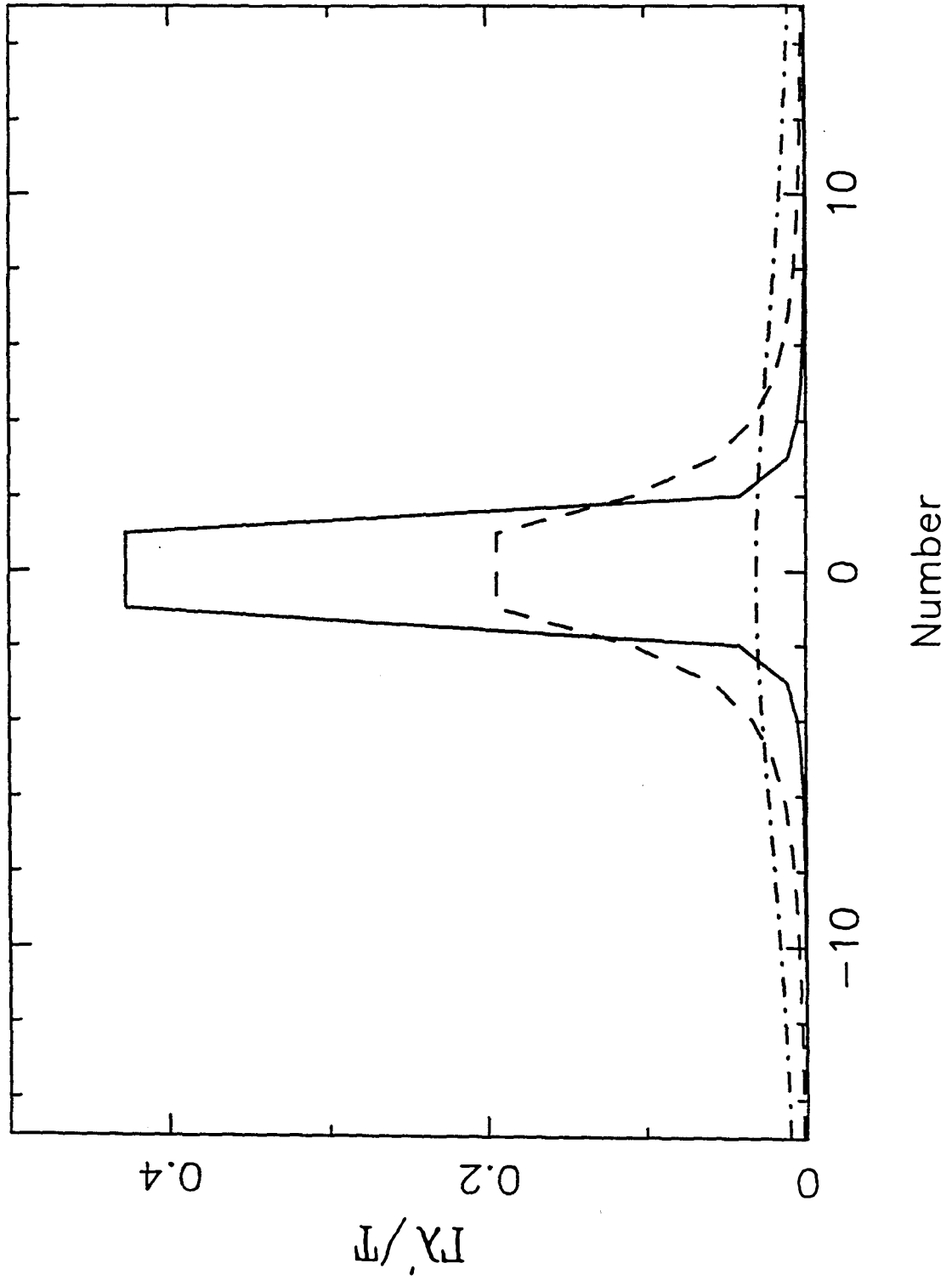


Figure 2

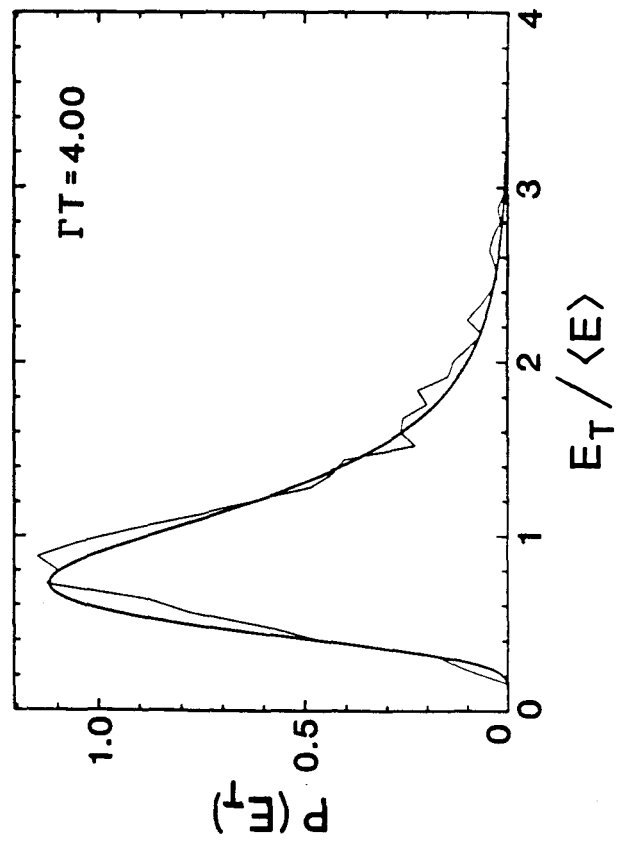
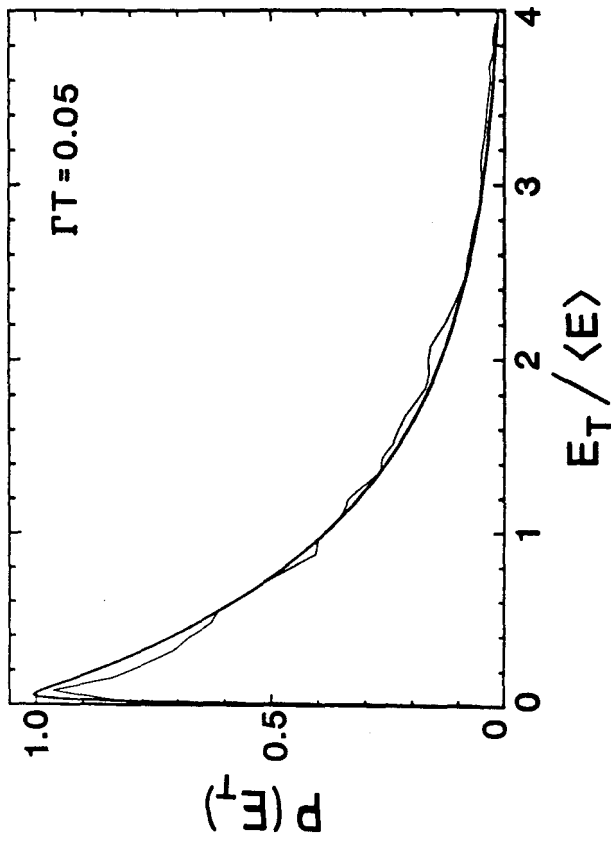
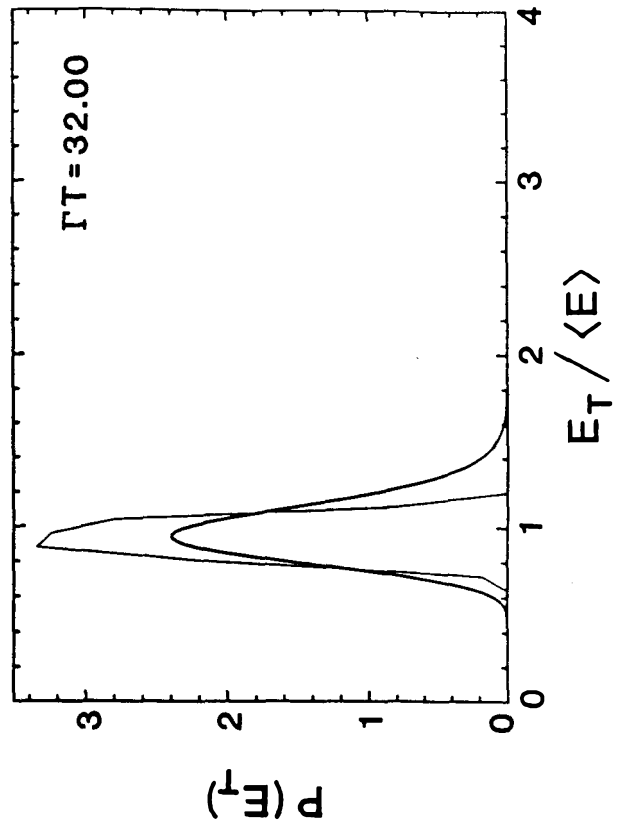
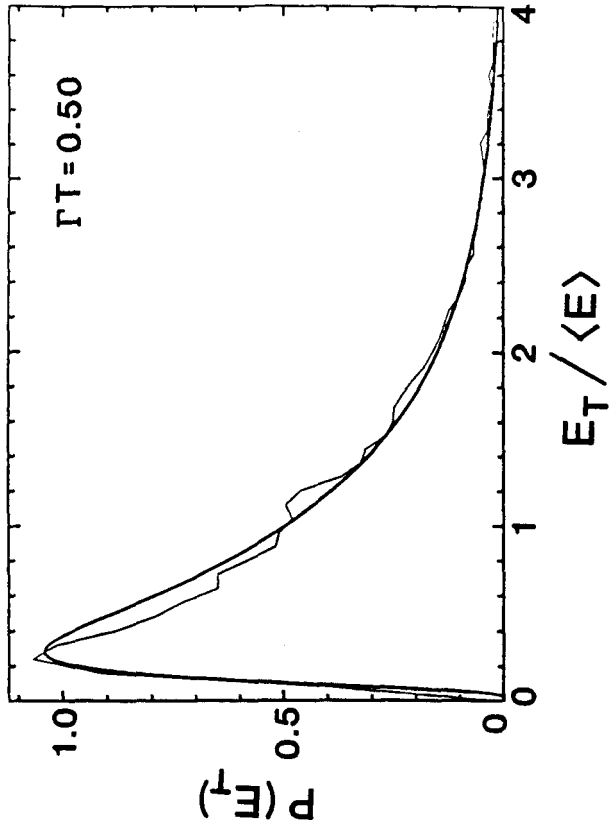
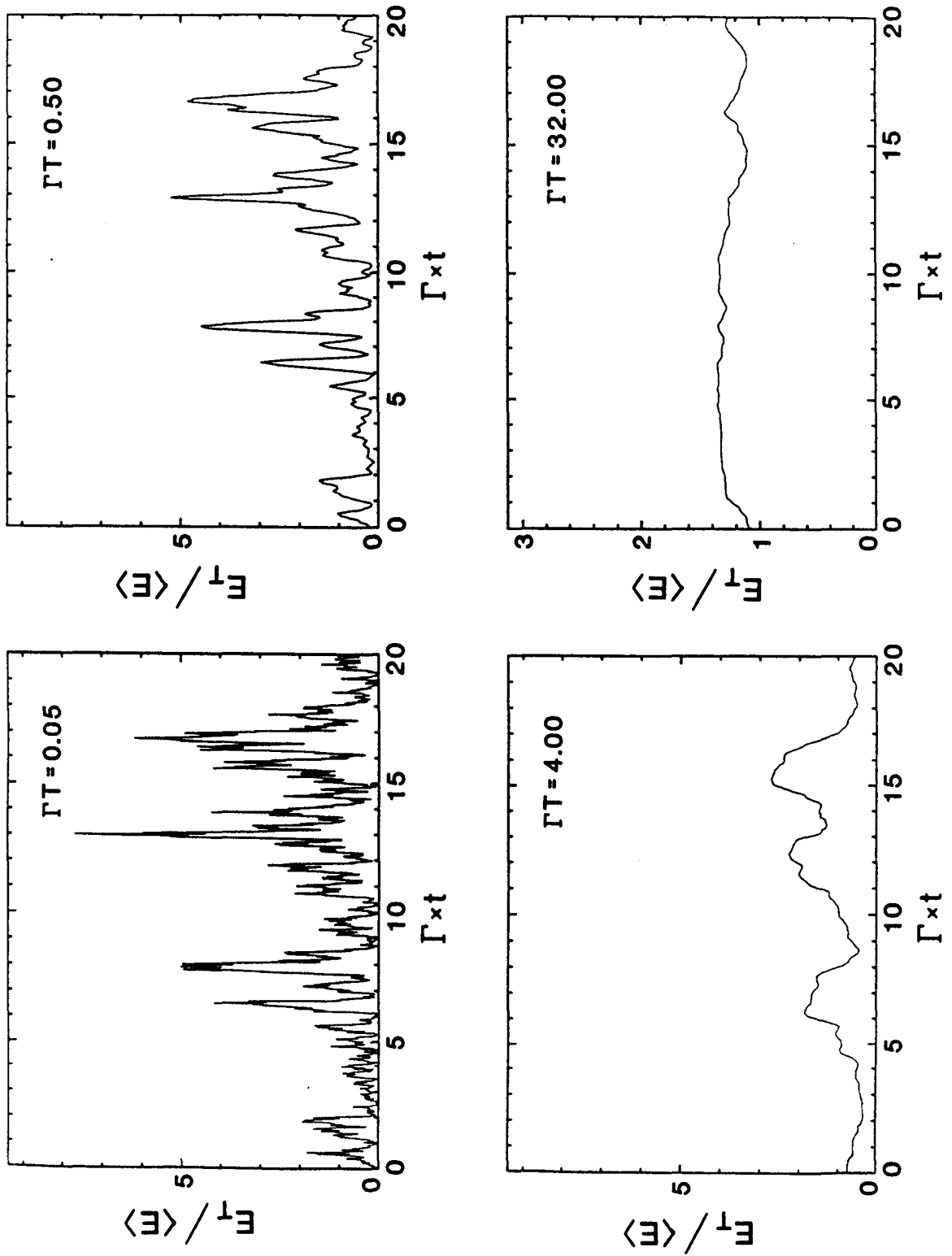


Figure 3



CHAPTER 5

3-mode Couplings of Solar p-modes

To be submitted to the **Astrophysical Journal**

3-mode Couplings of Solar p-modes

Pawan Kumar and Peter Goldreich

California Institute of Technology, Pasadena, California

ABSTRACT

We evaluate the rates at which nonlinear interactions transfer energy among the acoustic modes of a plane parallel, stratified atmosphere which resembles the outer part of the Sun including the convection zone and the optically thin region above the photosphere upto the temperature minimum. The acoustic modes are assigned energies such that their photospheric velocities match those of the Sun's p-modes. The nonlinearity parameter is the acoustic Mach number, M , the ratio of the total acoustic velocity due to all of the modes to the sound speed. For $M^2 \ll 1$ the leading nonlinear interactions are those of lowest order in M which couple 3-modes. We show that every p-mode in the 5-minute band is involved in many resonant triplets. As a consequence, the energy transfer rates are independent of the mode linewidths. Because M increases with height, the dominant contributions to the 3-mode coupling coefficients occur in the upper part of the convection zone and in the optically thin atmosphere and the coupling coefficients tend to increase with ω and k_h .

Nonlinear interactions which involve 2 trapped modes and 1 propagating mode drain energy from the trapped modes. They are far more effective than interactions among 3 trapped modes which tend to drive the modes toward equipartition of energy. Thus, every trapped p-mode suffers a net loss of energy due to its nonlinear interactions. Estimates of the nonlinear energy transfer rates are plagued by two uncertainties. Some of the coefficients which couple 2 trapped modes to a propagating mode formally diverge if the isothermal atmosphere is extended to infinity; physically, this reflects the exponential growth of the acoustic Mach number with height in the isothermal atmosphere. The energy transfer rates are sensitive to the unknown energies of the high frequency trapped modes. Plausible assumptions lead to energy transfer rates which range from 10 to 100 percent of the products of the mode energies and linewidths. Thus, we can only speculate on whether nonlinear mode coupling is an important damping process for the solar p-modes. Its observational signature would be a decrease in the energy per mode with increasing ℓ at fixed ω . Moreover, it might be, at least in part, responsible for the steep decline in the energy per mode at frequencies above 3 mHz which is usually attributed to radiative damping.

Our investigation indirectly bears on the question of the stability of the p-modes. We have evaluated the rates at which 3-mode couplings transfer energy to the f-modes. The f-mode energies are comparable to those of p-modes with the same frequencies. Every calculation of which we are aware predicts stability for the f-modes. Thus, even if the excitation of the p-modes is due to overstability, the excitation of the f-modes would require a separate explanation. The most plausible hypothesis would be that nonlinear interactions transfer energy from overstable p-modes to the f-modes. However, our calculations indicate that nonlinear interactions tend to damp rather than to excite the f-modes. This result favors the hypothesis that the Sun's f-modes, and by implication its p-modes as well, are stochastically excited by turbulent convection.

I. INTRODUCTION

In this paper we develop a method for evaluating nonlinear interactions among acoustic modes. We apply our method to calculate the rates of energy transfer among the p-modes of a plane parallel model atmosphere. The properties of the atmosphere and the energies of the modes are chosen to resemble those of the Sun. These rates are then compared to the mode lifetimes to assess whether nonlinear interactions play a significant role in establishing the mode energies. The investigation is motivated by our desire to decide which mechanism is responsible for the excitation of the solar p-modes.

One might question why, more than 25 years after the discovery of the 5-minute oscillations of the Sun by Leighton, Noyes and Simon (1961) and Evans and Michard (1962), we are reduced to taking this indirect approach to determine how these oscillations are excited. The answer is simple. There are two leading contenders for the excitation mechanism, self excitation by the opacity (κ) mechanism (Ando and Osaki 1975, Goldreich and Keeley 1977a) and stochastic excitation by turbulent convection (Goldreich and Keeley 1977b). Unfortunately, neither observation nor theory has been able to establish which, if either, is the correct choice. The linear stability of the solar p-modes is unresolved despite several theoretical investigations aimed at providing a conclusive answer (Ando and Osaki 1975, Goldreich and Keeley 1977a, Christensen-Dalsgaard and Frandsen 1982, Antia, Chitre and Narashima 1986, Kidman and Cox 1984). Its resolution must await significant advances in modeling the interaction of turbulent convection with pulsation and in treating radiative transfer in the transition region between high and low optical depth. The inconclusive nature of previous stability calculations is apparent; small and uncertain effects control the delicate balance between stability and overstability. Calculations of the stochastic excitation of the solar modes are plagued by the lack of an adequate theory for the interaction of acoustic radiation with turbulence, although there is encouraging recent progress on this front (Goldreich and Kumar

1987).

Given the current situation it is not clear how best to proceed to determine the mechanism responsible for the excitation of the p-modes. An alternative to refining the stability calculations or the theory of the interaction of acoustic radiation with turbulence is to assume that the modes are either stable or overstable and then to explore the implications of each assumption. As discussed below, this approach suggests that knowledge of the rates at which nonlinear interactions transfer energy among the p-modes would indirectly help to resolve the issue of mode stability.

If we assume that at least some of the p-modes are linearly overstable, there must be a nonlinear mechanism which saturates the instability and accounts for the observed amplitudes of the modes. An obvious possibility is that overstable modes transfer energy to damped modes. The lowest order mode couplings involve near resonant mode triplets. In order to serve as an amplitude limiting process, these 3-mode couplings must be able to drain the energy from the overstable modes on their linear e-folding timescales.

If the solar p-modes are linearly damped, the power in the 5-minute band probably results from the emission and absorption of acoustic radiation by turbulence near the top of the Sun's convection zone. The 3-mode couplings are less crucial if the p-modes are stable. However, they still act to redistribute energy among the different modes. This raises the question of whether an individual mode is more strongly coupled to the turbulent convection or to other acoustic modes.

The paper is organized as follows. In Section II we describe the plane parallel atmosphere and the properties of its acoustic modes. We apply a Hamiltonian method to derive the lowest order nonlinear interactions, the 3-mode couplings, in Section III. Section IV outlines the main features of the numerical procedure we use to calculate the rates at which 3-mode interactions transfer energy among the p-modes. We compare these calculated rates to the observed linewidths, and explore the implications of this comparison for identifying the excitation mechanism of the

solar p-modes, in Section V.

II. P-MODES OF THE MODEL ATMOSPHERE

Our computations are performed for the p-modes of a plane parallel atmosphere. To begin we imagine that the system has horizontal cross sectional area, A , and is enclosed between rigid vertical walls. Ultimately, we take the limit $A \rightarrow \infty$. The atmosphere sits in a uniform gravitational field and is composed of two layers, the lower adiabatic and the upper isothermal. The thermodynamic variables, pressure, density and temperature, are continuous across the interface between the two layers. However, the density gradient is not. The adiabatic index, Γ , is set equal to $5/3$ in both layers. The atmospheric parameters are listed in Table 1. They are chosen so that the atmosphere resembles the region of the Sun between the bottom of the convection zone and the temperature minimum. Except for its top few scale heights the solar convection zone is nearly adiabatic, and the optically thin region above the solar photosphere may be crudely represented as isothermal. However, the upper part of the Sun’s convective envelope possesses both a superadiabatic region and ionization zones of which our model atmosphere takes no account.

We take the vertical coordinate, z , to increase in the direction of the gravitational acceleration, \vec{g} , from $z = z_t$ at the interface between the two layers to $z = z_b$ at the bottom of the adiabatic zone. Because the unperturbed atmosphere is both static and plane parallel, all of the variables associated with the modes depend on x , y and t as $\exp i(\vec{k}_h \cdot \vec{x} - \omega t)$ where \vec{k}_h is the horizontal wave vector and ω is the radian frequency.¹ We adopt the Eulerian enthalpy perturbation, $Q = p_1/\rho$, where p_1 is the Eulerian pressure perturbation and ρ is the unperturbed density, as the dependent variable in the wave equation.

In the adiabatic atmosphere the linear wave equation reads

¹ The magnitude of \vec{k}_h is related to the angular order, ℓ , of the corresponding solar mode by $k_h R_\odot = \ell$.

$$\frac{d^2 Q}{dz^2} + \frac{3}{2z} \frac{dQ}{dz} + \left(\frac{\omega^2}{c^2} - k_h^2 \right) Q = 0, \quad (1)$$

where the adiabatic sound speed, c , satisfies $c^2 = 2gz/3$. The displacement vector, $\vec{\xi}$, is related to Q by

$$\vec{\xi}_h = i \frac{\vec{k}_h Q}{\omega^2}, \quad \xi_z = \frac{1}{\omega^2} \frac{dQ}{dz}. \quad (2)$$

Changing the independent variable from z to $x = z^{1/2}$ transforms equation (1) into

$$\frac{d^2 Q}{dx^2} + \frac{2}{x} \frac{dQ}{dx} + \left(\frac{6\omega^2}{g} - 4k_h^2 x^2 \right) Q = 0, \quad (3)$$

which reduces to the differential equation for spherical Bessel functions of zeroth order in the limit $k_h \rightarrow 0$.

Equation (3) is a classic example of a differential equation with two turning points. A simple WKB analysis yields the approximate analytic solution

$$Q \propto \frac{1}{z^{1/2}} \exp i \left(\int^z dz' k_z(z') + \delta \right), \quad (4)$$

where δ is a constant phase which is determined by the boundary conditions and

$$k_z(z) = \sqrt{\frac{3\omega^2}{2gz} - k_h^2}. \quad (5)$$

The upper and lower turning points are at

$$z_1 \approx \frac{2g}{3\omega^2} \quad (6)$$

and

$$z_2 \approx \frac{3\omega^2}{2gk_h^2}. \quad (7)$$

Between the turning points, $z_1 < z < z_2$, the WKB *envelopes* of the components of $\vec{\xi}$ satisfy

$$\xi_h \propto \frac{1}{z^{1/2}}, \quad \xi_z \propto \frac{1}{z}. \quad (8)$$

Since

$$\frac{k_z}{k_h} \approx \sqrt{\frac{z_2}{z} - 1}, \quad (9)$$

ξ_z is the dominant component of $\vec{\xi}$ except very close to the lower turning point.

In the isothermal atmosphere linear, adiabatic wave propagation is governed by

$$\frac{d^2 Q}{dz^2} + \frac{5g}{3c_0^2} \frac{dQ}{dz} + \left(\frac{\omega^2}{c_0^2} - k_h^2 + \frac{2g^2 k_h^2}{3c_0^2 \omega^2} \right) Q = 0, \quad (10)$$

where c_0 is the adiabatic sound speed. The displacement vector, $\vec{\xi}$, is related to Q by

$$\vec{\xi}_h = i \frac{k_h \vec{Q}}{\omega^2} \quad \xi_z = \left(\omega^2 - \frac{2g^2}{3c_0^2} \right)^{-1} \left(\frac{dQ}{dz} + \frac{2g}{3c_0^2} Q \right). \quad (11)$$

The differential equation (10) has constant coefficients so it may be solved analytically. The acoustic cutoff frequency, ω_{ac} , separates the evanescent from the propagating solutions. Expressed in terms of the scale height,

$$H = \frac{3c^2}{5g}, \quad (12)$$

the relation for ω_{ac} reads

$$\left(\frac{2\omega_{ac}H}{c_0} \right)^2 = \frac{1}{2} \left\{ [1 + (2k_h H)^2] + \sqrt{[1 + (2k_h H)^2]^2 - \frac{96}{25}(2k_h H)^2} \right\}. \quad (13)$$

As the above equation shows, ω_{ac} decreases with increasing k_h , but its dependence on k_h is weak for $k_h H \ll 1$ and, in this limit, equation (13) simplifies to $\omega_{ac} \approx c_0/2H = 5g/(6c_0)$. For $\omega < \omega_{ac}$ both solutions of equation (10) grow exponentially with height with inverse scale lengths given by

$$\kappa_{\pm} H = \frac{1}{2} \left\{ 1 \pm \sqrt{1 - \left(\frac{2\omega H}{c_0} \right)^2 + (2k_h H)^2 \left[1 - \frac{24}{25} \left(\frac{c_0}{2\omega H} \right)^2 \right]} \right\}. \quad (14)$$

The more slowly growing solution is the appropriate one for evanescent disturbances which originate within the adiabatic layer. For $k_h H \ll 1$ the expression for its inverse scale simplifies to

$$\kappa_{-H} \approx \frac{1}{2} \left[1 - \sqrt{1 - \left(\frac{\omega}{\omega_{ac}} \right)^2} \right]. \quad (15)$$

The propagating solutions of equation (10) also grow exponentially with height with $\kappa H = 1/2$ as required by flux conservation.

The eigenfrequencies and their associated eigenfunctions are obtained, for a given value of k_h , by numerically integrating equation (1) through the adiabatic layer and then matching the solutions to the analytic solutions of equation (10) in the isothermal layer. The evanescent solutions of the latter equation are taken for the trapped modes; otherwise, upward propagating waves are the correct choice. The remaining boundary conditions, most conveniently expressed in terms of ξ_z , are that $\xi_z(z_b) = 0$ and $\xi_z(z_t)$ is continuous. It is easy to verify that the latter condition implies the continuity of both Q and $\vec{\xi}_h$ across $z = z_t$. In addition to its value of \vec{k}_h , each normal mode is specified by the number of nodes, n , in its vertical displacement eigenfunction. As a shorthand notation, we often denote the pair (\vec{k}_h, n) by a single Greek letter.

The $k_h - \omega$ diagram for the p-modes of the model atmosphere is displayed in Figure 1. It looks quite similar to that for the solar p-modes except at small k_h where the finite depth of the adiabatic layer is responsible for changing the curvature of the dispersion ridges. The return to normal curvature is marked by the clustering of the ridges along a thin, almost vertical, line. There is an additional, barely perceptible, curvature variation along each ridge at $\omega \approx 5.5 \times 10^{-2}$ Hz which is associated with the transition between trapped and propagating modes. For k_h sufficiently large that bottom effects are negligible, the dispersion curves are well

fitted by the analytic formula

$$\omega = \frac{4}{3} g k_h \left(n + \frac{3}{4} \right). \quad (16)$$

Equation (16) is deduced by interpolating between the dispersion relation for the fundamental mode, $n = 0$, obtained by setting the Lagrangian density perturbation equal to 0, and the dispersion relation for large n derived from a WKB analysis.

A detailed comparison of the dispersion curves for the model atmosphere with those for the Sun reveals that, for $n > 0$ and large k_h , the former lie systemically above the latter.² This difference arises because, at depth, the temperature is lower at a given pressure in the Sun than in the model atmosphere; the lowering of the temperature gradient due to the reduction of Γ in the ionization zones more than compensates for the superadiabatic temperature gradient at the top of the convection zone in determining the run of temperature with depth in the Sun. The higher temperature of the model atmosphere leads to a higher sound speed and thus to higher frequency p-modes.

Expanding $\vec{\xi}$ in the terms of the normal modes of the system, we obtain

$$\vec{\xi} = \sum_{\alpha} \sqrt{\frac{\omega_{\alpha} J_{\alpha}}{2A}} \left\{ \vec{\xi}_{\alpha}(z) \exp(i\vec{k}_h \cdot \vec{x} - i\phi_{\alpha}) + \vec{\xi}_{\alpha}^{*}(z) \exp(-i\vec{k}_h \cdot \vec{x} + i\phi_{\alpha}) \right\}, \quad (17)$$

where the sum over α is three dimensional, two dimensions for \vec{k}_h and one for n . The phase $\phi_{\alpha}(t) = \omega_{\alpha} t + \epsilon_{\alpha}$. The eigenfunctions are normalized such that³

² Of course, the $n = 0$ curves are in excellent agreement because we have chosen the density at the top of the adiabatic layer of the model atmosphere to match that of the solar photosphere.

³ Only the trapped modes are strictly orthogonal. However, the propagating modes of interest to us have large enough Q 's so that we may neglect the imaginary parts of their frequencies and include them among the orthogonal modes.

$$\omega_\alpha^2 \int dz \rho \vec{\xi}_{k_h, n}^- \cdot \vec{\xi}_{k_h, m}^* = \delta_{n, m}. \quad (18)$$

We define the mass per unit surface area in mode α to be the ratio of its energy per unit surface area to its mean square surface velocity;

$$\mathcal{M}_\alpha \equiv \frac{1}{\omega^2 |\vec{\xi}_\alpha(0)|^2}. \quad (19)$$

Since $|\vec{\xi}(z)|$ grows exponentially with height in the isothermal layer (cf. eqns [14] and [15]), \mathcal{M}_α decreases exponentially with the height of the layer in which the surface velocity is defined. The sensitivity of \mathcal{M}_α to height is small for $\omega \ll \omega_{ac}$ and increases monotonically with ω . The p-mode masses derived from our model atmosphere, $4\pi R_\odot^2 \mathcal{M}_\alpha$, are slightly larger at low ℓ and slightly smaller at high ℓ than those derived from a standard solar model. The model masses track the solar ones fairly well as ω varies in spite of the limitations of the model atmosphere in representing the Sun.

III. 3-MODE COUPLINGS

a) Hamiltonian Formalism

We adopt a Hamiltonian approach to the calculation of mode coupling. The Hamiltonian is expanded in powers of the displacement vector $\vec{\xi}$. The second order terms yield the linear differential equations (1) and (10) for the normal modes and the third order terms describe their nonlinear interactions. We assume that the interactions among the modes are sufficiently weak so that they may be determined perturbatively.

The second and third order parts of the Hamiltonian density, appropriate to the adiabatic perturbations of a static configuration composed of a perfect gas, take the form (cf. Appendix I)

$$\mathcal{H} = \mathcal{H}_2 + \mathcal{H}_3, \quad (20)$$

where

$$\mathcal{H}_2 = \frac{\rho}{2} \left(\frac{\partial \vec{\xi}}{\partial t} \right)^2 + \frac{P}{2} \left[(\Gamma - 1)(\vec{\nabla} \cdot \vec{\xi})^2 + \xi_{i,j} \xi_{j,i} \right], \quad (21)$$

and

$$\mathcal{H}_3 = -P \left[\frac{(\Gamma - 1)^2}{6} (\vec{\nabla} \cdot \vec{\xi})^3 + \frac{(\Gamma - 1)}{2} (\vec{\nabla} \cdot \vec{\xi}) \xi^{i,j} \xi^{j,i} + \frac{1}{3} \xi^{i,j} \xi^{j,k} \xi^{k,i} \right]. \quad (22)$$

We evaluate the 3-mode couplings among the acoustic modes of the plane parallel, stratified atmosphere described in the previous section. Expressing the second order Hamiltonian density, \mathcal{H}_2 , in the terms of the normal modes and integrating it over volume, we find

$$H_2 \equiv \int d^3x \mathcal{H}_2 = \sum_{\alpha} \omega_{\alpha} J_{\alpha} = \sum_{\alpha} E_{\alpha}. \quad (23)$$

Thus, the energy in mode α , $E_{\alpha} = \omega_{\alpha} J_{\alpha}$.

Next, we expand \mathcal{H}_3 in the terms of the normal modes and integrate it over space to obtain

$$\begin{aligned}
 H_3 &\equiv \int d^3x \mathcal{H}_3 \\
 &= \sum_{\alpha_{s\alpha}, \beta_{s\beta}, \gamma_{s\gamma}} \sqrt{\frac{E_\alpha E_\beta E_\gamma}{8A}} K_{\alpha_{s\alpha} \beta_{s\beta} \gamma_{s\gamma}} \exp[-i(s_\alpha \phi_\alpha + s_\beta \phi_\beta + s_\gamma \phi_\gamma)].
 \end{aligned} \tag{24}$$

The terms in the above sum are restricted by the conservation of horizontal momentum expressed through the matching condition on the horizontal wavevectors,

$$s_\alpha \vec{k}_{h\alpha} + s_\beta \vec{k}_{h\beta} + s_\gamma \vec{k}_{h\gamma} = 0, \tag{25}$$

where α, β, γ refer to different modes of oscillation and the symbols $s_\alpha, s_\beta, s_\gamma$ take on the values +1 or -1.

The coefficient $K_{\alpha_{s\alpha} \beta_{s\beta} \gamma_{s\gamma}}$ which appears in equation (24) is symmetrical under the interchange of indices $\alpha_{s\alpha}, \beta_{s\beta}$ and $\gamma_{s\gamma}$. It is defined by

$$\begin{aligned}
 K_{\alpha_{s\alpha} \beta_{s\beta} \gamma_{s\gamma}} &= - \int dz \frac{P}{6} \left[(\Gamma - 1)^2 (\vec{\nabla} \cdot \vec{\xi}_{\alpha_{s\alpha}}) (\vec{\nabla} \cdot \vec{\xi}_{\beta_{s\beta}}) (\vec{\nabla} \cdot \vec{\xi}_{\gamma_{s\gamma}}) \right. \\
 &\quad \left. + \xi_{\alpha_{s\alpha}}^{i,j} \xi_{\beta_{s\beta}}^{j,k} \xi_{\gamma_{s\gamma}}^{k,i} + \xi_{\beta_{s\beta}}^{i,j} \xi_{\alpha_{s\alpha}}^{j,k} \xi_{\gamma_{s\gamma}}^{k,i} \right. \\
 &\quad \left. + (\Gamma - 1) \left\{ (\vec{\nabla} \cdot \vec{\xi}_{\alpha_{s\alpha}}) \xi_{\beta_{s\beta}}^{i,j} \xi_{\gamma_{s\gamma}}^{j,i} + (\vec{\nabla} \cdot \vec{\xi}_{\beta_{s\beta}}) \xi_{\gamma_{s\gamma}}^{i,j} \xi_{\alpha_{s\alpha}}^{j,i} + (\vec{\nabla} \cdot \vec{\xi}_{\gamma_{s\gamma}}) \xi_{\alpha_{s\alpha}}^{i,j} \xi_{\beta_{s\beta}}^{j,i} \right\} \right],
 \end{aligned} \tag{26}$$

where the complex conjugate eigenfunction should be used for $s_\mu = -1$.

Our system has now been reduced to that of N interacting harmonic oscillators with action-angle variables, J_α, ϕ_α . In terms of these variables the Hamiltonian reads

$$H = \vec{\omega} \cdot \vec{J} + H_{int}(\vec{J}, \vec{\phi}). \tag{27}$$

The Hamilton equations then yield

$$\frac{\partial \vec{\phi}}{\partial t} \equiv \dot{\vec{\phi}} = \frac{\partial H}{\partial \vec{J}}, \quad (28)$$

and

$$\frac{\partial \vec{J}}{\partial t} \equiv \dot{\vec{J}} = -\frac{\partial H}{\partial \vec{\phi}}. \quad (29)$$

Substituting for H_3 from equation (24) in the Hamilton equations (28) and (29), we find the evolution equations for mode α due to a single triplet:

$$\frac{d\phi_\alpha}{dt} = \omega_\alpha + \frac{6\omega_\alpha |K_{\alpha_s\alpha\beta_s\beta\gamma_s\gamma}|}{\sqrt{8A}} \sqrt{\frac{E_\beta E_\gamma}{E_\alpha}} \cos(\Phi + \delta_3), \quad (30)$$

and

$$\frac{dJ_\alpha}{dt} = \frac{12s_\alpha |K_{\alpha_s\alpha\beta_s\beta\gamma_s\gamma}|}{\sqrt{8A}} \sqrt{E_\alpha E_\beta E_\gamma} \sin(\Phi + \delta_3), \quad (31)$$

where Φ and δ_3 are defined by

$$\Phi \equiv s_\alpha \phi_\alpha + s_\beta \phi_\beta + s_\gamma \phi_\gamma. \quad (32)$$

and

$$K_{\alpha_s\alpha\beta_s\beta\gamma_s\gamma} = |K_{\alpha_s\alpha\beta_s\beta\gamma_s\gamma}| \exp(i\delta_3). \quad (33)$$

The combinatorial factors of 6 and 12 in equations (30) and (31) arise because the triplet (α, β, γ) occurs 6 times for each choice of α in equation (24).

b) Master Equation

For simplicity, we begin by calculating dE_α/dt due to the interactions among the single triplet (α, β, γ) and then sum the result over all possible triplets which involve mode α . Finally, we take the expectation value of the resulting expression to obtain the master equation which governs the expectation value of the rate at which nonlinear interactions change the energy of mode α .

We solve equations (30) and (31) perturbatively. The zeroth order values of ϕ_α and J_α are taken to be the actual values at some arbitrarily chosen time t . The

corrections of order n at time $t + \tau$ are computed with the right hand sides of the equations evaluated to order $n - 1$. This procedure, carried out to first order for ϕ_α and to second order for J_α , yields

$$\phi_\alpha^{(1)}(t + \tau) = \frac{6\omega_\alpha |K_{\alpha s_\alpha \beta s_\beta \gamma s_\gamma}|}{\sqrt{8A} \Delta\omega} \sqrt{\frac{E_\beta^{(0)} E_\gamma^{(0)}}{E_\alpha^{(0)}}} [\sin(\Delta\omega \tau + \epsilon_3 + \delta_3) - \sin(\epsilon_3 + \delta_3)], \quad (34)$$

$$J_\alpha^{(1)}(t) = -\frac{12 s_\alpha |K_{\alpha s_\alpha \beta s_\beta \gamma s_\gamma}|}{\sqrt{8A} \Delta\omega} \sqrt{E_\alpha^{(0)} E_\beta^{(0)} E_\gamma^{(0)}} [\cos(\Delta\omega \tau + \epsilon_3 + \delta_3) - \cos(\epsilon_3 + \delta_3)], \quad (35)$$

and

$$J_\alpha^{(2)}(t) = \frac{18 |K_{\alpha s_\alpha \beta s_\beta \gamma s_\gamma}|^2}{A (\Delta\omega)^2} \sin^2\left(\frac{\Delta\omega \tau}{2}\right), \quad (36)$$

$$\left(\omega_\alpha E_\beta^{(0)} E_\gamma^{(0)} + s_2 \omega_\beta E_\alpha^{(0)} E_\gamma^{(0)} + s_2 \omega_\gamma E_\alpha^{(0)} E_\beta^{(0)}\right),$$

where

$$\epsilon_3 \equiv s_\alpha \epsilon_\alpha^{(0)} + s_\beta \epsilon_\beta^{(0)} + s_\gamma \epsilon_\gamma^{(0)}, \quad (37)$$

and

$$s_1 \equiv \frac{s_\beta}{s_\alpha} \quad s_2 \equiv \frac{s_\gamma}{s_\alpha}. \quad (38)$$

We simplify equation (36) by setting

$$\frac{1}{(\Delta\omega)^2} \sin^2\left(\frac{\Delta\omega \tau}{2}\right) \approx \frac{\pi \tau}{2} \delta(\Delta\omega), \quad (39)$$

which is an expression of approximate energy conservation

$$\Delta\omega \equiv s_\alpha \omega_\alpha + s_\beta \omega_\beta + s_\gamma \omega_\gamma \approx 0. \quad (40)$$

Next, we sum equation (36) over all the triplets which contain mode α and take the limit $A \rightarrow \infty$. The latter step involves the replacement

$$\lim_{A \rightarrow \infty} \sum_{\vec{k}_{h\beta}, \vec{k}_{h\gamma}} = \frac{1}{(2\pi)^4} \int d^2 k_{h\beta} d^2 k_{h\gamma}. \quad (41)$$

The horizontal wave vector matching condition given by equation (25) introduces a term $(2\pi)^2 \delta(s_\alpha \vec{k}_{h\alpha} + s_\beta \vec{k}_{h\beta} + s_\gamma \vec{k}_{h\gamma})$ which reduces the double integral to a single one over $d^2 k_{h\beta}$. We make the change of variable

$$d^2 k_{h\beta} = k_{h\beta} dk_{h\beta} d\theta_{\alpha\beta} = k_{h\beta} \frac{d\theta_{\alpha\beta}}{d\omega_\gamma} dk_{h\beta} d\omega_\gamma, \quad (42)$$

and use

$$\cos \theta_{\alpha\beta} = s_1 \frac{k_{h\gamma}^2 - k_{h\alpha}^2 - k_{h\beta}^2}{2k_{h\alpha} k_{h\beta}}, \quad (43)$$

to arrive at

$$\frac{d\theta_{\alpha\beta}}{d\omega_\gamma} = \frac{-s_1 2k_{h\gamma}}{\sqrt{[(k_{h\alpha} + k_{h\beta})^2 - k_{h\gamma}^2] [k_{h\gamma}^2 - (k_{h\alpha} - k_{h\beta})^2]}} \frac{dk_{h\gamma}}{d\omega_\gamma}. \quad (44)$$

Taken together these operations yield

$$\begin{aligned} \left\langle \frac{dE_{\vec{k}_{h\alpha}}}{dt} \right\rangle &= \frac{9\omega_\alpha}{\pi} \sum_{n_\beta, n_\gamma} \int dk_{h\beta} \frac{|K_{\alpha\beta\beta\gamma}|^2 k_{h\beta} k_{h\gamma}}{\sqrt{[(k_{h\alpha} + k_{h\beta})^2 - k_{h\gamma}^2] [k_{h\gamma}^2 - (k_{h\alpha} - k_{h\beta})^2]}} \\ &\quad \times \frac{dk_{h\gamma}}{d\omega_\gamma} \{ \omega_\alpha E_\beta E_\gamma + s_1 \omega_\beta E_\alpha E_\gamma + s_2 \omega_\gamma E_\alpha E_\beta \}. \end{aligned} \quad (45)$$

We note that $0 \leq \theta_{\alpha\beta} < 2\pi$ and that $\theta_{\alpha\beta}$ and $2\pi - \theta_{\alpha\beta}$ correspond to the same value of $k_{h\gamma}$. This accounts for the factor of 2 which the integral over ω_γ introduces into equation (45).

In writing equation (45) we have defined $\langle dE_\alpha/dt \rangle \equiv \omega_\alpha J_\alpha^{(2)}(t + \tau)/\tau$. The triangular brackets denoting expectation value are called for because we discard the direct contribution which $J_\alpha^{(1)}$ makes to dE_α/dt since its expectation value vanishes.

The expression for $d\langle E_\alpha \rangle / dt$ given in equation (45) is the fundamental formula of this paper.⁴ In carrying out the integral over k_{h_β} it is important to avoid double counting modes. The frequency matching equation (40) implies that either one or both of s_1 and s_2 are negative. In the former case we choose $s_2 = -1$ and take the integral over those modes for which $\omega_\gamma \geq \omega_\beta$. In the latter case, $s_1 = s_2 = -1$, the integral is restricted to modes with $\omega_\beta \leq \omega_\alpha/2$.

⁴ In deriving the master equation we have implicitly assumed that each mode is involved in many triplets which satisfy the frequency matching equation (40) to within the sum of the linewidths of the 3 modes. Otherwise, the steps taken in equations (39) and (41), which lead to an expression that is independent of the linewidths, could not be justified. We estimate the number of couplings per solar p-mode in section V.

IV. NUMERICAL PROCEDURE AND RESULTS

a) Class 1 And Class 2 Triplets

The 3-mode couplings separate naturally into 2 classes.

Class 1 consists of all the possible triplets for which one mode has frequency greater than ω_{ac} , the acoustic cutoff frequency in the isothermal atmosphere. The high frequency mode is only partially trapped and thus has negligible energy. This type of 3-mode coupling produces a net transfer of energy from the trapped modes to the propagating mode. We denote by $\Upsilon_{\alpha}^{(1)}$ the rate at which the energy in mode α decays as the result of these couplings. To compute $\Upsilon_{\alpha}^{(1)}$ we set $E_{\gamma} = 0$ and $s_2 = -1$ in equation (45) and sum over all the class 1 triplets which involve mode α .

Class 2 contains the remaining resonant triplets, those which involve only trapped modes. Each 3-mode coupling in this class drives the modes it connects towards equipartition of energy. Since the trapped modes with frequencies just below ω_{ac} have the lowest energies, these interactions tend to transfer energy from the lower to the higher frequency modes. To compute $\Upsilon_{\alpha}^{(2)}$, the net rate at which 3-mode couplings in class 2 change the energy of mode α , we sum over all those class 2 triplets which include mode α .

We note that $\Upsilon_{\alpha}^{(1)}$ is always negative but $\Upsilon_{\alpha}^{(2)}$ may have either sign.

b) Mode Energies

Mode energies are required as input to the calculations of energy transfer rates given by equation (45). Libbrecht and Zirin have accurately measured the surface velocities of the low degree, $\ell \lesssim 20$, solar p-modes in the 5-minute band. We determine mode energies by multiplying their mean square velocities by mode masses appropriate to the line forming level for their observations. We adopt these mode energies for our calculations making the assumption that the mode energy is independent of ℓ . While this assumption is theoretically plausible, its observational

support is shaky. The most relevant high degree, $\ell \lesssim 200$ results indicate that the rms surface velocities do not vary with ℓ (Libbrecht, Popp, Kaufman and Penn 1986). Since the mode mass decreases by about a factor of 3 between $\ell = 0$ and $\ell = 200$ there may be a slow decline in mode energy with increasing ℓ . Our assumption of ℓ -independent mode energy tends to overestimate the importance of nonlinear mode coupling if the mode energies really do decline with increasing ℓ .

Reliable mode energies have only been determined for modes with periods longer than about 4 minutes where the mode energy is about an order of magnitude lower than at the peak of the 5-minute band. Consequently, the energies we assign to the high frequency trapped modes are not much better than guesses. This leads to large uncertainties in the energy transfer rates due to class 1 couplings since many of these involve a high frequency trapped mode.

The total mean square surface velocity is obtained by summing the contributions from all of the modes. We have

$$v^2 \equiv \lim_{A \rightarrow \infty} \frac{1}{A} \int d^2x_h \left(\frac{\partial \xi_z}{\partial t} \right)^2 = \sum_{n_\alpha} \int \frac{d^2k_{h_\alpha}}{(2\pi)^2} \frac{E_\alpha}{M_\alpha}. \quad (46)$$

The mode energies we adopt yield $v_{rms} \approx 0.8 \text{ km s}^{-1}$ at the interface between the adiabatic and isothermal layers. At higher levels v_{rms} is larger, the precise value depends on the energies of the unobserved, high frequency, trapped modes.

c) Computational Method

Starting with mode α we find all pairs of modes which satisfy the horizontal wavevector and frequency matching conditions given by equations (25) and (40). To do so, we slide the position of mode β along the portion of each ridge in the $k_h - \omega$ diagram which lies below the acoustic cutoff frequency, ω_{ac} . For specified values $k_{h_\alpha}, \omega_\alpha$ and $k_{h_\beta}, \omega_\beta$, the values of $k_{h_\gamma}, \omega_\gamma$ correspond to the intersections of the lines $\omega_\gamma = \omega_\alpha \pm \omega_\beta$ with the ridges in the $k - \omega$ diagram that lie between the boundaries $|k_{h_\alpha} - k_{h_\beta}| \leq k_{h_\gamma} \leq k_{h_\alpha} + k_{h_\beta}$.

The coupling coefficient for each triplet is computed using equation (26). The two energy transfer rates for mode α , $\Upsilon_\alpha^{(1)}$ and $\Upsilon_\alpha^{(2)}$, are obtained by summing the contributions from all the class 1 and class 2 triplets which involve mode α .

d) 3-Mode Coupling Coefficients

Physically, we expect the nonlinear mode interaction to be strongest in regions where the appropriate nonlinearity parameter, the acoustic Mach number, is large. Mathematically, the local contribution to the 3-mode coupling coefficient is proportional to the product of the unperturbed pressure and the gradients of the displacement eigenfunctions of the 3 modes (cf. eq. [26]). Let us separate the contributions to $K_{\alpha\beta\gamma}$ from the adiabatic and isothermal layers and examine each individually.

The situation is simpler in the adiabatic layer and we begin with it. Here, $P \propto z^{5/2}$. The dominant term in gradient of the displacement is $\partial\xi_z/\partial z$ whose envelope diminishes as $z^{-3/2}$ for $z_1 < z < z_2$ and as $\exp(-k_h z)$ for $z > z_2$ (cf. eq. [8]). This gives a local 3-mode coupling strength which decreases at least as fast as z^{-2} for z greater than the largest z_1 of the 3 modes. Thus, the contribution to the 3-mode coupling coefficient from the adiabatic layer is concentrated close to its upper boundary.

Nonlinear mode coupling in the isothermal layer is complicated by the exponential increase with height of $\vec{\xi}$ (cf. eq. [15]) which, for some triplets, overwhelms the exponential decrease of the pressure in the integrand for the coupling coefficient. Coupling coefficients which formally diverge in an infinite isothermal atmosphere are primarily associated with class 1 triplets, especially those for which the frequency of at least one of the trapped modes is not far below the acoustic cutoff. A physically plausible way to bound the coupling coefficients is to choose the upper limit in their defining integral to be the height at which the acoustic Mach number reaches unity. Unfortunately, the validity of the perturbation expansion becomes questionable at this point; higher order couplings have comparable strengths to the

3-mode couplings there.

Even the coefficients which are formally convergent show a pronounced increase in magnitude with increasing ω and k_H of the modes they couple. This dependence is due to the increased concentration in the upper layers of the atmosphere of modes with high values of ω and k_h . This is responsible for the small masses of these modes (cf. Table 2).

Figure 2 displays the integrand of the mode coupling coefficient for a variety of triplets.

e) Energy Transfer Rates

We compute net energy transfer rates for a selected sample of modes whose parameters are listed in Table 2. The computed values of $\Upsilon_\alpha^{(1)}$ and $\Upsilon_\alpha^{(2)}$, are listed in Tables 3a and 3b. An obvious feature is that every trapped mode is losing energy due to its nonlinear interactions. Of course, class 1 couplings drain the energy of the trapped modes by transferring it to propagating modes. However, even class 2 couplings, which conserve the energy of the trapped modes, damp all modes except those in a narrow frequency range bounded from above by ω_{ac} . This is a consequence of the steep decline in the energy per mode as ω approaches ω_{ac} from below.

The lifetimes (the inverses of the linewidths) of the low degree solar p-modes near the peak of the 5-minute band are of order several days (Libbrecht and Zirin 1986, Isaak 1986). In addition, at fixed k_h the mode lifetime appears to decrease monotonically with increasing ω . The significance of the nonlinear interactions is measured by comparing the damping rate, $\eta_\alpha \equiv \Upsilon_\alpha/E_\alpha$, to the linewidth for each mode. The values of the former, computed from the entries in Tables 2 and 3, are compiled in Table 4. These calculations have been carried out for a variety of choices of the thickness of the isothermal atmosphere and for the mode energies in the unobserved high frequency range.

The values of η_α are quite sensitive to the thickness of the isothermal layer and to the energies of the high frequency modes. With a thin isothermal layer and small energies for the high frequency modes, the damping times for the 5-minute modes of low degree are several months, much longer than the observed lifetimes. However, with a thick isothermal layer and large energies for the high frequency modes, the damping times for the low degree 5-minute modes drop to several days, close to the observationally determined lifetimes.

The scale length for the exponential growth of the eigenfunctions in the isothermal layer decreases with frequency (cf. eq. [15]). This accounts for the increase with frequency of the sensitivity of the damping times to the thickness of the isothermal layer.

The values of η_α listed in Table 4 display a few abrupt changes over small ranges of $k_{h\alpha}$. These are puzzling but do not signal an error in our computations. Rather, they may be traced to the availability or unavailability of triplets which couple mode α to modes on a particular ridge, usually the fundamental, $n = 0$, ridge.

f) Error Tests

The energy transfer rates are the end product of a fairly long series of calculations. Their numerical values are the major result of our investigation and we want to insure that they are correct. In order to minimize the chances for errors we devised and performed a set of tests of various parts of the calculations.

Approximate analytic eigenfunctions were derived to check the eigenfunctions determined by the numerical solution of the differential equations (1) and (10). These analytic eigenfunctions were used to compute 3-mode coupling coefficients, $K_{\alpha\beta\gamma}$, which were compared to those computed from the numerical eigenfunctions.

In our calculations of $\Upsilon_\alpha^{(1)}$ and $\Upsilon_\alpha^{(2)}$ we varied the number of choices of mode β for a given mode α . We also interchanged the roles of modes β and γ in these

calculations. Finally, we summed $\Upsilon_{\alpha}^{(2)}$ over all the trapped modes to verify that the class 2 couplings conserve their total energy.

V. DISCUSSION AND CONCLUSIONS

a) Number of Resonant Triplets per Solar P-Mode

Let us estimate the number of resonant triplets which involve a particular mode α . By a resonant triplet we mean one which satisfies the frequency matching condition given by equation (40) to within the sum of the linewidths of the 3 modes. For simplicity, we consider a restricted set of couplings for which ω and ℓ for all 3 modes (α, β, γ) lie within intervals $\Delta\omega/\omega_* \lesssim 1$ and $\Delta\ell/\ell_* \lesssim 1$ about the fiducial values ω_* and ℓ_* .⁵ Moreover, we assume that all the modes have similar linewidths $\Delta\omega \approx \omega/Q$ where Q is the quality factor.

Given mode α there are $N_\beta \sim n_* \ell_*^2$ choices for mode β .⁶ With both α and β determined the angular momentum addition rules allow of order ℓ_* possible choices of ℓ for mode γ . However, for $\ell_* \gg 1$ one Clebsch-Gordon coupling coefficient is much larger than the others and ℓ_γ is essentially unique.⁷ Approximate energy conservation determines ω_γ to within a tolerance of order ω_*/Q . Thus, the probability that an appropriate mode γ exists to complete the resonant triple is $N_\gamma \sim n_*/Q$. Multiplying this probability by the number of possible choices for mode β we obtain an estimate of

$$\mathcal{N} \equiv N_\beta N_\gamma \sim \frac{n_*^2 \ell_*^3}{Q} \quad (47)$$

for the number of resonant triplets which involve mode α .

The solar p-modes in the 5-minute band have $Q \sim 10^3$ and (n, ℓ) combinations ranging from $(25, 0)$ to $(0, 10^3)$. As examples, we take the limiting cases $(n_*, \ell_*) = (20, 10)$ and $(n_*, \ell_*) = (1, 700)$. These choices yield $\mathcal{N} \sim 4 \times 10^1$ and $\mathcal{N} \sim 5 \times 10^2$,

⁵ In the remainder of this subsection we use the radial order, n , instead of ω , together with ℓ and m to specify a mode.

⁶ For each (n, ℓ) pair $-\ell \leq m \leq \ell$.

⁷ For $\ell_* \gg 1$ the rules for the addition of ℓ reduce to those for the addition of k_h .

respectively. Thus, we may safely conclude that each 5-minute mode is coupled to many other modes.

b) Significance of Nonlinear Mode Coupling

Nonlinear interactions transfer energy among the p-modes. The most important nonlinear interactions are those which couple 2 trapped modes to a propagating mode (class 1 triplets). These drain the energies of the trapped modes. As a consequence, all of the trapped modes suffer a net loss of energy due to nonlinear mode interactions.

These damping times may be compared to the observationally determined lifetimes of the solar p-modes. Unfortunately, this comparison is currently restricted, by lack of adequate observational data, to low degree modes near the peak of the 5-minute band. Moreover, there are significant residual uncertainties in the nonlinear damping rates associated with the upper limit we choose for the integrals which give the divergent coupling coefficients and with the energies we adopt for high frequency trapped modes. These uncertainties preclude our reaching any firm conclusion regarding the importance of nonlinear interactions in affecting the energies of the solar p-modes.

The observational consequences of the 3-mode couplings, if they are significant, would follow from the dependence of the damping rates on ℓ and ω . The increase in damping rate with increasing ℓ might give rise to a decline of the energy per mode with increasing ℓ at fixed ω . Furthermore, the rapid increase in damping rate as ω approaches ω_{ac} from below might be, at least in part, responsible for the steep decline in the energy per mode at the high frequency end of the 5-minute band. This decline is generally attributed to radiative damping but calculations of that process are not secure enough to rule out the existence of another, possibly dominant, contributor.

In initiating this investigation, one of our goals was to help to establish the

mechanism which excites the solar p-modes. If our calculations had conclusively shown that nonlinear mode couplings are unimportant, we would have gone a long way toward eliminating overstability as the excitation mechanism. It turns out that we can not do this. Instead, we are left with an ambiguous result. However, it still provides us with a good, although indirect, reason to doubt whether overstability is important. The argument runs as follows. Although previous calculations have disagreed on the stability of the p-modes, they have all predicted that the f-modes with periods near 5-minutes are stable. Presumably, this is a consequence of the incompressible nature of the f-modes. Thus, even if some p-modes are overstable, the excitation of the f-modes, which have comparable energies per mode to the p-modes of similar period, remains to be explained. The obvious suggestion, that the f-modes receive their energy from the p-modes via nonlinear mode coupling, conflicts with our finding that nonlinear interactions damp the f-modes just as they do the p-modes. Of course, this statement depends on the energies we adopt for the f-modes, which in the 5-minute range we have taken from observation. We have artificially reduced the energies we assign to selected 5-minute f-modes in our calculations to the point that nonlinear interactions no longer damp them. This occurs for energies which are about four orders of magnitude lower than those determined from observation. Such is the overwhelming strength of the class 1 couplings relative to those of class 2.

Since the f-modes are probably not overstable, and they are definitely not receiving their energy from the p-modes, they must be excited by some other mechanism. It seems likely that the same mechanism excites the p-modes and that they are also stable. This mechanism is probably stochastic excitation by turbulent convection.

APPENDIX

The equations of inviscid fluid dynamics of a perfect gas with adiabatic index Γ follow from varying the Lagrangian (Newcomb 1962)

$$L = \int d\mathbf{x}_0 \rho_0(\mathbf{x}_0) \left(\frac{v^2}{2} - \frac{P(\mathbf{x})}{(\Gamma - 1)\rho(\mathbf{x})} - \phi(\mathbf{x}) \right). \quad (\text{A1})$$

The background configuration is specified by $\rho_0(\mathbf{x}_0)$, $P_0(\mathbf{x}_0)$ and $\mathbf{v}_0 = 0$. The variation is achieved by displacing the position of each fluid element from \mathbf{x}_0 to $\mathbf{x} = \mathbf{x}_0 + \vec{\xi}$, where $\vec{\xi}$ is the Lagrangian displacement. The conservation laws of mass and entropy imply

$$\rho d\mathbf{x} = \rho_0 d\mathbf{x}_0 \quad \Rightarrow \quad \rho = \rho_0 \mathcal{J}^{-1}, \quad (\text{A2})$$

and

$$P\rho^{-\Gamma} = P_0\rho_0^{-\Gamma} \quad \Rightarrow \quad P = P_0 \mathcal{J}^{-\Gamma}, \quad (\text{A3})$$

where \mathcal{J} is the Jacobian of the transformation. The Lagrangian can be written in terms of \mathcal{J} and the background variables as

$$L = \int d\mathbf{x}_0 \left(\frac{\rho_0 v^2}{2} - \frac{P_0 \mathcal{J}^{1-\Gamma}}{\rho_0(\Gamma - 1)} - \phi(\mathbf{x}_0 + \vec{\xi}) \right). \quad (\text{A4})$$

The Jacobian

$$\mathcal{J} = \det \left(\frac{\partial \mathbf{x}}{\partial \mathbf{x}_0} \right) = \det \left(1 + \frac{\partial \vec{\xi}}{\partial \mathbf{x}_0} \right), \quad (\text{A5})$$

may be rewritten as

$$\mathcal{J} = 1 + (\vec{\nabla} \cdot \vec{\xi}) - \frac{1}{2} \xi^{i,j} \xi^{j,i} + \frac{1}{2} (\vec{\nabla} \cdot \vec{\xi})^2 + \frac{1}{3} \xi^{i,j} \xi^{j,k} \xi^{k,i} - \frac{(\vec{\nabla} \cdot \vec{\xi})}{2} \xi^{i,j} \xi^{j,i} + \frac{1}{6} (\vec{\nabla} \cdot \vec{\xi})^3. \quad (\text{A6})$$

Expanding the Lagrangian in powers of the displacement, $\vec{\xi}$, with the aid of equation (A6), we obtain the second and third order Lagrangian densities,

$$\mathcal{L}_2 = \frac{\rho_0}{2} \left| \frac{\partial \vec{\xi}}{\partial t} \right|^2 - \frac{P_0}{2} \left[(\Gamma - 1) (\vec{\nabla} \cdot \vec{\xi})^2 + \xi^{i,j} \xi^{j,i} \right] - \frac{\rho_0}{2} \phi_{,ij} \xi_i \xi_j, \quad (\text{A7})$$

and

$$\mathcal{L}_3 = P_0 \left[\frac{(\Gamma - 1)^2}{6} (\vec{\nabla} \cdot \vec{\xi})^3 + \frac{(\Gamma - 1)}{2} (\vec{\nabla} \cdot \vec{\xi}) \xi^{i,j} \xi^{j,i} + \frac{1}{3} \xi^{i,j} \xi^{j,k} \xi^{k,i} \right] - \frac{\rho_0}{6} \phi_{,ijk} \xi_i \xi_j \xi_k. \quad (\text{A8})$$

The final terms in \mathcal{L}_2 and \mathcal{L}_3 vanish for a uniform gravitational field .

The Hamiltonian and Lagrangian densities are related by

$$\mathcal{H} = \frac{\delta \mathcal{L}}{\delta \partial_t \xi_i} \partial_t \xi_i - \mathcal{L}. \quad (\text{A9})$$

Using equations (A7), (A8) and (A9), we derive the second and third order Hamiltonian densities,

$$\mathcal{H}_2 = \frac{\rho_0}{2} \left| \frac{\partial \vec{\xi}}{\partial t} \right|^2 + \frac{P_0}{2} \left[(\Gamma - 1) (\vec{\nabla} \cdot \vec{\xi})^2 + \xi^{i,j} \xi^{j,i} \right], \quad (\text{A10})$$

and

$$\mathcal{H}_3 = -\mathcal{L}_3. \quad (\text{A11})$$

REFERENCES

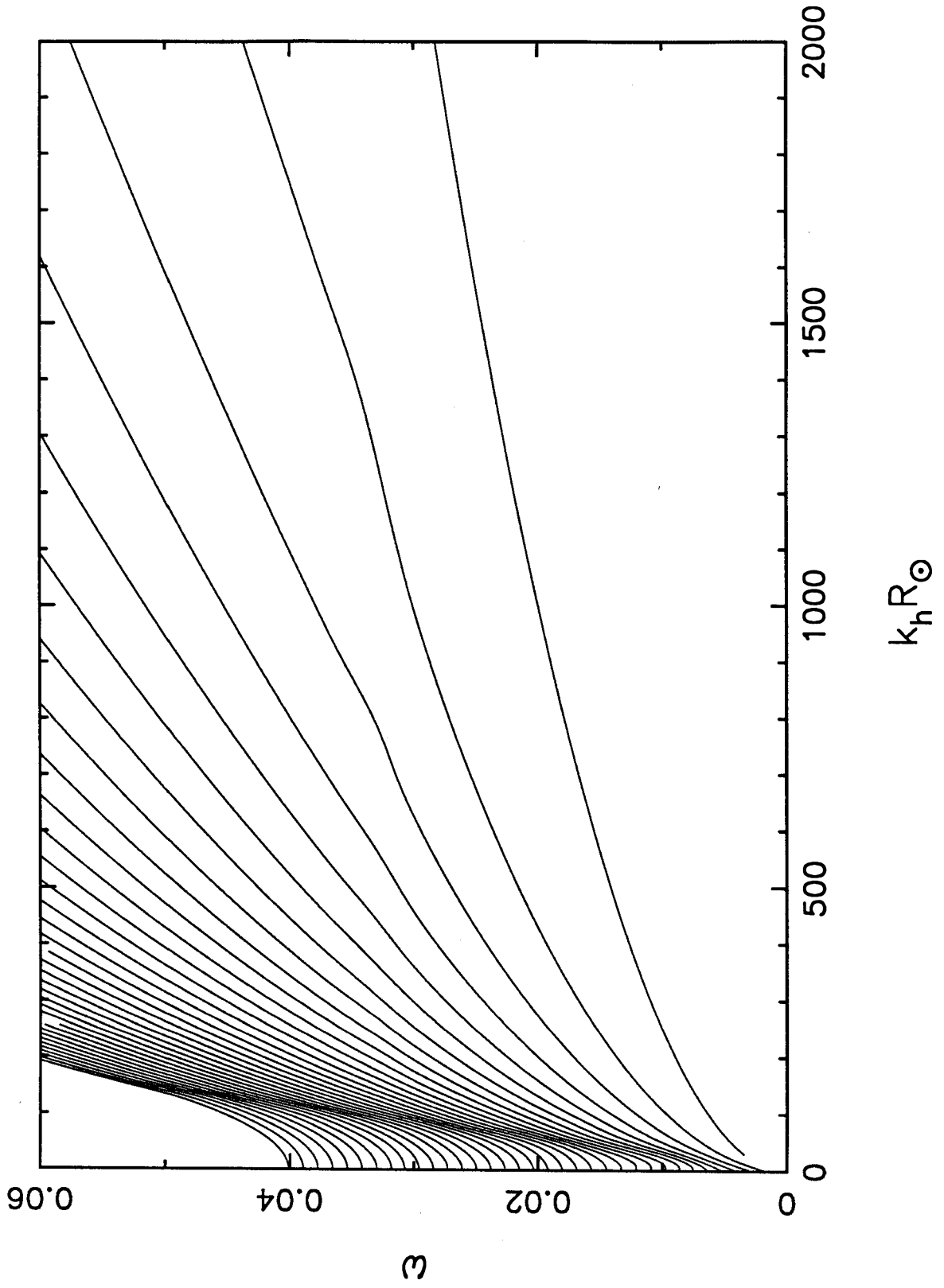
- Ando, H. and Osaki, Y., 1975, *Publ. Astro. Soc. Japan*, **27**, 581.
- Antia, H.M., Chitre, S.M. and Narashima, D., 1986, *Ap. Sp. Sci.*, **118**, 169.
- Christensen-Dalsgaard, J. and Frandsen, S., 1982, *Solar Phys.*, **82**, 165.
- Evans, J.W. and Michard, R., 1962, *Ap. J.*, **136**, 493.
- Goldreich, P. and Keeley, D.A., 1977a, *Ap. J.*, **211**, 934.
- Goldreich, P. and Keeley, D.A., 1977b, *Ap. J.*, **212**, 243.
- Isaak, G.R. 1986, in *Seismology of the Sun and the Distant Stars*, ed. D.O. Gough (Dordrecht: Reidel), 223.
- Kidman, R.B. and Cox, A.N., 1984, in *Solar Seismology from Space*, eds. R.K. Ulrich, J. Harvey, E.J. Rhodes Jr. and J. Toomre.
- Leighton, R.B., Noyes, R.W., and Simon, G.W. 1961, *Ap. J.*, **135**, 474.
- Libbrecht, K.G., and Zirin, H., 1986, *Ap. J.*, **308**, 413.
- Libbrecht, K.G., Popp, B.D., Kaufman, J.M., and Penn, M.J., 1986, *Nature*, **323**, 235.
- Newcomb, W.A., 1962, *Nuclear Fusion: Supplement Part 2*, 451.

FIGURE CAPTIONS

Figure 1: is $k_h - \omega$ diagram for the model atmosphere whose parameters are given in table 1. k_h has been multiplied by R_\odot to obtain a dimensionless number which can be identified with the degree, ℓ , of solar p-modes.

Figure 2: displays the absolute integrand of the coupling coefficient (cf. eq. [26]) as a function of z , the distance in the adiabatic atmosphere, for four different triplets. From top left clockwise the frequencies (radian sec^{-1}) and $k_h R_\odot$ of the three modes in each of the four triplets are: $\{(0.0125, 107), (0.01113, 310), (0.02363, 280)\}$, $\{(0.0225, 545), (0.00927, 215), (0.03176, 717)\}$, $\{(0.0225, 545), (0.03053, 1034), (0.0530, 751)\}$ and $\{(0.0125, 107), (0.02997, 991), (0.04248, 892)\}$. Absolute values of the coupling coefficients in the adiabatic and the isothermal part of the atmosphere are also listed at the top of each figure. Note the rapid increase in their values with increasing value for the sum of the frequencies of the modes in the triplet.

Figure 1



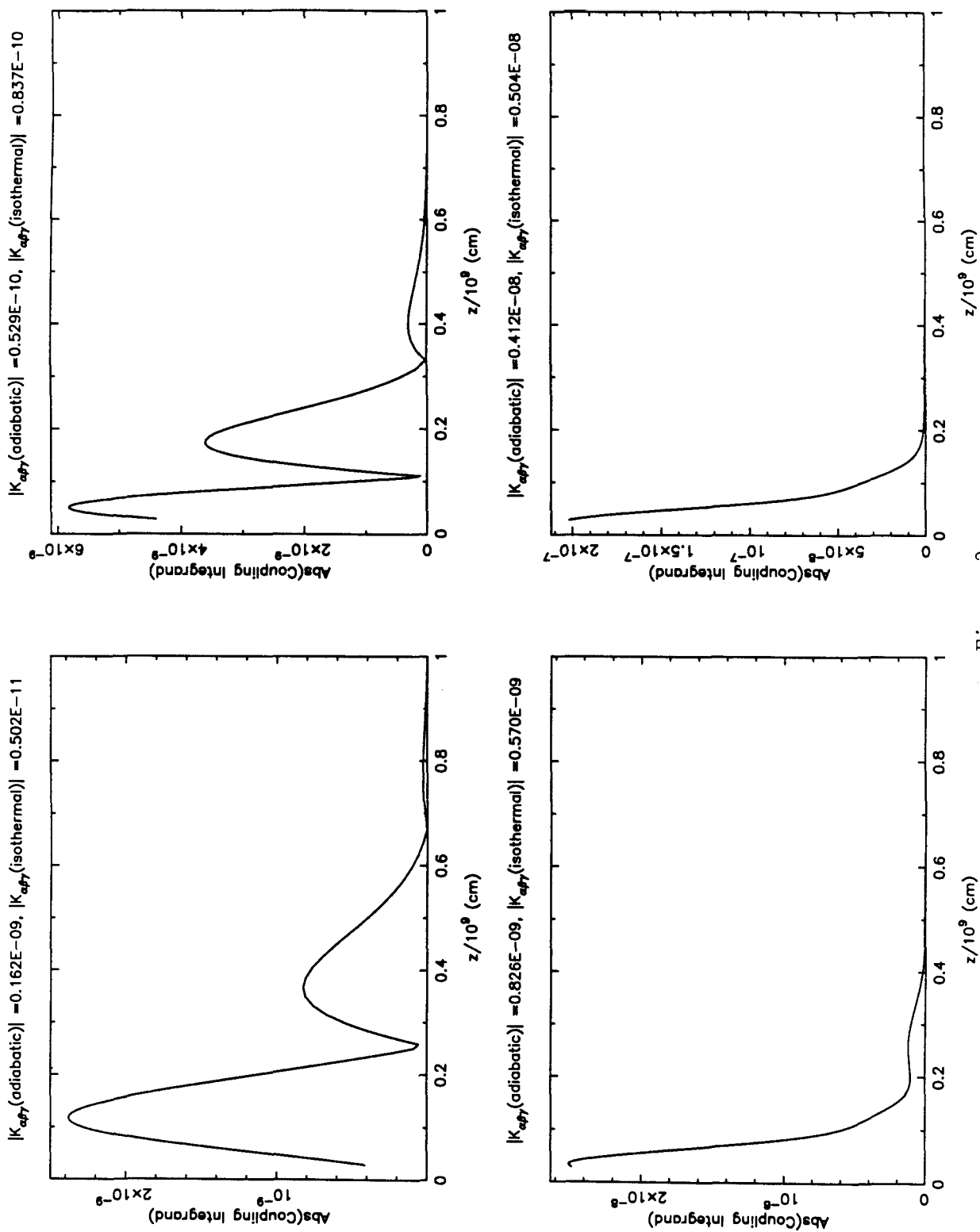


Figure 2

Table 1.

	Top of adiabatic atmosphere	Bottom of adiabatic atmosphere
z (cm)	2.85×10^7	3.38×10^{10}
P ($\text{gm cm}^{-1} \text{sec}^{-2}$)	6.20×10^4	3.0×10^{12}
ρ (gm cm^{-3})	1.96×10^{-7}	8.0×10^{-3}
g	$27750 \text{ cm sec}^{-2}$	
ω_{crit}	$0.03185 \text{ rad sec}^{-1}$	
adiabatic constant	1.666667	

Table 2.

ω (rad/sec)	Period (minute)	$k_h R_\odot$	n	$M_\alpha^\dagger/10^{25}$ (gm)	$E_\alpha/10^{27}$ (egrs)	$E'_\alpha/10^{27}$ (egrs)
0.0110	9.52	21.5	8	25.20	1.76	1.76
0.0110	9.52	41.0	5	30.70	1.76	1.76
0.0110	9.52	60.5	3	18.50	1.76	1.76
0.0110	9.52	82.7	2	11.70	1.76	1.76
0.0110	9.52	130.0	1	6.84	1.76	1.76
0.0110	9.52	303.0	0	3.16	1.76	1.76
0.0125	8.38	37.5	8	15.50	3.31	3.31
0.0125	8.38	61.9	4	11.90	3.31	3.31
0.0125	8.38	107.0	2	7.32	3.31	3.31
0.0125	8.38	167.5	1	4.48	3.31	3.31
0.0125	8.38	391.3	0	1.38	3.31	3.31
0.0150	6.98	43.1	10	8.92	5.98	5.98
0.0150	6.98	112.6	3	4.19	5.98	5.98
0.0150	6.98	153.6	2	2.87	5.98	5.98
0.0150	6.98	241.9	1	2.16	5.98	5.98
0.0150	6.98	563.6	0	0.58	5.98	5.98
0.0175	5.98	50.0	11	7.42	12.70	12.70
0.0175	5.98	100.1	5	3.50	12.70	12.70
0.0175	5.98	153.6	3	2.53	12.70	12.70
0.0175	5.98	328.7	1	0.98	12.70	12.70
0.0175	5.98	767.3	0	0.29	12.70	12.70
0.0200	5.24	63.2	11	4.81	14.50	14.50
0.0200	5.24	158.5	4	1.56	14.50	14.50
0.0200	5.24	200.2	3	1.27	14.50	14.50
0.0200	5.24	273.1	2	0.92	14.50	14.50
0.0200	5.24	429.5	1	0.57	14.50	14.50
0.0200	5.24	1002.2	0	0.15	14.50	14.50
0.0225	4.65	63.2	14	2.85	3.25	3.25
0.0225	4.65	108.4	8	1.85	3.25	3.25
0.0225	4.65	200.2	4	0.95	3.25	3.25
0.0225	4.65	346.1	2	0.60	3.25	3.25
0.0225	4.65	544.9	1	0.39	3.25	3.25
0.0225	4.65	1267.7	0	0.10	3.25	3.25
0.0250	4.19	74.4	15	2.25	0.82	0.82
0.0250	4.19	151.5	7	1.11	0.82	0.82
0.0250	4.19	204.3	5	0.84	0.82	0.82
0.0250	4.19	247.4	4	0.70	0.82	0.82
0.0250	4.19	314.1	3	0.56	0.82	0.82
0.0250	4.19	428.1	2	0.41	0.82	0.82
0.0250	4.19	674.8	1	0.27	0.82	0.82
0.0250	4.19	1565.1	0	0.07	0.82	0.82
0.0275	3.81	162.6	8	0.92	0.35	0.12
0.0275	3.81	211.3	6	0.72	0.35	0.12
0.0275	3.81	300.2	4	0.51	0.35	0.12
0.0275	3.81	380.9	3	0.41	0.35	0.12
0.0275	3.81	520.6	2	0.30	0.35	0.12
0.0275	3.81	822.2	1	0.20	0.35	0.12
0.0275	3.81	1893.9	0	0.05	0.35	0.12

Table 2. (continued)

ω (rad/sec)	Period (minute)	$k_h R_\odot$	n	$M_\alpha^\dagger/10^{25}$ (gm)	$E_\alpha/10^{27}$ (egrs)	$E'_\alpha/10^{27}$ (egrs)
0.0310	3.38	132.1	13	1.03	0.06	0.02
0.0310	3.38	234.9	7	0.56	0.06	0.02
0.0310	3.38	385.7	4	0.34	0.06	0.02
0.0310	3.38	492.1	3	0.28	0.06	0.02
0.0310	3.38	674.1	2	0.21	0.06	0.02
0.0310	3.38	1073.8	1	0.12	0.06	0.02

E_α and E'_α are two different energy spectrums used to calculate the energy transfer rates of modes due to 3-mode coupling. They are different only for frequencies ≥ 0.026 rad sec⁻¹, where the observational results are not available.

$\dagger M_\alpha = 4\pi R_\odot^2 \mathcal{M}_\alpha$, where \mathcal{M}_α is the surface mass density in mode α defined by equation (19).

Table 3a.

ω (rad/sec)	$k_h R_\odot$	$\Upsilon_\alpha^{(1)}$ (erg/sec) d/H=2.5 [†]	$\Upsilon_\alpha^{(2)}$ (erg/sec) d/H=2.5 [†]	$\Upsilon_\alpha^{(1)}$ (erg/sec) d/H=5.0 [†]	$\Upsilon_\alpha^{(2)}$ (erg/sec) d/H=5.0 [†]
0.0110	21.5	-8.78x10 ¹⁹	-3.53x10 ¹⁶	-1.24x10 ²⁰	-5.91x10 ¹⁶
0.0110	41.0	-8.92x10 ¹⁹	-3.92x10 ¹⁶	-1.18x10 ²⁰	-6.66x10 ¹⁶
0.0110	60.5	-1.72x10 ²⁰	-1.93x10 ¹⁷	-2.66x10 ²⁰	-3.47x10 ¹⁷
0.0110	82.7	-1.67x10 ²⁰	-7.54x10 ¹⁸	-2.43x10 ²⁰	-1.41x10 ¹⁹
0.0110	130.0	-2.68x10 ²⁰	-6.39x10 ¹⁸	-3.68x10 ²⁰	-1.18x10 ¹⁹
0.0110	303.0	-1.43x10 ²¹	-1.16x10 ¹⁹	-1.85x10 ²¹	-2.10x10 ¹⁹
0.0125	37.5	-1.35x10 ²⁰	-2.00x10 ¹⁷	-1.78x10 ²⁰	-3.46x10 ¹⁷
0.0125	61.9	-2.50x10 ²⁰	-2.89x10 ¹⁷	-3.25x10 ²⁰	-4.97x10 ¹⁷
0.0125	107.0	-4.53x10 ²⁰	-7.03x10 ¹⁷	-5.79x10 ²⁰	-1.17x10 ¹⁸
0.0125	167.5	-1.00x10 ²¹	-5.07x10 ¹⁸	-1.25x10 ²¹	-8.68x10 ¹⁸
0.0125	391.3	-7.32x10 ²¹	-4.13x10 ¹⁹	-9.50x10 ²¹	-7.78x10 ¹⁹
0.0150	43.1	-8.67x10 ²⁰	-3.69x10 ¹⁸	-1.13x10 ²¹	-6.79x10 ¹⁸
0.0150	112.6	-2.89x10 ²¹	-3.88x10 ¹⁸	-3.65x10 ²¹	-7.04x10 ¹⁸
0.0150	153.6	-4.38x10 ²¹	-5.36x10 ¹⁸	-5.47x10 ²¹	-9.73x10 ¹⁸
0.0150	241.9	-8.61x10 ²¹	-6.27x10 ¹⁸	-1.06x10 ²²	-1.15x10 ¹⁹
0.0150	563.6	-3.49x10 ²²	-4.33x10 ¹⁹	-4.25x10 ²²	-8.32x10 ¹⁹
0.0175	50.0	-5.28x10 ²¹	-5.58x10 ¹⁷	-6.43x10 ²¹	-1.00x10 ¹⁸
0.0175	100.1	-1.08x10 ²²	-1.68x10 ¹⁸	-1.32x10 ²²	-3.07x10 ¹⁸
0.0175	153.6	-1.44x10 ²²	-1.82x10 ¹⁸	-1.70x10 ²²	-3.28x10 ¹⁸
0.0175	328.7	-3.42x10 ²²	-4.79x10 ¹⁸	-3.81x10 ²²	-8.71x10 ¹⁸
0.0175	767.3	-1.99x10 ²³	-2.23x10 ¹⁹	-2.21x10 ²³	-4.25x10 ¹⁹
0.0200	63.2	-6.77x10 ²¹	-2.74x10 ¹⁷	-5.68x10 ²¹	-5.19x10 ¹⁷
0.0200	158.5	-2.44x10 ²²	-2.95x10 ¹⁷	-2.51x10 ²²	-5.39x10 ¹⁷
0.0200	200.2	-3.38x10 ²²	-6.45x10 ¹⁷	-3.51x10 ²²	-1.19x10 ¹⁸
0.0200	273.1	-4.76x10 ²²	-6.94x10 ¹⁷	-5.00x10 ²²	-1.30x10 ¹⁸
0.0200	429.5	-9.03x10 ²²	-1.51x10 ¹⁸	-9.19x10 ²²	-2.87x10 ¹⁸
0.0200	1002.2	-5.12x10 ²³	-8.43x10 ¹⁸	-5.31x10 ²³	-1.68x10 ¹⁹
0.0225	63.2	-2.50x10 ²¹	-6.14x10 ¹⁵	-1.93x10 ²¹	-1.14x10 ¹⁶
0.0225	108.4	-4.78x10 ²¹	-9.38x10 ¹⁵	-3.48x10 ²¹	-1.72x10 ¹⁶
0.0225	200.2	-1.03x10 ²²	-2.37x10 ¹⁶	-7.51x10 ²¹	-4.44x10 ¹⁶
0.0225	346.1	-2.50x10 ²²	-3.46x10 ¹⁶	-2.28x10 ²²	-6.54x10 ¹⁶
0.0225	544.9	-5.04x10 ²²	-9.57x10 ¹⁶	-5.01x10 ²²	-1.89x10 ¹⁷
0.0225	1267.7	-2.34x10 ²³	-5.15x10 ¹⁷	-2.41x10 ²³	-1.05x10 ¹⁸
0.0250	74.4	-1.63x10 ²¹	6.04x10 ¹⁵	-1.16x10 ²¹	8.35x10 ¹⁵
0.0250	151.5	-3.49x10 ²¹	9.72x10 ¹⁵	-2.45x10 ²¹	1.34x10 ¹⁶
0.0250	204.3	-4.74x10 ²¹	1.21x10 ¹⁶	-3.36x10 ²¹	1.67x10 ¹⁶
0.0250	247.4	-6.33x10 ²¹	1.51x10 ¹⁶	-4.56x10 ²¹	2.08x10 ¹⁶
0.0250	314.1	-8.81x10 ²¹	1.39x10 ¹⁶	-6.40x10 ²¹	1.92x10 ¹⁶
0.0250	428.1	-1.31x10 ²²	2.33x10 ¹⁶	-9.79x10 ²¹	3.24x10 ¹⁶
0.0250	674.8	-2.48x10 ²²	1.72x10 ¹⁶	-2.61x10 ²²	2.40x10 ¹⁶
0.0250	1565.1	-1.23x10 ²³	0.00x10 ⁰	-1.36x10 ²³	0.00x10 ⁰
0.0275	162.6	-3.32x10 ²¹	3.05x10 ¹⁷	-2.83x10 ²¹	4.56x10 ¹⁷
0.0275	211.3	-4.00x10 ²¹	3.60x10 ¹⁷	-3.58x10 ²¹	5.40x10 ¹⁷
0.0275	300.2	-6.46x10 ²¹	5.62x10 ¹⁷	-5.79x10 ²¹	8.43x10 ¹⁷
0.0275	380.9	-8.25x10 ²¹	5.26x10 ¹⁷	-7.62x10 ²¹	7.91x10 ¹⁷
0.0275	520.6	-1.15x10 ²²	4.85x10 ¹⁷	-1.01x10 ²²	7.31x10 ¹⁷
0.0275	822.2	-2.19x10 ²²	3.93x10 ¹⁷	-2.98x10 ²²	6.04x10 ¹⁷
0.0275	1893.9	-9.20x10 ²²	0.00x10 ⁰	-1.27x10 ²³	0.00x10 ⁰

Table 3a. (continued)

ω (rad/sec)	$k_h R_\odot$	$\Upsilon_\alpha^{(1)}$ (erg/sec) $d/H=2.5^\dagger$	$\Upsilon_\alpha^{(2)}$ (erg/sec) $d/H=2.5^\dagger$	$\Upsilon_\alpha^{(1)}$ (erg/sec) $d/H=5.0^\dagger$	$\Upsilon_\alpha^{(2)}$ (erg/sec) $d/H=5.0^\dagger$
0.0310	132.1	-1.75×10^{21}	1.96×10^{19}	-4.24×10^{21}	3.57×10^{19}
0.0310	234.9	-2.68×10^{21}	3.81×10^{19}	-5.85×10^{21}	6.96×10^{19}
0.0310	385.7	-4.74×10^{21}	5.42×10^{19}	-9.44×10^{21}	9.88×10^{19}
0.0310	492.1	-5.47×10^{21}	5.43×10^{19}	-1.06×10^{22}	1.00×10^{20}
0.0310	674.1	-7.84×10^{21}	4.50×10^{19}	-1.53×10^{22}	8.27×10^{19}
0.0310	1073.8	-1.28×10^{22}	1.49×10^{19}	-3.90×10^{22}	2.77×10^{19}

$^\dagger d$ is the thickness of the isothermal atmosphere and H is the pressure scale height.

Table 3b.

ω (rad/sec)	$k_h R_\odot$	$\Upsilon_\alpha^{(1)}$ (erg/sec) d/H=2.5	$\Upsilon_\alpha^{(2)}$ (erg/sec) d/H=2.5	$\Upsilon_\alpha^{(1)}$ (erg/sec) d/H=5.0	$\Upsilon_\alpha^{(2)}$ (erg/sec) d/H=5.0
0.0110	21.5	-8.78x10 ¹⁹	-3.61x10 ¹⁶	-1.24x10 ²⁰	-6.05x10 ¹⁶
0.0110	41.0	-8.91x10 ¹⁹	-3.99x10 ¹⁶	-1.18x10 ²⁰	-6.78x10 ¹⁶
0.0110	60.5	-1.71x10 ²⁰	-1.95x10 ¹⁷	-2.64x10 ²⁰	-3.50x10 ¹⁷
0.0110	82.7	-1.66x10 ²⁰	-7.62x10 ¹⁸	-2.41x10 ²⁰	-1.42x10 ¹⁹
0.0110	130.0	-2.73x10 ²⁰	-6.48x10 ¹⁸	-3.73x10 ²⁰	-1.19x10 ¹⁹
0.0110	303.0	-8.45x10 ²⁰	-1.18x10 ¹⁹	-1.12x10 ²¹	-2.14x10 ¹⁹
0.0125	37.5	-1.41x10 ²⁰	-2.02x10 ¹⁷	-1.86x10 ²⁰	-3.50x10 ¹⁷
0.0125	61.9	-2.60x10 ²⁰	-2.94x10 ¹⁷	-3.38x10 ²⁰	-5.04x10 ¹⁷
0.0125	107.0	-4.20x10 ²⁰	-7.21x10 ¹⁷	-5.40x10 ²⁰	-1.20x10 ¹⁸
0.0125	167.5	-5.96x10 ²⁰	-5.14x10 ¹⁸	-7.55x10 ²⁰	-8.80x10 ¹⁸
0.0125	391.3	-4.50x10 ²¹	-4.17x10 ¹⁹	-5.92x10 ²¹	-7.84x10 ¹⁹
0.0150	43.1	-2.77x10 ²⁰	-3.71x10 ¹⁸	-3.70x10 ²⁰	-6.82x10 ¹⁸
0.0150	112.6	-1.33x10 ²¹	-3.91x10 ¹⁸	-1.68x10 ²¹	-7.09x10 ¹⁸
0.0150	153.6	-2.22x10 ²¹	-5.39x10 ¹⁸	-2.76x10 ²¹	-9.79x10 ¹⁸
0.0150	241.9	-5.24x10 ²¹	-6.31x10 ¹⁸	-6.28x10 ²¹	-1.16x10 ¹⁹
0.0150	563.6	-3.10x10 ²²	-4.36x10 ¹⁹	-3.69x10 ²²	-8.36x10 ¹⁹
0.0175	50.0	-2.67x10 ²¹	-5.62x10 ¹⁷	-2.83x10 ²¹	-1.01x10 ¹⁸
0.0175	100.1	-5.88x10 ²¹	-1.69x10 ¹⁸	-6.36x10 ²¹	-3.09x10 ¹⁸
0.0175	153.6	-8.47x10 ²¹	-1.83x10 ¹⁸	-8.86x10 ²¹	-3.30x10 ¹⁸
0.0175	328.7	-2.78x10 ²²	-4.83x10 ¹⁸	-2.91x10 ²²	-8.76x10 ¹⁸
0.0175	767.3	-1.68x10 ²³	-2.25x10 ¹⁹	-1.83x10 ²³	-4.28x10 ¹⁹
0.0200	63.2	-6.71x10 ²¹	-2.76x10 ¹⁷	-5.65x10 ²¹	-5.23x10 ¹⁷
0.0200	158.5	-2.06x10 ²²	-2.98x10 ¹⁷	-1.86x10 ²²	-5.43x10 ¹⁷
0.0200	200.2	-2.78x10 ²²	-6.50x10 ¹⁷	-2.49x10 ²²	-1.20x10 ¹⁸
0.0200	273.1	-3.86x10 ²²	-6.99x10 ¹⁷	-3.44x10 ²²	-1.30x10 ¹⁸
0.0200	429.5	-7.53x10 ²²	-1.52x10 ¹⁸	-6.89x10 ²²	-2.88x10 ¹⁸
0.0200	1002.2	-4.38x10 ²³	-8.50x10 ¹⁸	-4.41x10 ²³	-1.70x10 ¹⁹
0.0225	63.2	-2.48x10 ²¹	-6.21x10 ¹⁵	-1.91x10 ²¹	-1.15x10 ¹⁶
0.0225	108.4	-4.71x10 ²¹	-9.48x10 ¹⁵	-3.44x10 ²¹	-1.73x10 ¹⁶
0.0225	200.2	-1.03x10 ²²	-2.39x10 ¹⁶	-7.57x10 ²¹	-4.49x10 ¹⁶
0.0225	346.1	-2.00x10 ²²	-3.50x10 ¹⁶	-1.60x10 ²²	-6.61x10 ¹⁶
0.0225	544.9	-3.70x10 ²²	-9.66x10 ¹⁶	-3.04x10 ²²	-1.90x10 ¹⁷
0.0225	1267.7	-1.99x10 ²³	-5.19x10 ¹⁷	-1.94x10 ²³	-1.06x10 ¹⁸
0.0250	74.4	-1.62x10 ²¹	6.06x10 ¹⁵	-1.15x10 ²¹	8.37x10 ¹⁵
0.0250	151.5	-3.25x10 ²¹	9.75x10 ¹⁵	-2.25x10 ²¹	1.34x10 ¹⁶
0.0250	204.3	-4.24x10 ²¹	1.22x10 ¹⁶	-2.93x10 ²¹	1.67x10 ¹⁶
0.0250	247.4	-5.33x10 ²¹	1.51x10 ¹⁶	-3.68x10 ²¹	2.08x10 ¹⁶
0.0250	314.1	-7.41x10 ²¹	1.39x10 ¹⁶	-5.08x10 ²¹	1.92x10 ¹⁶
0.0250	428.1	-1.08x10 ²²	2.34x10 ¹⁶	-7.43x10 ²¹	3.25x10 ¹⁶
0.0250	674.8	-1.93x10 ²²	1.73x10 ¹⁶	-1.46x10 ²²	2.40x10 ¹⁶
0.0250	1565.1	-1.02x10 ²³	0.00x10 ⁰	-1.04x10 ²³	0.00x10 ⁰
0.0275	162.6	-9.22x10 ²⁰	3.22x10 ¹⁷	-6.75x10 ²⁰	4.82x10 ¹⁷
0.0275	211.3	-1.07x10 ²¹	3.81x10 ¹⁷	-8.01x10 ²⁰	5.71x10 ¹⁷
0.0275	300.2	-1.83x10 ²¹	5.95x10 ¹⁷	-1.40x10 ²¹	8.93x10 ¹⁷
0.0275	380.9	-2.41x10 ²¹	5.59x10 ¹⁷	-1.94x10 ²¹	8.40x10 ¹⁷
0.0275	520.6	-3.45x10 ²¹	5.16x10 ¹⁷	-2.72x10 ²¹	7.77x10 ¹⁷
0.0275	822.2	-5.69x10 ²¹	4.16x10 ¹⁷	-4.76x10 ²¹	6.39x10 ¹⁷
0.0275	1893.9	-2.84x10 ²²	0.00x10 ⁰	-3.44x10 ²²	0.00x10 ⁰

Table 3b. (continued)

ω (rad/sec)	$k_h R_\odot$	$\Upsilon_\alpha^{(1)}$ (erg/sec) d/H=2.5	$\Upsilon_\alpha^{(2)}$ (erg/sec) d/H=2.5	$\Upsilon_\alpha^{(1)}$ (erg/sec) d/H=5.0	$\Upsilon_\alpha^{(2)}$ (erg/sec) d/H=5.0
0.0310	132.1	-4.16×10^{20}	1.97×10^{19}	-6.53×10^{20}	3.59×10^{19}
0.0310	234.9	-7.47×10^{20}	3.83×10^{19}	-1.22×10^{21}	7.00×10^{19}
0.0310	385.7	-1.46×10^{21}	5.45×10^{19}	-2.45×10^{21}	0.99×10^{20}
0.0310	492.1	-1.62×10^{21}	5.46×10^{19}	-2.50×10^{21}	1.00×10^{20}
0.0310	674.1	-2.38×10^{21}	4.53×10^{19}	-3.87×10^{21}	8.32×10^{19}
0.0310	1073.8	-3.26×10^{21}	1.50×10^{19}	-5.22×10^{21}	2.79×10^{19}

The tables 3a and 3b use different energy spectrums to calculate the energy transfer rates. Table 3a uses energy spectrum E_α whereas table 3b uses E'_α (see table 2).

Table 4.

ω (rad/sec)	$k_h R_\odot$	η_α^\dagger (sec ⁻¹) d/H=2.5	η_α (sec ⁻¹) d/H=5.0	$\eta_\alpha'^\dagger$ (sec ⁻¹) d/H=2.5	η_α' (sec ⁻¹) d/H=5.0
0.0110	21.5	-4.99x10 ⁻⁸	-7.06x10 ⁻⁸	-4.99x10 ⁻⁸	-7.06x10 ⁻⁸
0.0110	41.0	-5.07x10 ⁻⁸	-6.70x10 ⁻⁸	-5.06x10 ⁻⁸	-6.69x10 ⁻⁸
0.0110	60.5	-9.76x10 ⁻⁸	-1.51x10 ⁻⁷	-9.71x10 ⁻⁸	-1.50x10 ⁻⁷
0.0110	82.7	-9.93x10 ⁻⁸	-1.46x10 ⁻⁷	-9.88x10 ⁻⁸	-1.45x10 ⁻⁷
0.0110	130.0	-1.56x10 ⁻⁷	-2.16x10 ⁻⁷	-1.59x10 ⁻⁷	-2.19x10 ⁻⁷
0.0110	303.0	-8.20x10 ⁻⁷	-1.06x10 ⁻⁶	-4.87x10 ⁻⁷	-6.50x10 ⁻⁷
0.0125	37.5	-4.10x10 ⁻⁸	-5.39x10 ⁻⁸	-4.28x10 ⁻⁸	-5.62x10 ⁻⁸
0.0125	61.9	-7.57x10 ⁻⁸	-9.83x10 ⁻⁸	-7.85x10 ⁻⁸	-1.02x10 ⁻⁷
0.0125	107.0	-1.37x10 ⁻⁷	-1.75x10 ⁻⁷	-1.27x10 ⁻⁷	-1.63x10 ⁻⁷
0.0125	167.5	-3.03x10 ⁻⁷	-3.80x10 ⁻⁷	-1.82x10 ⁻⁷	-2.31x10 ⁻⁷
0.0125	391.3	-2.22x10 ⁻⁶	-2.89x10 ⁻⁶	-1.37x10 ⁻⁶	-1.81x10 ⁻⁶
0.0150	43.1	-1.46x10 ⁻⁷	-1.90x10 ⁻⁷	-4.70x10 ⁻⁸	-6.30x10 ⁻⁸
0.0150	112.6	-4.85x10 ⁻⁷	-6.11x10 ⁻⁷	-2.24x10 ⁻⁷	-2.82x10 ⁻⁷
0.0150	153.6	-7.33x10 ⁻⁷	-9.17x10 ⁻⁷	-3.73x10 ⁻⁷	-4.63x10 ⁻⁷
0.0150	241.9	-1.44x10 ⁻⁶	-1.77x10 ⁻⁶	-8.78x10 ⁻⁷	-1.05x10 ⁻⁶
0.0150	563.6	-5.85x10 ⁻⁶	-7.12x10 ⁻⁶	-5.19x10 ⁻⁶	-6.18x10 ⁻⁶
0.0175	50.0	-4.16x10 ⁻⁷	-5.06x10 ⁻⁷	-2.10x10 ⁻⁷	-2.23x10 ⁻⁷
0.0175	100.1	-8.47x10 ⁻⁷	-1.04x10 ⁻⁶	-4.63x10 ⁻⁷	-5.01x10 ⁻⁷
0.0175	153.6	-1.13x10 ⁻⁶	-1.34x10 ⁻⁶	-6.67x10 ⁻⁷	-6.98x10 ⁻⁷
0.0175	328.7	-2.69x10 ⁻⁶	-3.00x10 ⁻⁶	-2.19x10 ⁻⁶	-2.29x10 ⁻⁶
0.0175	767.3	-1.57x10 ⁻⁵	-1.74x10 ⁻⁵	-1.32x10 ⁻⁵	-1.44x10 ⁻⁵
0.0200	63.2	-4.67x10 ⁻⁷	-3.92x10 ⁻⁷	-4.63x10 ⁻⁷	-3.90x10 ⁻⁷
0.0200	158.5	-1.68x10 ⁻⁶	-1.73x10 ⁻⁶	-1.42x10 ⁻⁶	-1.28x10 ⁻⁶
0.0200	200.2	-2.33x10 ⁻⁶	-2.42x10 ⁻⁶	-1.92x10 ⁻⁶	-1.72x10 ⁻⁶
0.0200	273.1	-3.28x10 ⁻⁶	-3.45x10 ⁻⁶	-2.66x10 ⁻⁶	-2.37x10 ⁻⁶
0.0200	429.5	-6.23x10 ⁻⁶	-6.34x10 ⁻⁶	-5.19x10 ⁻⁶	-4.75x10 ⁻⁶
0.0200	1002.2	-3.53x10 ⁻⁵	-3.66x10 ⁻⁵	-3.02x10 ⁻⁵	-3.04x10 ⁻⁵
0.0225	63.2	-7.69x10 ⁻⁷	-5.93x10 ⁻⁷	-7.64x10 ⁻⁷	-5.89x10 ⁻⁷
0.0225	108.4	-1.47x10 ⁻⁶	-1.07x10 ⁻⁶	-1.45x10 ⁻⁶	-1.06x10 ⁻⁶
0.0225	200.2	-3.16x10 ⁻⁶	-2.31x10 ⁻⁶	-3.18x10 ⁻⁶	-2.33x10 ⁻⁶
0.0225	346.1	-7.70x10 ⁻⁶	-7.03x10 ⁻⁶	-6.14x10 ⁻⁶	-4.92x10 ⁻⁶
0.0225	544.9	-1.55x10 ⁻⁵	-1.54x10 ⁻⁵	-1.14x10 ⁻⁵	-9.35x10 ⁻⁶
0.0225	1267.7	-7.21x10 ⁻⁵	-7.41x10 ⁻⁵	-6.12x10 ⁻⁵	-5.97x10 ⁻⁵
0.0250	74.4	-1.98x10 ⁻⁶	-1.41x10 ⁻⁶	-1.99x10 ⁻⁶	-1.41x10 ⁻⁶
0.0250	151.5	-4.24x10 ⁻⁶	-2.98x10 ⁻⁶	-3.98x10 ⁻⁶	-2.76x10 ⁻⁶
0.0250	204.3	-5.76x10 ⁻⁶	-4.08x10 ⁻⁶	-5.19x10 ⁻⁶	-3.59x10 ⁻⁶
0.0250	247.4	-7.69x10 ⁻⁶	-5.54x10 ⁻⁶	-6.53x10 ⁻⁶	-4.51x10 ⁻⁶
0.0250	314.1	-1.07x10 ⁻⁵	-7.78x10 ⁻⁶	-9.08x10 ⁻⁶	-6.23x10 ⁻⁶
0.0250	428.1	-1.59x10 ⁻⁵	-1.19x10 ⁻⁵	-1.32x10 ⁻⁵	-9.10x10 ⁻⁶
0.0250	674.8	-3.01x10 ⁻⁵	-3.17x10 ⁻⁵	-2.37x10 ⁻⁵	-1.79x10 ⁻⁵
0.0250	1565.1	-1.50x10 ⁻⁴	-1.65x10 ⁻⁴	-1.25x10 ⁻⁴	-1.27x10 ⁻⁴
0.0275	162.6	-9.45x10 ⁻⁶	-8.06x10 ⁻⁶	-7.62x10 ⁻⁶	-5.58x10 ⁻⁶
0.0275	211.3	-1.14x10 ⁻⁵	-1.02x10 ⁻⁵	-8.84x10 ⁻⁶	-6.62x10 ⁻⁶
0.0275	300.2	-1.84x10 ⁻⁵	-1.65x10 ⁻⁵	-1.51x10 ⁻⁵	-1.16x10 ⁻⁵
0.0275	380.9	-2.35x10 ⁻⁵	-2.17x10 ⁻⁵	-1.99x10 ⁻⁵	-1.60x10 ⁻⁵
0.0275	520.6	-3.27x10 ⁻⁵	-2.87x10 ⁻⁵	-2.85x10 ⁻⁵	-2.25x10 ⁻⁵
0.0275	822.2	-6.23x10 ⁻⁵	-8.49x10 ⁻⁵	-4.70x10 ⁻⁵	-3.93x10 ⁻⁵
0.0275	1893.9	-2.62x10 ⁻⁴	-3.61x10 ⁻⁴	-2.35x10 ⁻⁴	-2.84x10 ⁻⁴

Table 4. (continued)

ω (rad/sec)	$k_h R_\odot$	η_α^\dagger (sec ⁻¹) d/H=2.5	η_α (sec ⁻¹) d/H=5.0	$\eta_\alpha'^\dagger$ (sec ⁻¹) d/H=2.5	η_α' (sec ⁻¹) d/H=5.0
0.0310	132.1	-2.81x10 ⁻⁵	-6.81x10 ⁻⁵	-1.76x10 ⁻⁵	-2.74x10 ⁻⁵
0.0310	234.9	-4.29x10 ⁻⁵	-9.37x10 ⁻⁵	-3.15x10 ⁻⁵	-5.10x10 ⁻⁵
0.0310	385.7	-7.59x10 ⁻⁵	-1.51x10 ⁻⁴	-6.27x10 ⁻⁵	-1.05x10 ⁻⁴
0.0310	492.1	-8.78x10 ⁻⁵	-1.70x10 ⁻⁴	-6.94x10 ⁻⁵	-1.07x10 ⁻⁴
0.0310	674.1	-1.26x10 ⁻⁴	-2.47x10 ⁻⁴	-1.04x10 ⁻⁴	-1.68x10 ⁻⁴
0.0310	1073.8	-2.08x10 ⁻⁴	-6.32x10 ⁻⁴	-1.44x10 ⁻⁴	-2.31x10 ⁻⁴

$\dagger \eta_\alpha \equiv (\Upsilon_\alpha^{(1)} + \Upsilon_\alpha^{(2)})/E_\alpha$, and is the inverse decay time of the mode α due to 3-mode couplings. η_α and η_α' have been calculated using the energy spectrums E_α and E'_α respectively (see table 2).